STUDY OF NONLINEAR ANALYSIS AND CHAOS IN VIBRATIONS AND FLUIDS

A Dissertation

by

JING TIAN

Submitted to the Office of Graduate and Professional Studies of
Texas A&M University
in partial fulfillment of the requirements for the degree of

DOCTOR OF PHILOSOPHY

Chair of Committee,	Goong Chen
Committee Members,	Siu A. Chin
	Prabir Daripa
	Peter Howard
Head of Department,	Emil Straube

August 2016

Major Subject: Mathematics

ABSTRACT

Chaos and turbulence are two important topics in nonlinear dynamics. In this study, two problems related to chaos and turbulence modelling are presented. They are the chaotic vibration phenomenon in high-dimensional partial differential equations and the emergence of the Navier-Stokes-alpha model for channel flows.

The study of the chaotic vibration phenomenon in high-dimensional partial differential equations is explained from both the numerical and theoretical aspects. In the numerical perspective, we have studied the chaotic vibration phenomenon of the 2D wave equation through numerical simulations. Based on the finite-volume method, we have built our own solver "img2Foam" in the Computational Fluid Dynamics software OpenFOAM (Open source Field Operation and Manipulation). We have implemented several numerical simulations containing both chaotic and non-chaotic cases. As for the theoretical perspective, we give a rigorous proof for the chaotic vibration phenomenon of the 2D non-strictly hyperbolic equation. After introducing two linear operators, the initial system of the 2D non-strictly hyperbolic equation is converted into a system of two coupled first order equations. By using the method of characteristics, we have found the explicit solution formulas of the new system. We have also found a regime of the parameters when the chaotic vibration phenomenon occurs by applying the period-doubling bifurcation theorem. Numerical simulations are presented to validate the theoretical results.

Inspired by the concept of the regular part of the weak attractor of the 3D Navier-Stokes equations, we concentrate on a restricted class of fluid flows to explore the transition from the Navier-Stokes equations to the Navier-Stokes-alpha model for channel flows. The Navier-Stokes equations have been widely used to describe the

motion of viscous incompressible fluid flows. As an averaged version of the Navier-Stokes equations, the Navier-Stokes-alpha model has solid mathematical properties as well as reliable experimental matches. Therefore, the Navier-Stokes-alpha model is taken as an approximation for the dynamics of appropriately averaged turbulent fluid flows. We are interested in finding a connection between Navier-Stokes equations and the Navier-Stokes-alpha model in terms of the physical properties of the fluid flow. Given the hypothesis that the turbulence described by the Navier-Stokes-alpha model was partly due to the roughness of the walls, the transition from the Navier-Stokes equations into the Navier-Stokes-alpha model is presented by introducing a Reynolds type averaging.

DEDICATION

I would like to dedicate this dissertation to my beloved parents, who have supported me throughout my life.

ACKNOWLEDGEMENTS

I would like to express my utmost gratitude to my adviser, Professor Goong Chen for his continuous support of my Ph.D. studies. His patient guidance and tremendous help make this work possible. My sincere thanks also go to Professor Ciprian Foias for his research collaboration and encouragement. I am very grateful to my committee members, Professors Siu Chin, Prabir Daripa and Peter Howard, for their kind service and useful comments on this dissertation. My thanks also go to Professors Harold Boas, Zhaosheng Feng and David Manuel for their diligent help and suggestions during my Ph.D. studies.

I would also like to thank the Department of Mathematics at Texas A&M University and Qatar National Research Fund QNRF Grant #5−674−1−114 for providing me with assistantships. An acknowledgment is also given to Mrs. Monique Steward and Mrs. Floyd Sherry for their help.

Finally, I want to thank all my friends, who make my life full of love.

TABLE OF CONTENTS

LIST OF FIGURES

FIGURE Page

1. INTRODUCTION

Chaos and turbulence have always been important areas of research in nonlinear dynamic phenomenon. In this dissertation, two problems related to chaos and turbulence modeling are presented: the chaotic vibration phenomenon in high-dimensional partial differential equations and the emergence of the Navier-Stokes-alpha model for channel flows.

Chaotic vibration phenomena have been shown to exist in second order ordinary differential equations as well as one-dimensional partial differential equations. It is still a challenge to study chaotic vibration phenomena in high-dimensional partial differential equations. As will be presented in sections 2 and 3, we have studied the chaotic phenomenon of a 2D wave equation and a non-strictly hyperbolic equation, respectively. The wave equation is an important second-order linear partial differential equation for modeling wave propagation, such as acoustic and electromagnetic waves or a vibrating membrane. Inspired by the results of the chaotic vibration phenomenon of the 1D wave equation [9, 14, 8], in section 2, we present the study of the chaotic vibration phenomenon of a 2D wave equation by numerical simulations. We use a user-friendly software OpenFOAM (Open source Field Operation And Manipulation) to conduct the numerical experiments. By writing the C++ codes to create and implement an application called *img2Foam*, we have obtained the numerical solutions of the 2D wave equation of certain initial and boundary conditions. The discretization method used in OpenFOAM is the finite-volume method. By choosing different parameters, we obtain the results of both the chaotic and non-chaotic cases.

We are also interested in studying the chaotic phenomenon of high-dimensional partial differential equations theoretically. In section 3, we focus on a 2D non-strictly hyperbolic equation. First, we introduce two linear operators and Riemann invariants, which enable us to convert the initial system into a system of two coupled first order equations. The well-posedness of these two systems are equivalent, so we concentrate the investigation on the new system. We have found explicit solution formulas of the first order equations by using the method of characteristics. After that, we have studied the dynamic properties of the composite functions in the system. By applying the period-doubling bifurcation theorem, we characterize a regime of the parameters when the chaotic vibration phenomenon occurred due to the *energy-injection* boundary condition and the *distributed self-regulation* boundary condition. Numerical simulations are provided to validate the theoretical results.

In section 4, we share the study of the emergence of the Navier-Stokes-alpha model in channel flow, as it is related to turbulence modeling. The Navier-Stokes equations (NSE) have been widely used to describe the motion of viscous incompressible fluid flows, while the Navier-Stokes-alpha model (NS-α) is a mathematical model for the dynamics of appropriately averaged turbulent fluid flows. Our aim is to obtain a simple Reynolds type averaging which transforms the NSE into the NS-α. For this purpose, we concentrate on a restricted class of fluid flows. This class, denotes by $\mathcal{P}$, is defined (recurrently) by five assumptions, for which we have provided the respective rationales. The definition of the class $\mathcal{P}$ is inspired by the concept of the regular part of the weak attractor of the 3D NSE [23] as well as by that of the sigma weak attractor defined in [4].

The innovative aspect of the investigation here is the hypothesis that the turbulence described by the NS-α is partly due to the roughness of the walls. Therefore, we have introduced a specifically designed mathematical model for the effect of the wall roughness upon the fluid flows by adopting one of Mandelbrot's paradigms [35], which in this case, is that the roughness is the sum of a self-similar decreasing sequence of rugosities. The model is based on the hypothesis that the effect of each of the smaller rugosities is concentrated mainly on the flow eddies of linear size comparable with the magnitudes of the rugosities. After introducing the Reynolds averaging and roughness model, we are able to transform the NSE into the NS-α.

In section 5, the concluding remarks of the dissertation are provided.

2. CHAOTIC VIBRATION PHENOMENON OF A 2D WAVE EQUATION AND OTHER NUMERICAL EXPERIMENTS

2.1 Background

Computational fluid dynamics (CFD) is a constantly growing field with an impact on both science and industry. It is a branch of fluid mechanics that solves and analyzes problems involving fluid flows by using numerical analysis and algorithms. High performance computing, such as supercomputers, is often used to perform the calculations in CFD computation. A basic procedure of a CFD computation includes three parts:

(i) Preprocessing: defining the geometry, generating meshes, defining the physical modeling (equations) and defining boundary and initial conditions.

(ii) Simulating: solving the equations.

(iii) Post-processing: analyzing and creating visualizations.

Recently, one popular software used in CFD is OpenFOAM* (Open source Field Operation And Manipulation). The OpenFOAM package is an object-oriented numerical simulation toolkit written in C++ language [2]. It has been widely used in the CFD computations. One advantage of OpenFOAM is its friendly syntax for tensor operations and partial differential equations (PDE) that enables us to create custom solvers. Running OpenFOAM is a process of running *applications*. *Applications* are written by the syntax introduced by OpenFOAM [2]. There are two categories of applications: *solvers* and *utilities*. *Solvers* perform the actual calculation to solve continuum mechanics problems, i.e., *simpleFOAM* is a steady-state solver for incompressible turbulent flow. *Utilities* can be used to generate the mesh,

*OpenFOAM is a registered trade mark of OpenCFD Limited.

set-up the simulation case and process the results, i.e., *blockMesh* can be used to generate meshes.

The discretization method used in OpenFOAM is the finite-volume method (FVM). It is one of the three popular discretization methods in Numerical Analysis. The other two are the finite-element method and the finite-difference method. FVM is a method that represents and evaluates partial differential equations in the form of algebraic equations [31]. The values are calculated at each node point. "Finite volume" refers to the small volume surrounding each node point [31]. The main tool used in the finite volume method is the *divergence theorem*. Usually, we take the volume integrals on both sides of the equation. By applying the divergence theorem, the volume integrals that contain a divergence term in the equation are converted into surface integrals [31]. FVM is conservative. Another advantage of the FVM, which also becomes an advantage of OpenFOAM, is that it can be used to deal with unstructured meshes.

2.2 Numerical Simulations of a 2D Wave Equation

The study of nonlinear vibrations in mechanical and electronic systems has always been an important area of research by scientists and engineers [39]. Recently, one of the primary emphases of such research is on chaotic phenomena. Chaotic phenomena have been shown to exist in second order ordinary differential equations as well as first order partial differential equations. In a series of papers [9, 14, 8], Chen and his team studied the chaotic vibrating phenomenon in the 1D wave equation. One system they studied was (from [9]))

$$
\begin{aligned}
&w_{tt}(x,\ t) - w_{xx}(x,\ t) = 0, \qquad 0 < x < 1,\ t > 0,\\
&w_x(0,\ t) = -\eta w_t(0,\ t), \qquad \eta > 0,\ \eta \neq 1,\\
&w_x(1,\ t) = \alpha w_t(1,\ t) - \beta w_t(1,\ t)^3, \qquad t > 0;\ \alpha, \beta > 0,\\
&w(x,\ 0) = w_0(x),\ w_t(x,\ 0) = w_1(x), \qquad 0 \leq x \leq 1.
\end{aligned}
$$

By applying the method of characteristics, they proved the chaotic phenomenon existed in the above system.

However the method of characteristics is generally not easily applicable in 2D or higher dimensions, so in this section we apply the numerical tools to study the chaotic vibration phenomenon of wave equation in the high dimensions.

2.2.1 Approaches and Objectives

2.2.1.1 Objectives

The wave equation is an important second-order linear partial differential equation for modeling wave propagation, such as acoustic and electromagnetic waves, and a vibrating membrane.

Inspired by the 1D results, we are interested in exploring the chaotic phenomenon of the 2D wave equation. Consider the equation:

$$\frac{\partial^2 w}{\partial t^2} = {c_0}^2 \nabla^2 w, \tag{2.1}$$

where c_0 is the propagation speed of the wave, and we take $c_0 = 1$ in our case. The domain is a $1m * 1m$ square.

The boundary conditions are:

$$w = 0.\ when\ x = 0, \tag{2.2}$$

$$\frac{\partial w}{\partial x} = \alpha \frac{\partial w}{\partial t} - \beta (\frac{\partial w}{\partial t})^3.\ when\ x = 1, \tag{2.3}$$

$$w = 0.\ when\ y = 0, \tag{2.4}$$

$$\frac{\partial w}{\partial y} = 0.\ when\ y = 1. \tag{2.5}$$

The initial conditions are:

$$w(x, y, 0) = 0.02(\frac{4}{\pi}(1 - cos(\pi y)) - \frac{7y}{4} + \frac{7}{8\pi} sin(2\pi y)) \tag{2.6}$$

$$*(\frac{4}{\pi}(1 - cos(\pi x)) - \frac{7x}{4} + \frac{7}{8\pi} sin(2\pi x)), \tag{2.7}$$

$$w_t(x, y, 0) = 0.02(4sin(\pi y) + 3.5sin^2(\pi y))(4sin(\pi x) + 3.5sin^2(\pi x)). \tag{2.8}$$

2.2.1.2 Approaches

(1) Solving Mechanism

We use a CFD software OpenFOAM to solve this equation. Running OpenFOAM consists of three steps [2]:

(i) Preprocessing: (a) mesh generation; (b) boundary and initial conditions; (c) physical properties and control settings; (d) discretization and solver settings,

(ii) Running an application: usually on a supercomputer,

(iii) Post-processing: by using the software Paraview for visualization.

(a) Mesh generation

Our domain consists of a square of side length $d = 1m$ in the $x - y$ plane. A uniform mesh of 100 by 100 cells will be used. The z direction with a subdivision "1" shows this is a 2D case, also the front and back faces are set as type empty. After these settings, the mesh generator supplied with OpenFOAM called "blockMesh" generates meshes from a description specified in the blockMesh dictionary.

(b) Boundary and initial conditions

We have three types of boundary conditions here: (2.2) and (2.4) are the "fixed-Value" type, and (2.5) is the "zeroGradient" type. For the two initial conditions (2.6) and (2.8), we use the "codeStream" function to write those expressions into the "internalField" file.

(c) Physical properties and controls

We set "c_0" to be 1 in the "transportProperties" file. The time step is $6 * 10^{-5}s$.

(2) Discretization of the Equation and Solver Settings

We implemented our own application called "img2Foam". The main code in this solver is:

$$solve(fvm :: d2dt2(w) == c02 * fvc :: laplacian(w)). \tag{2.9}$$

Here fvm means finite volume method. The fvm is defined for implicit equations. In the fvm solving process, the equation is solved iteratively. Instead of producing an immediate solution (like the fvc), fvm namespace produces a fvMatrix object which is a matrix form coefficients. While, fvc means finite volume calculus. It is used to solve explicit equations and will generate a field.

The scheme for *d2dt2* is Euler, and for Laplacian is Gauss linear uncorrected. The definition point of physical quantities is taken at the barycenter of each control volume (CV) (see Fig. 2.1).

For the left side of (2.1), taking integration over the CV with the time-invariant

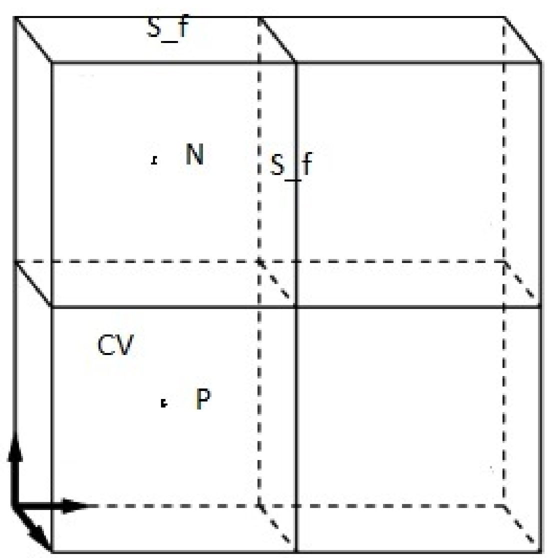

Figure 2.1: The mesh settings

volume V and applying the central differencing scheme ([36]), we obtain:

$$\frac{\partial^2}{\partial t^2}\int_V w dV \approx \frac{w^{n+1} - 2w^n + w^{n-1}}{\triangle t^2} V,$$

where, w^{n+1}, w^n and w^{n-1} denote the values of w at the $(n+1)-th$, $n-th$ and $(n-1)-th$ steps of the time step $\triangle t$.

For the right hand side of (2.1), integrating over the control volume with the time-invariant volume V and applying the divergence theorem, we obtain ([36]):

$$\int_V {c_0}^2 \nabla^2 w dV = {c_0}^2 \int_S dS \cdot \bigtriangledown w \approx {c_0}^2 \sum_f S_f \frac{w_N - w_P}{|d_{PN}|},$$

where S_f denotes the face area of face f. w_N and w_P are the values of w at the centers of the adjacent cells N and P.

After discretization, (2.1) becomes:

$$\frac{w_P^{n+1} - 2w_P^n + w_P^{n-1}}{\triangle t^2} V \approx {c_0}^2 \sum_f S_f \frac{w_N^n - w_P^n}{|d_{PN}|}. \tag{2.10}$$

Then we use the "PCG" (preconditioned conjugate gradient) solver in OpenFOAM to solve this linear equation.

The fvscheme we use in OpenFOAM is:

Euler implicit

$solve(fvm :: d2dt2(w) == c02 * fvm :: laplacian(w));$

d2dt2Schemes

{

d2dt2(w) Euler;

}

laplacianScheme

{

laplacian(w) Gauss linear uncorrected;

laplacian(w_0) Gauss linear uncorrected;

}.

(3) Discretization of the Boundary Condition

For the boundary condition (2.3), since at $x = 1$, the boundary condition is $\frac{\partial w}{\partial x} = \frac{\partial w}{\partial n_b}$. So we need to discretize it to calculate the surface normal gradient of w at the time step $n+1$ at the boundary face barycenter b, namely $\frac{\partial w}{\partial n_b}|^{n+1}$ ([36]). w subscripted by P denotes the values of w at the barycenter of boundary-internal CV, and w subscripted by b (see Fig. 2.2) denotes the values of w at the barycenter of boundary face. $\triangle n$ is the distance between the two barycenters. By applying a backward difference scheme to the time derivative of (2.3), we have

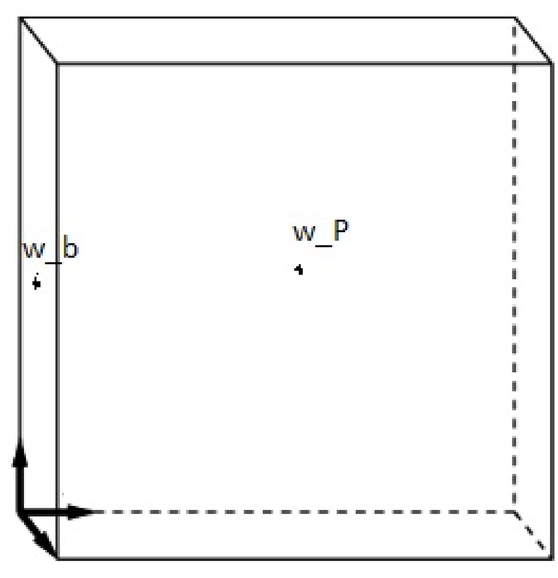

Figure 2.2: The boundary mesh

$$\frac{\partial w}{\partial n_b}|^{n+1} = \alpha(\frac{w_P^{n+1} - w_P^n}{\triangle t}) - \beta(\frac{w_P^{n+1} - w_P^n}{\triangle t})^3.$$

After we obtain the value of $\frac{\partial w}{\partial n_b}|^{n+1}$ from w_P^{n+1} and w_P^n, we can apply

$$\frac{\partial w}{\partial n_b}|^{n+1} = \frac{w_b^{n+1} - w_P^{n+1}}{\triangle n} \tag{2.11}$$

to obtain the value of w_b^{n+1} on the boundary.

Remark 1. *The above solving mechanism can also be used to solve the system*

$$\frac{\partial^2 w}{\partial t^2} = {c_0}^2 \nabla^2 w,$$

$$w = 0. \ when \ x = 0,$$

$$\frac{\partial w}{\partial x} = \alpha\frac{\partial w}{\partial t} - \beta(\frac{\partial w}{\partial t})^3. \ when \ x = 1,$$

$$w = 0. \ when \ y = 0,$$

$$\frac{\partial w}{\partial y} = \alpha\frac{\partial w}{\partial t} - \beta(\frac{\partial w}{\partial t})^3. \ when \ y = 1,$$

$$\begin{aligned} w(x, y, 0) = 0.02(&\frac{4}{\pi}(1 - cos(\pi y)) - \frac{7y}{4} + \frac{7}{8\pi} sin(2\pi y)) \\ &*(\frac{4}{\pi}(1 - cos(\pi x)) - \frac{7x}{4} + \frac{7}{8\pi} sin(2\pi x)), \end{aligned}$$

$$w_t(x, y, 0) = 0.02(4sin(\pi y) + 3.5sin^2(\pi y))(4sin(\pi x) + 3.5sin^2(\pi x)).$$

2.2.2 Simulation Results

2.2.2.1 Benchmark

We consider the initial-value problem for the 3D wave equation on a unit cube with the boundary $\partial\Omega$:

$$u_{tt} - c^2\Delta u = 0,$$
$$u(x_1, x_2, x_3, 0) = e^{-[(x_1-0.5)+(x_2-0.5)+(x_3-0.5)]},$$
$$u_t(x_1, x_2, x_3, 0) = \psi(x_1, x_2, x_3) = -c * \sqrt{3} * e^{-[(x_1-0.5)+(x_2-0.5)+(x_3-0.5)]},$$
$$u(x_1, x_2, x_3, t)|_{\partial\Omega} = e^{-[(x_1-0.5)+(x_2-0.5)+(x_3-0.5)]-c*\sqrt{3}*t}, (x_1, x_2, x_3) \in \partial\Omega.$$

By comparing the u values at point (0.025, 0.025, 0.025), we have two results: one is from OpenFOAM; one is from the exact solution formula: $u(x_1, x_2, x_3, t) = e^{-[(x_1-0.5)+(x_2-0.5)+(x_3-0.5)]-c*\sqrt{3}*t}$.

Below are the results from OpenFOAM (Fig. 2.3) and the exact solution (Fig. 2.4).

From Fig. 2.3 and Fig. 2.4 we can find that the two results match well.

2.2.2.2 For the 2D Wave Equation Case

We run several cases and compare the results: $\alpha = 0.1,\ 0.3,\ 0.8,\ 3$, and $\beta = 1$.

By using the software “Paraview” , we can obtain the graphic results. In order to make a 3D video, we extract the data from OpenFOAM and use Matlab codes to make the movies.

By comparing the results of four cases: $\alpha = 0.1,\ \beta = 1$; $\alpha = 0.3,\ \beta = 1$, $\alpha = 0.8,\ \beta = 1$, and $\alpha = 3,\ \beta = 1$. We find that only when $\alpha = 0.8$, there is the

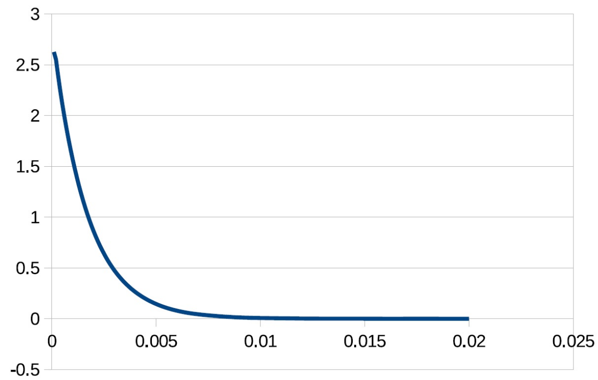

Figure 2.3: Result from OpenFOAM

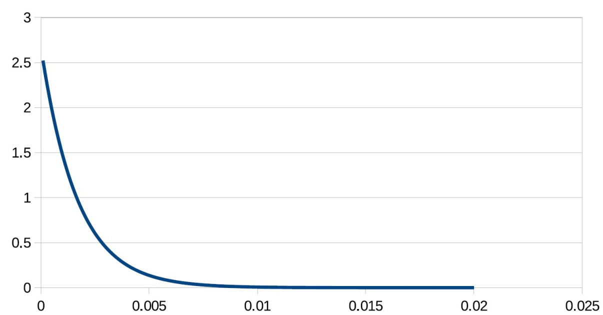

Figure 2.4: Result from the exact solution

occurrence of 2D chaotic phenomenon. Some graphic results are listed below (Fig. 2.5-2.8):

2.3 Other Numerical Experiments

2.3.1 Dumbbell Case

2.3.1.1 Basic Settings

The problem solved here is the propagation of a Gaussian acoustic pulse placed at a point in a dumbbell as an acoustic source. We consider the 3D wave equation:

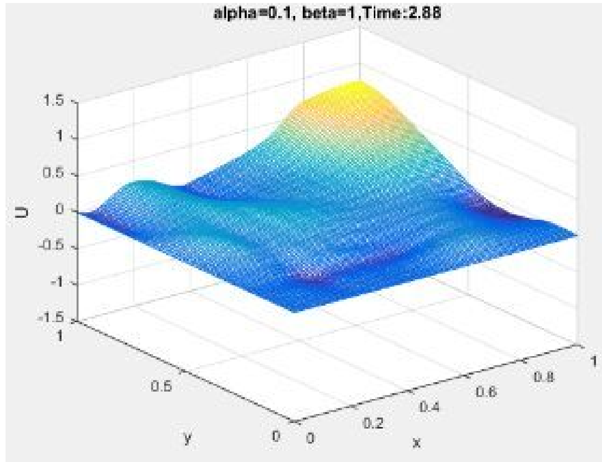

Figure 2.5: Case of alpha=0.1, t=2.88

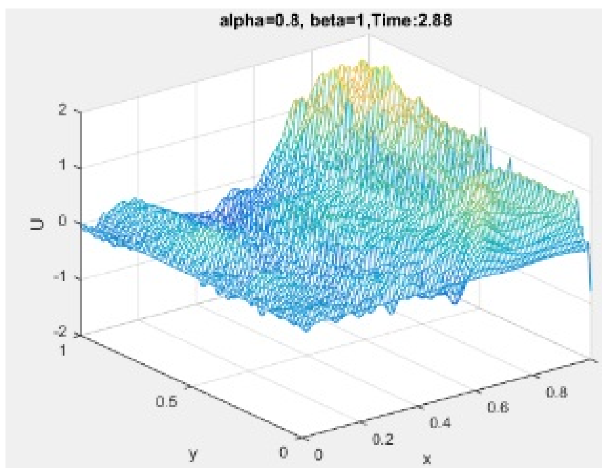

Figure 2.6: Case of alpha=0.8, t=2.88

$$\frac{\partial^2 \phi}{\partial t^2} = {c_0}^2 \nabla^2 \phi.$$

where $c_0 = 343.7m/s$ and density in the space is $1.205kg/m^3$.

Denote all the outside boundaries other than the small ball inside as Ω_1, and the

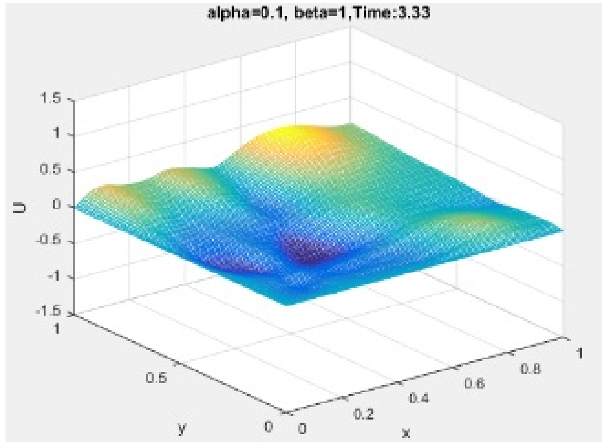

Figure 2.7: Case of alpha=0.1, t=3.33

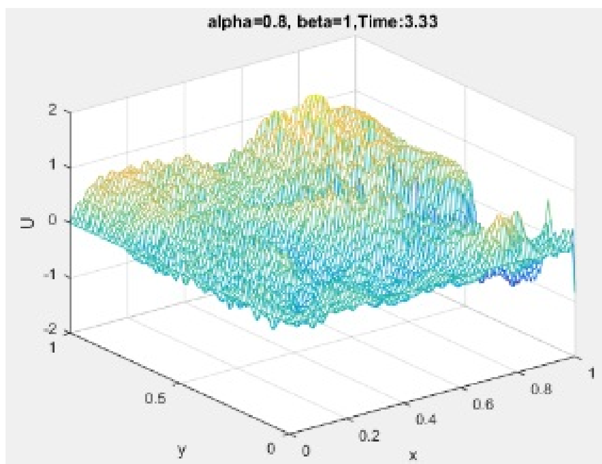

Figure 2.8: Case of alpha=0.8, t=3.33

boundary of the small ball inside as Ω_2.

We test three different types of boundary conditions:

(i) Convective boundary condition

$$\frac{\partial \phi}{\partial t} + V_n \frac{\partial \phi}{\partial n} = 0,$$

where V_n represents the convective velocity, which will be given in each case.

α is the acoustic absorption factor, and $\alpha = 1 - |\frac{V_n/c_0-1}{V_n/c_0+1}|^2$. If $\alpha = 0$, it is fully reflected. If $\alpha = 1$, it is fully absorbed. We study three types of conditions here:

(a) Ω_1 is assigned with an acoustic impendance of $343.7kg/m^2s$, which is equivalent to the acoustic absorption factor $\alpha = 1$.

Ω_2 is assigned with an acoustic impendance of $136791.7kg/m^2s$, which is equivalent to the acoustic absorption factor $\alpha = 0.01$.

(b) Ω_2 is assigned with an acoustic impendance of $343.7kg/m^2s$, which is equivalent to the acoustic absorption factor $\alpha = 1$.

Ω_1 is assigned with an acoustic impendance of $136791.7kg/m^2s$, which is equivalent to the acoustic absorption factor $\alpha = 0.01$.

(c) All the boundaries have the same boundary condition: $\alpha = 1$.

(ii) Dirichlet boundary condition: $\phi = 0$ at all the boundaries.

(iii) Neumann boundary condition: $\frac{\partial \phi}{\partial n} = 0$ at all the boundaries.

Running all the cases, we obtain the following graphic results (Fig. 2.9-2.23).

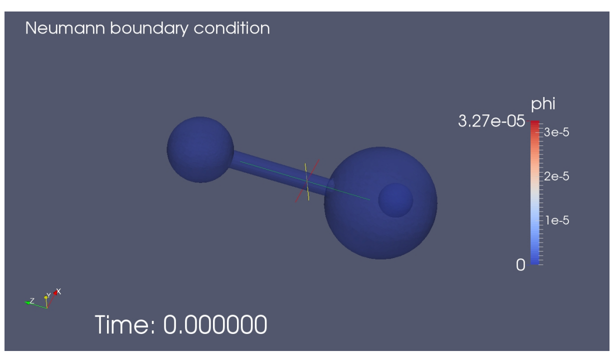

Figure 2.9: The case of Neumann boundary condition at t=0

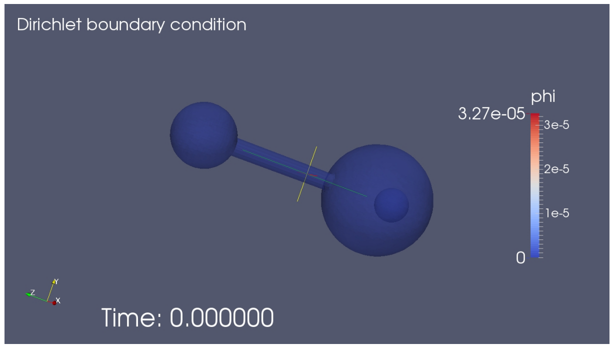

Figure 2.10: The case of Dirichlet boundary condition at t=0

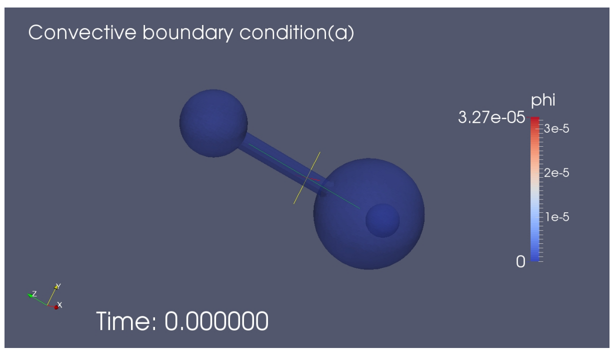

Figure 2.11: The case of Convective boundary condition (a) at t=0

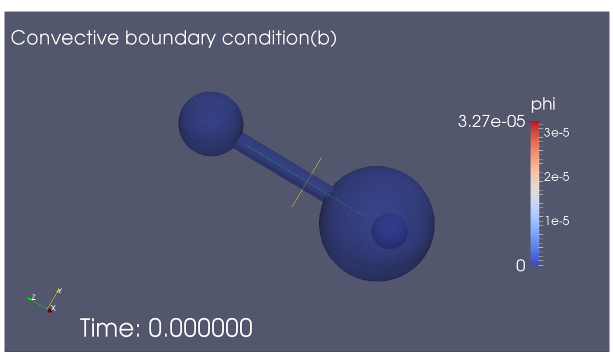

Figure 2.12: The case of Convective boundary condition (b) at t=0

2.3.1.2 Data Analysis

After running the applications and obtaining the video simulations, we can conduct the data analysis to compare the difference between each type of boundary

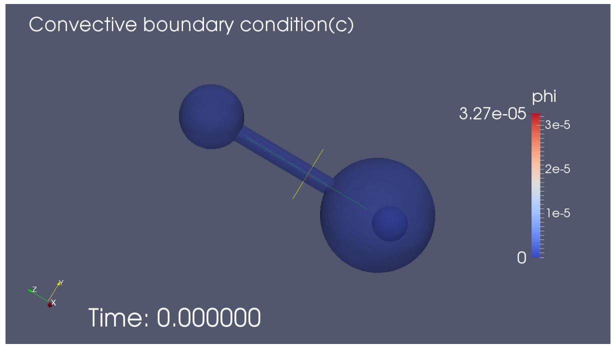

Figure 2.13: The case of Convective boundary condition (c) at t=0

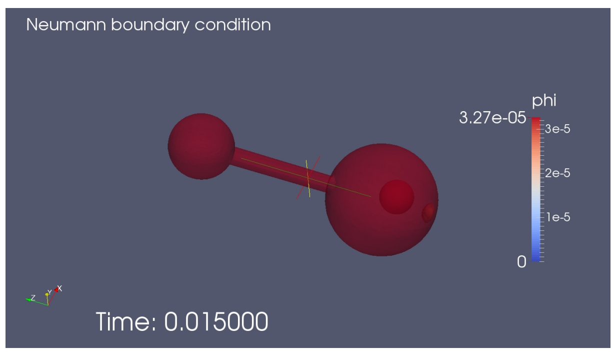

Figure 2.14: The case of Neumann boundary condition at t=0.015

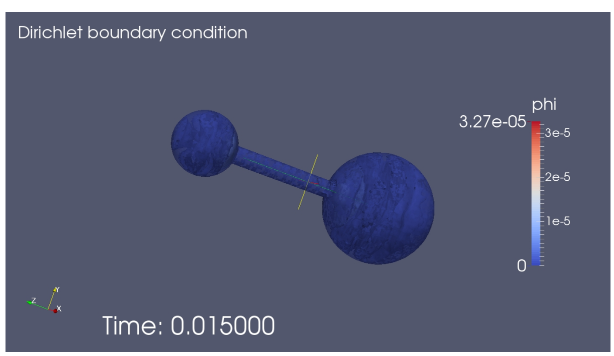

Figure 2.15: The case of Dirichlet boundary condition at t=0.015

conditions.

Sound is commonly shown as a waveform. The waveform is a 2D graph which

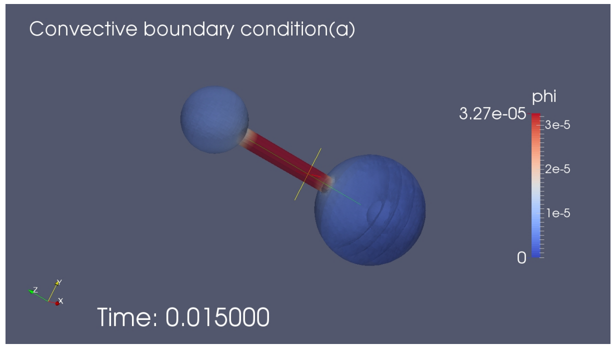

Figure 2.16: The case of Convective boundary condition (a) at t=0.015

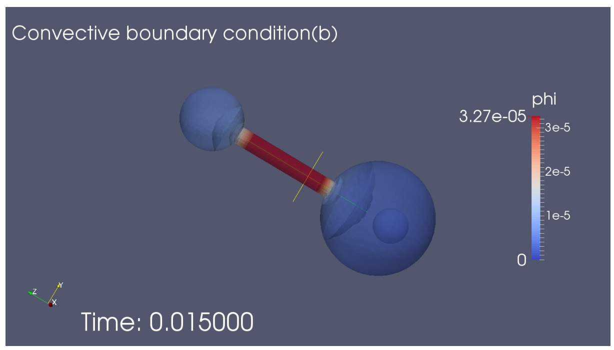

Figure 2.17: The case of Convective boundary condition (b) at t=0.015

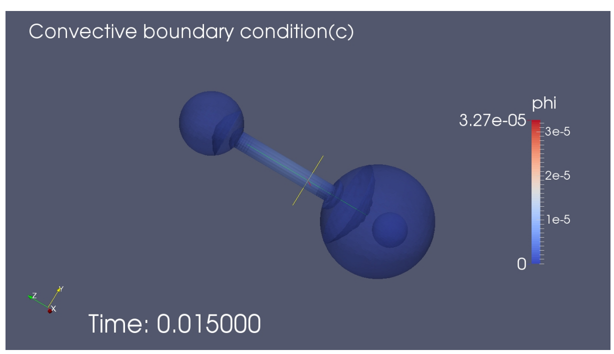

Figure 2.18: The case of Convective boundary condition (c) at t=0.015

displays the sound pressure as a function of time. Sound pressure is a measure of the variations in air pressure that we can observe as sound. The greater the change

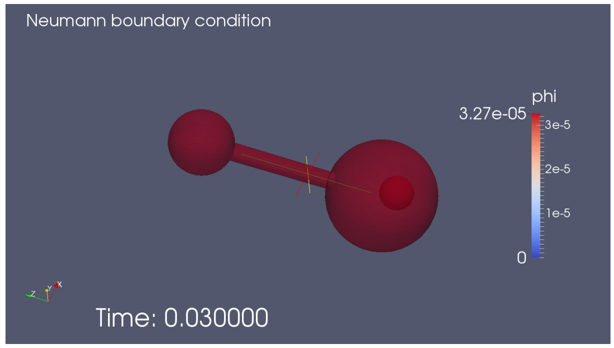

Figure 2.19: The case of Neumann boundary condition at t=0.03

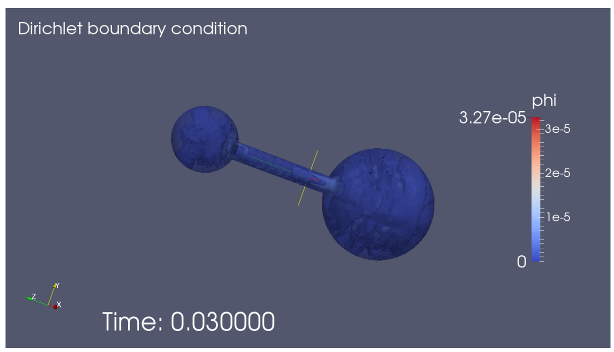

Figure 2.20: The case of Dirichlet boundary condition at t=0.03

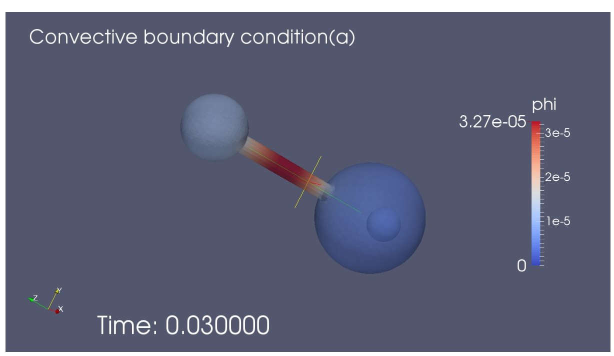

Figure 2.21: The case of Convective boundary condition (a) at t=0.03

in pressure, the louder the sound that we are able to hear. As we know, sound pressure is positive when the sound wave is compressing the medium through where

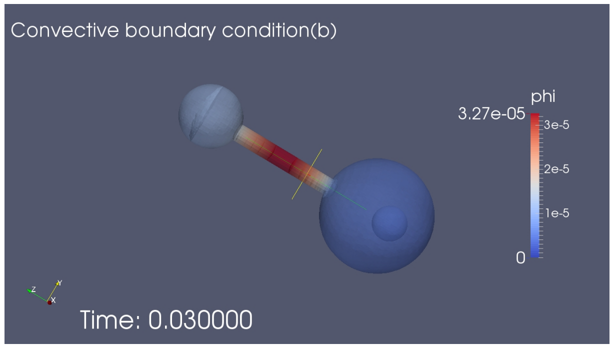

Figure 2.22: The case of Convective boundary condition (b) at t=0.03

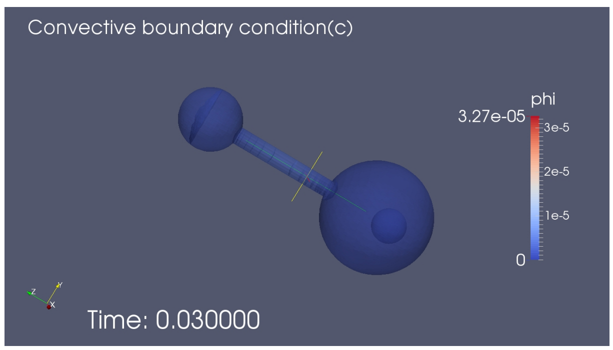

Figure 2.23: The case of Convective boundary condition (c) at t=0.03

it is traveling. It is negative when the medium is being expanded by the sound wave.

First, we aim to find the transient sound pressure waveforms [36] at a receiving point (0.0247773, 0.819853, -3.16938), which is located at the right end of the larger ball. The waveforms for each type of boundary conditions can be found in Figures 2.24-2.28.

Remark 2. *We can observe that the waveforms match with the patterns in the simulation results.*

1. All the waves are aperiodic (not periodic).

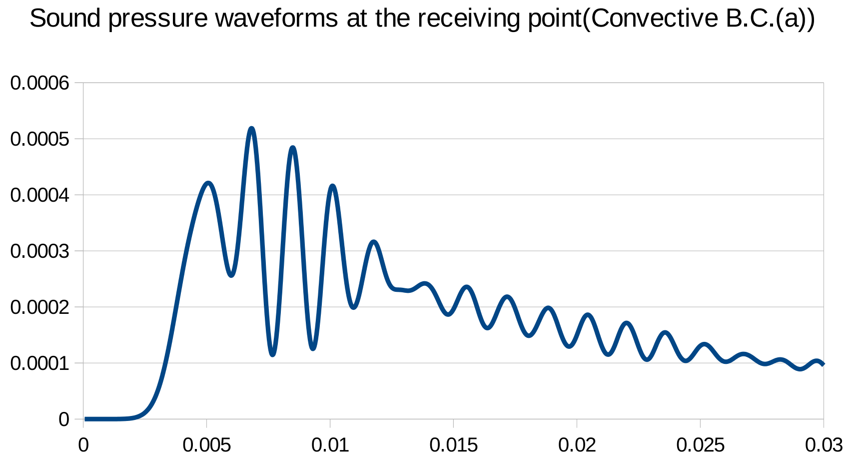

Figure 2.24: The waveform for the case of Convective B.C. (a)

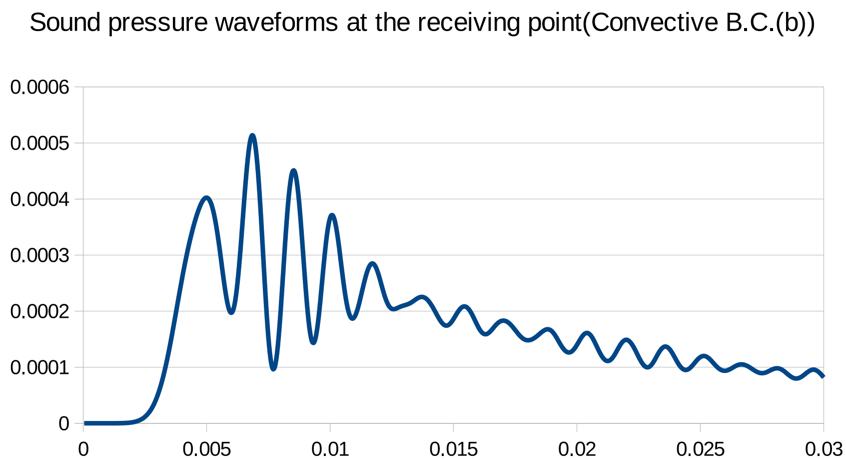

Figure 2.25: The waveform for the case of Convective B.C. (b)

2. All starting points are 0, which is the initial condition.

3. In each case under the convective B.C., the sound pressure is positive, since the sound wave is compressing the air. Moreover, the three cases under the convective B.C. have quite similar graphs, only a small difference on the value of each point.

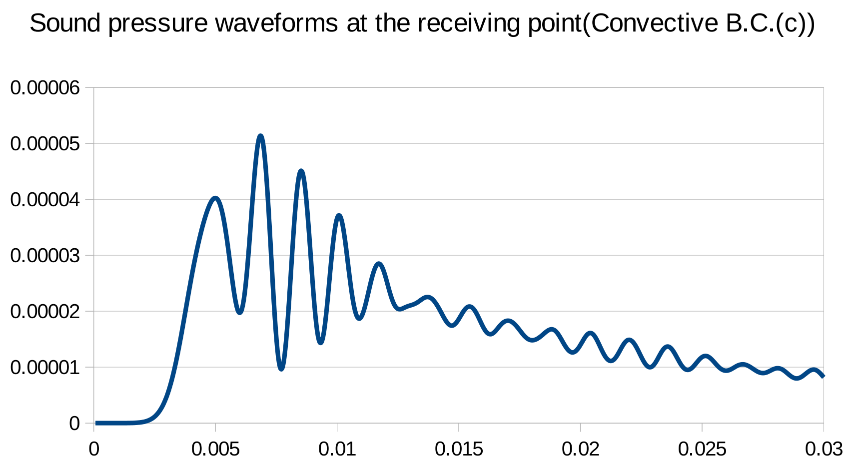

Figure 2.26: The waveform for the case of Convective B.C. (c)

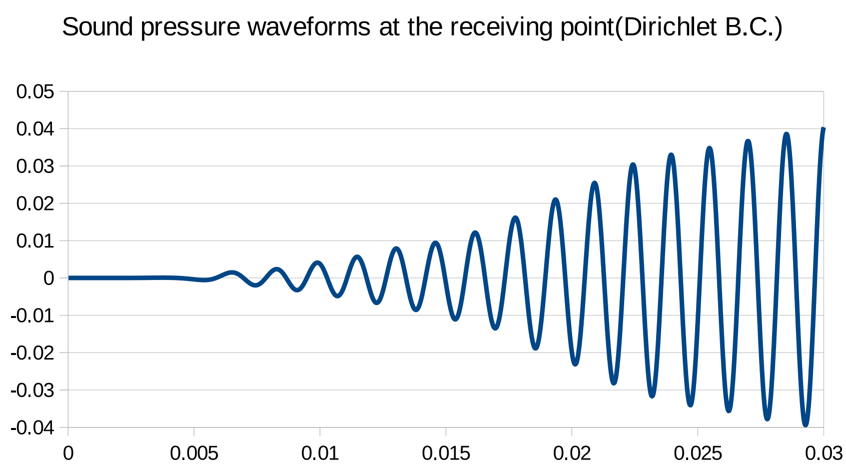

Figure 2.27: The waveform for the case of Dirichlet B.C.

4. In the case under the Dirichlet boundary condition, the graphics looks well-regulated. The amplitude grows linearly in time. For the Dirichlet boundary condition, the total energy is conserved.

In many applications, it is important to identify the spectral content of the signal.

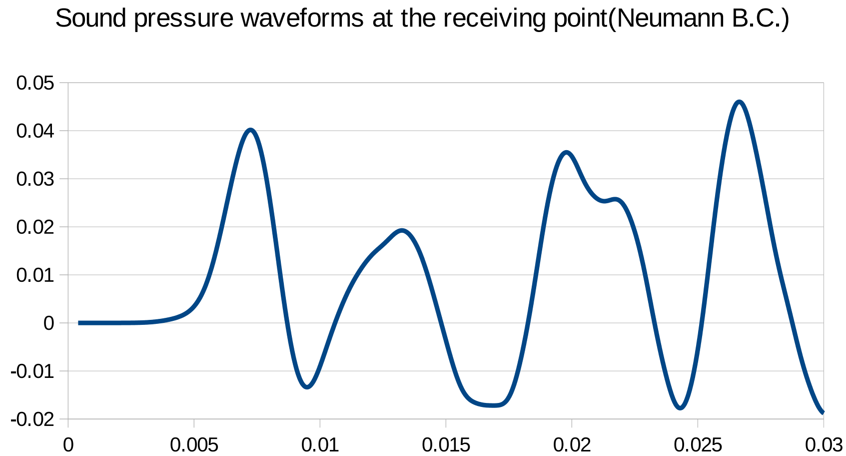

Figure 2.28: The waveform for the case of Neumann B.C.

Notice that the time waveforms in Figures 2.24-2.28 do not provide information about the spectral content of the signal [7]. To determine the frequency characteristics of the signal, we need to find a method to estimate the spectral content of it. One possible technique is to apply the Fast Fourier Transform (FFT) to the signal, and convert the time waveform into a frequency spectrum.

The Fourier transform can convert time domain waveform data into the frequency domain data [7]. Here is how it works: the transform breaks down the original time-based waveform into a series of sinusoidal terms; each of these sinusoidal terms has a unique frequency, magnitude, and phase [7]. This process successfully converts a waveform in the time domain into a series of sinusoidal functions which are easier to be described mathematically.

Using the FFT to transform a time domain signal to the frequency domain representation of the signal enables us to discover information that might be hidden in the time-domain waveform. For example, the square of the magnitude of the FFT is called the *power spectrum*, which characterizes how the energy of a signal is distributed in the frequency domain [7]. The power spectrum of a sound signal can show the relative intensity of the energy of a signal at each frequency for the entire signal. Details about the FFT algorithm can find in [7].

By using the fft function in Matlab, we can find the Single-Sided Amplitude Spectrum of each case in Figures 2.24-2.28. See Figures 2.29-2.33.

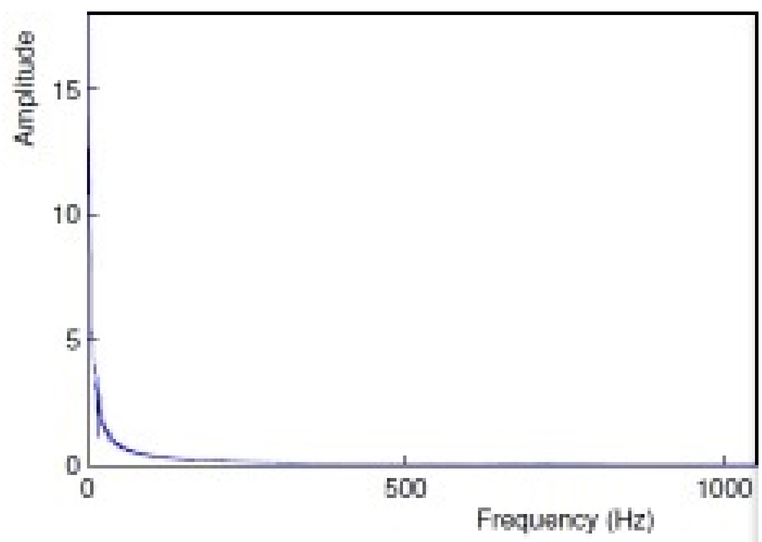

Figure 2.29: The Single-Sided Amplitude Spectrum for the case of Convective B.C. (a)

Remark 3. *The zero amplitude is meaningless.*

2.3.2 Propeller Case

(a) Background

Contra-rotating is a technique whereby parts of a mechanism rotate in opposite directions about a common axis. It is found (in certain cases) to be effective in producing a large torque, for example, aircraft propellers. Compared with Contra-rotating, Iso-rotating is another terminology, which means rotating in the same di-

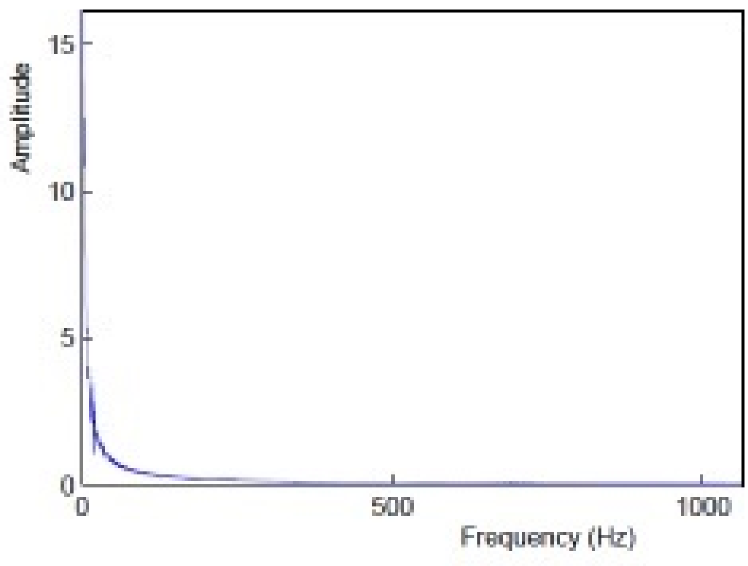

Figure 2.30: The Single-Sided Amplitude Spectrum for the case of Convective B.C. (b)

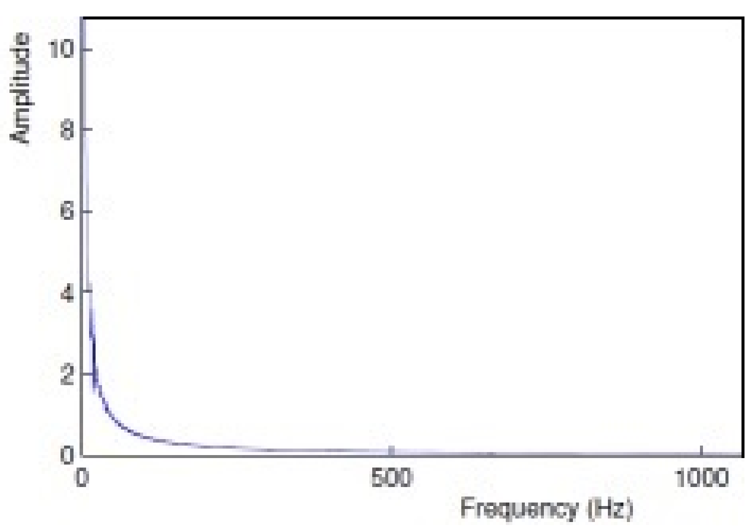

Figure 2.31: The Single-Sided Amplitude Spectrum for the case of Convective B.C. (c)

rection. Contra-rotating propellers are widely used in the marine transportation systems, in particular for large speed boats.

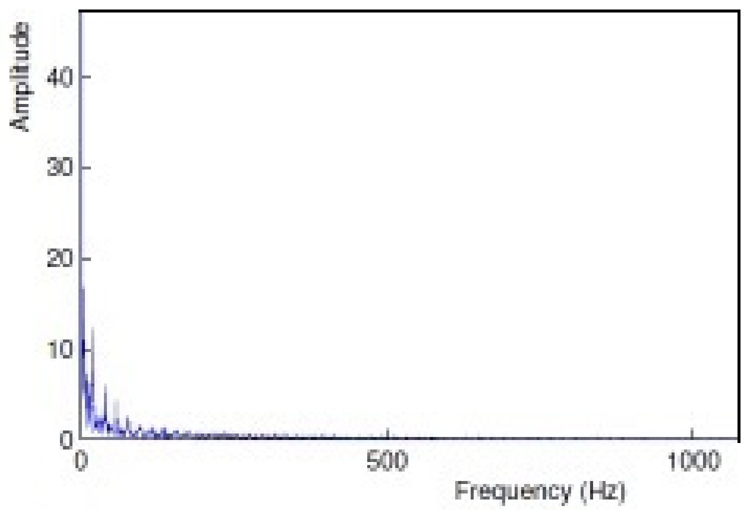

Figure 2.32: The Single-Sided Amplitude Spectrum for the case of Dirichlet B.C.

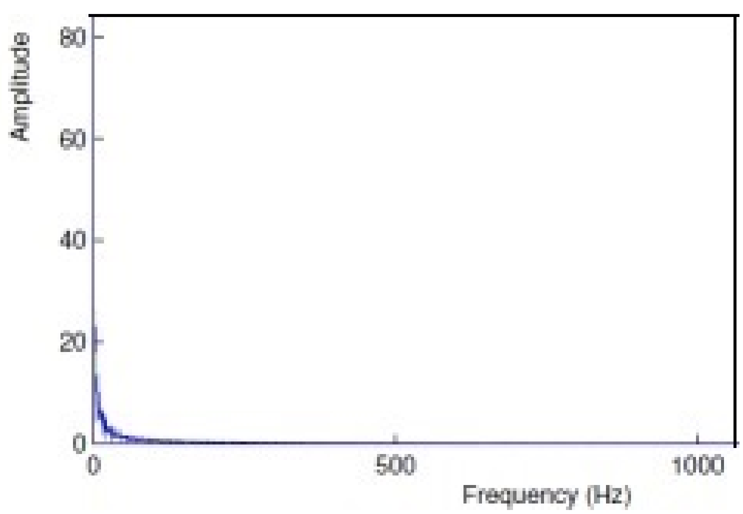

Figure 2.33: The Single-Sided Amplitude Spectrum for the case of Neumann B.C.

Contra-rotating propellers have also been used in Torpedoes to give the maximum possible speed within a limited diameter, and to counteract the torque that would tend to cause the torpedo to rotate around its own longitudinal axis [38]. The definitions of thrust and torque are explained below.

Thrust is a force that is described quantitatively by the Newton's second and third laws. When a system expels or accelerates the mass in one direction, the expelled mass will cause a force of equal magnitude in the opposite direction [3]. Thrust is the force applied to a surface in a direction perpendicular or normal to the surface.

Torque is the tendency of a force to rotate an object about an axis or pivot [29]. In other words, it measures how much a force acting on an object causes the object to rotate.

(b) Numerical simulations

In order to study the *thrust* and *torque* in the Contra-rotating propellers and Iso-rotating propellers, we implement some numerical simulations in OpenFOAM.

We choose the solver called "interPhaseChangeDyMFoam". It is a solver for incompressible fluids with phase-change. Our study is based on the "Propeller" case in the OpenFOAM tutorial. First, we change the geometry object by using surfaceTransformPoints. Then, we add a propeller into the domain of the blockMesh. We also need to modify the snappyHexMesh and all other files. A technique called "AMI" (arbitrary mesh interface) is applied in our case. It enables simulation across disconnected and adjacent mesh domains. AMI is particularly useful for rotating geometries. The RANS (Reynolds-Averaged Navier-Stokes) turbulence model is used in this case. The time step here is $6 * 10^{-5}$s.

We have run two cases:

(i) Iso-rotating:

both propellers have the same angular velocity: 419 rad/s.

(ii) Contra-rotating:

two propellers have the angular velocity: 419 rad/s and -419 rad/s, respectively.

Some video simulations can be watched:

https://www.dropbox.com/s/tpp9jl2jj4gjwvd/4.ogv?n=173504581.

Graph result can be find in Figure. 2.34.

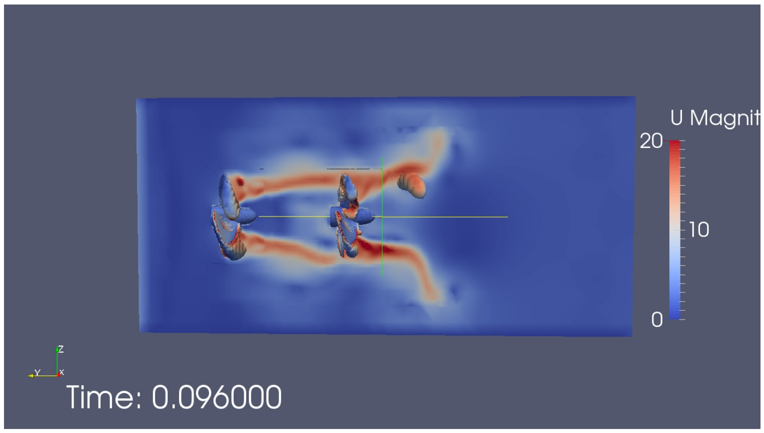

Figure 2.34: Iso-rotating case

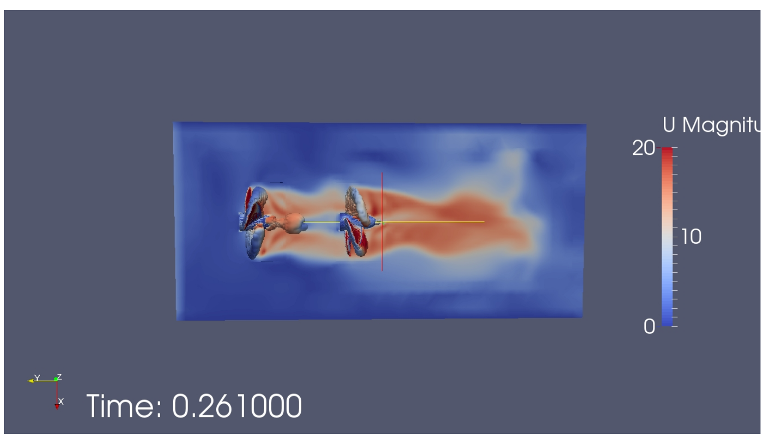

Figure 2.35: Contra-rotating case

We also have another experiment to compare three cases: a single propeller (with angular velocity 158 rad/s), two propeller rotate in the same direction (propellerTip has radial-velocity 9000 deg/s, propellerTip1 has radial-velocity 10000 deg/s), two Contra-rotating propellers (propellerTip has radial-velocity 9000 deg/s, propeller-Tip1 has radial-velocity -12000 deg/s). See Figures 2.36-2.39.

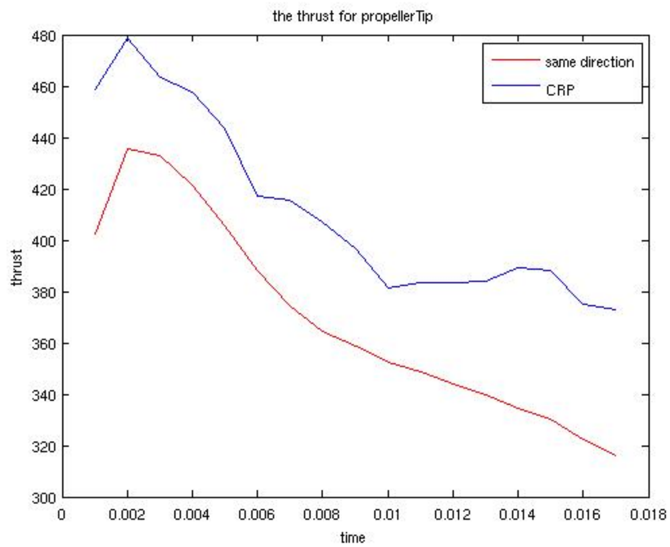

Figure 2.36: Thrust for propellerTip

2.4 Summary

In this section, using a CFD software "OpenFOAM" as our platform, we mainly study the chaotic vibration phenomenon of a 2D wave equation. Several simulations are obtained. There are also two other projects included in this section. The first one is the comparison of different types of boundary conditions in a 3D wave equation, while the second one is the comparison of Contra-rotating propellers and Iso-rotating propellers.

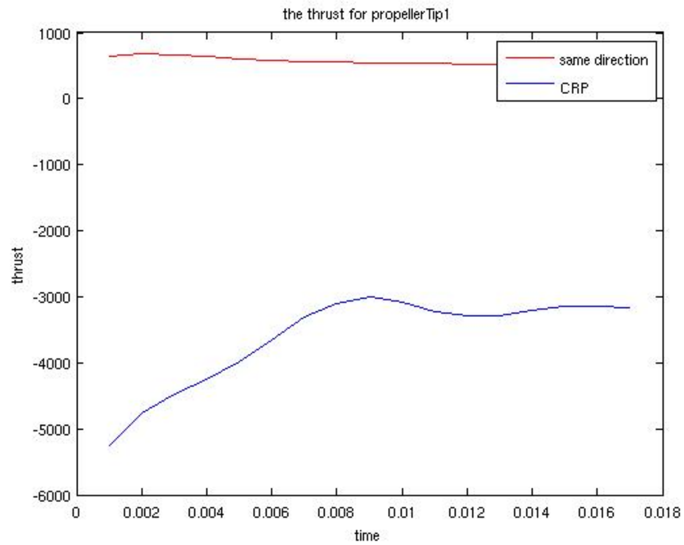

Figure 2.37: Thrust for propellerTip1

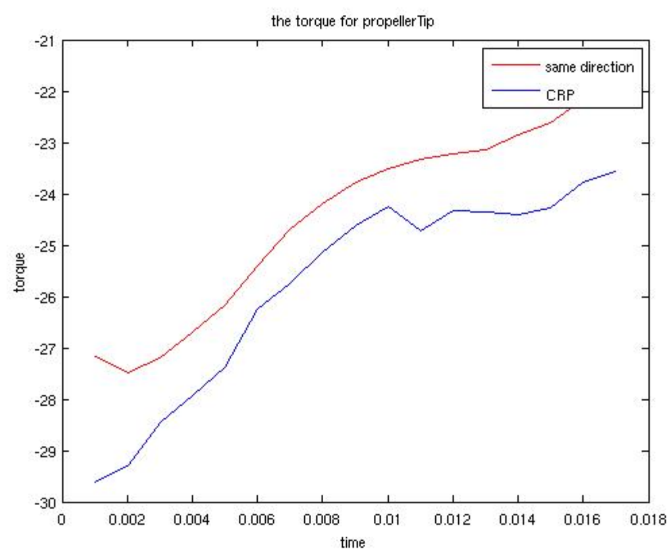

Figure 2.38: Torque for propellerTip

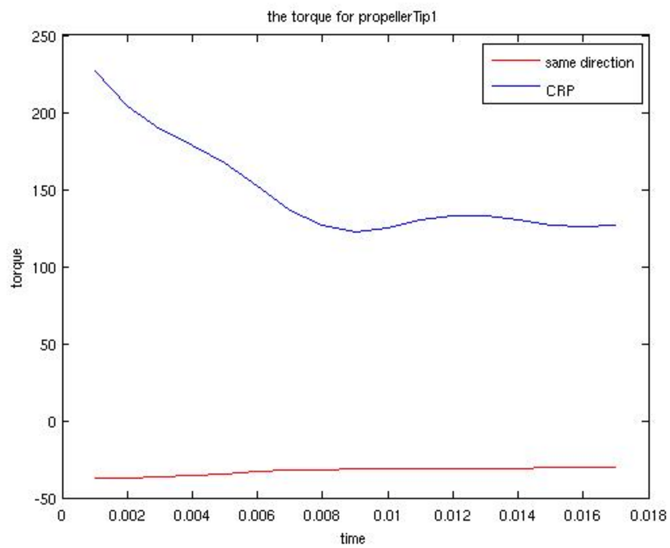

Figure 2.39: Torque for propellerTIp1

3. CHAOTIC VIBRATION PHENOMENON OF A 2D NON-STRICTLY HYPERBOLIC EQUATION *

In the previous section, we studied the chaotic vibration phenomenon of a 2D wave equation through numerical simulations. In this section, we will explore a theoretical study regarding the chaotic vibration phenomenon of a 2D non-strictly hyperbolic equation.

First, we recall several basic definitions (most of these definitions are cited from Wikipedia):

(1). *Jordan Curve*: a non-self-intersecting continuous loop, also been called *simple closed curve.*

(2). *Riemann Invariants*: mathematical transformations that make the equations more easily solvable. The Riemann invariants are constant along the characteristic curves of the equations.

(3). *Transport Equation*: a partial differential equation (PDE) of the form $u_t + cu_x = 0$.

(4). *Directional Derivative*: the directional derivative of function f in the direction $\overrightarrow{l}$ is

$$\nabla_{\overrightarrow{l}} f = \nabla f \cdot \frac{\overrightarrow{l}}{|\overrightarrow{l}|}.$$

(5). *Topological Conjugacy*: two functions are said to be topologically conjugate if there exists a homeomorphism that will conjugate one into the other.

(6). *Dynamical Systems*: systems in which a function describes the time dependence of a point in a geometrical space.

*Part of this section is reprinted from "Chaotic vibration of a 2D non-strictly hyperbolic equation" by G. Chen, L. Li and J. Tian, a paper in preparation [11].

(7). *Bifurcation*: a phenomenon that occurs when a small smooth change made to the parameter values causes a sudden "qualitative" or topological change in its behavior [5].

(8). *Period Doubling Bifurcation*: a bifurcation in which a small change in a parameter value leads to the system switching to a new behavior with twice the period of the original system [26].

(9). *Total Variation*: for a function g defined on a closed subset E of $\mathbb{R}$, the total variation $V_S(g)$ is defined as

$$V_E(g) = sup_{P(E)}\{\sum_{k=1}^{N} |g(x_k) - g(x_{k-1})|\},$$

where $P(E)$ represents a partition $x_0 < x_1 < \cdots < x_N$ of E.

An important tool we use in our work is the *method of characteristics.* So, we give a brief introduction about this tool:

Method of characteristics is a technique used to solve PDEs. It can reduce a PDE to a family of ordinary differential equations (ODEs) along which the solution can be integrated from some initial data. The curve along which the PDE becomes ODE is called *characteristic curves* or *characteristics.*

Also recall from [18] that the following partial differential equation

$$w_{tt} - \sum_{i,j}^{1,n} a_{i,j}(t) w_{x_i x_j} = 0, \tag{3.1}$$

under the *non-strict hyperbolicity* condition

$$\forall \xi \in \mathbb{R}^n,\ \sum_{i,j}^{1,n} a_{i,j}(t)\xi_i\xi_j \geq 0. \tag{3.2}$$

has been widely studied in literature. The well-posedness of the Cauchy problem of equation (3.1) is considered in many papers [18, 19]. In this section, we will study the chaotic vibration phenomenon of system (3.1) on a compact set $\Gamma \subseteq \mathbb{R}^n$ with $n \geq 2$. In [18, 19], they did not include any boundary conditions. When time-dependent boundary conditions are included in (3.1), analysis for well-posedness becomes much more complicated. However, if we consider the equation

$$w_{tt} - \Delta w - 2w_{xy} = 0, \tag{3.3}$$

we are able to apply the *method of characteristics* to analyze the chaotic behavior.

Starting from the case $n = 2$, let $\Gamma \subseteq \mathbb{R}^2$ and $\partial\Gamma$ be a *Jordan curve*. Assume $\partial\Gamma = \Gamma_1 \cup \Gamma_2 \cup \Gamma_3 \cup \Gamma_4$, where Γ_2 and Γ_4 are two directed lines with the direction $\overrightarrow{l} = (1, 1)$. Moreover, we assume that for any points $A \in \Gamma_1$ and $B \in \Gamma_3$, the segment AB belongs to Γ.

For simplicity, let $\Gamma \subseteq \mathbb{R}^2$ be given by

$$\mathring{\Gamma} = \{(x, y) \in \mathbb{R}^2 \mid -1 < x + y < 1,\ -1 < x - y < 1\}, \tag{3.4}$$

and $\partial\Gamma = \Gamma_1 \cup \Gamma_2 \cup \Gamma_3 \cup \Gamma_4$, where

$$\begin{aligned} \Gamma_1 =& \{(x, y) \in \Gamma \mid x + y = -1\}, \quad \Gamma_2 = \{(x, y) \in \Gamma \mid x - y = -1\}, \\ \Gamma_3 =& \{(x, y) \in \Gamma \mid x + y = 1\}, \quad \Gamma_4 = \{(x, y) \in \Gamma \mid x - y = 1\}. \end{aligned} \tag{3.5}$$

See Fig. 3.1.

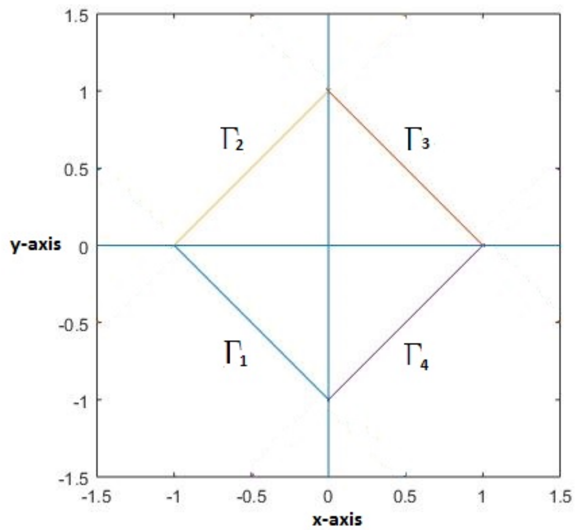

Figure 3.1: The domain Γ.

On the boundary Γ_1, we have a linear boundary condition

$$w_t(t,x,y) = -\eta \left(w_x(t,x,y) + w_y(t,x,y) \right), \ (x,y) \in \Gamma_1, \ t > 0, \ 0 < \eta \neq 1. \tag{3.6}$$

When $(x, y) \in \Gamma_3$, we have a nonlinear boundary condition

$$w_t(t,x,y) = \alpha \left(w_x(t,x,y) + w_y(t,x,y) \right) - \beta \left(w_x(t,x,y) + w_y(t,x,y) \right)^3, \quad t > 0, \tag{3.7}$$

where

$$0 < \alpha < 1, \qquad \beta > 0. \tag{3.8}$$

On Γ_2 and Γ_4, we have the Dirichlet boundary conditions:

$$w(t,x,y)=0,\ (x,y)\in\Gamma_2\cup\Gamma_4,\ t>0.$$

So, the system we study here is:

$$\begin{cases} w_{tt}=\Delta w+2w_{xy}, \quad (x,y)\in\mathring{\Gamma},\ t>0, \\ w_t=-\eta\left(w_x+w_y\right),\ (x,y)\in\Gamma_1,\ t>0, \\ w_t=\alpha(w_x+w_y)-\beta(w_x+w_y)^3,\ (x,y)\in\Gamma_3,\ t>0, \\ w(t,x,y)=0,\ (x,y)\in\Gamma_2\cup\Gamma_4,\ t>0, \\ w(0,x,y)=w_0(x,y),\ w_t(0,x,y)=w_1(x,y),\ (x,y)\in\Gamma, \end{cases} \tag{3.9}$$

where $0<\eta\neq 1, 0<\alpha<1, \beta>0$ and the initial conditions w_0 and w_1 satisfy

$$w_0\in C^2(\Gamma), \qquad w_1\in C^2(\Gamma). \tag{3.10}$$

and

$$\begin{aligned} &w_0(x,y)=w_1(x,y)=0,\ (x,y)\in\Gamma_2\cup\Gamma_4; \\ &w_1(x,y)=-\eta\left(\frac{\partial w_0}{\partial x}+\frac{\partial w_0}{\partial y}\right),\ (x,y)\in\Gamma_1; \\ &w_t=\alpha(\frac{\partial w_0}{\partial x}+\frac{\partial w_0}{\partial y})-\beta(\frac{\partial w_0}{\partial x}+\frac{\partial w_0}{\partial y})^3,\ (x,y)\in\Gamma_3. \end{aligned}$$

Remark 4. *When $\eta=1$, the system is not well-posed [33].*

At time $t>0$, the energy of the system (3.9) is

$$E(t)=\frac{1}{2}\int_\Gamma w_t^2+(w_x+w_y)^2dS. \tag{3.11}$$

Theorem 1. *Consider the system* (3.9) *and the energy functional*

$$\forall t > 0, \quad E(t) = \frac{1}{2}\int_{\Gamma} w_t^2 + (w_x + w_y)^2 dS \tag{3.12}$$

Then the derivative of the energy functional has the form below

$$\begin{gathered}\forall t > 0, \quad E'(t) = \sqrt{2}\eta \int_{\Gamma_1} (w_x + w_y)^2 d\sigma \\ +\sqrt{2}\int_{\Gamma_3} (w_x + w_y)^2 \left(\alpha - \beta(w_x + w_y)^2\right) d\sigma.\end{gathered} \tag{3.13}$$

Proof. Let w be up to C^2. Consider the vector field as follow

$$\mathbb{H} = (w_x + w_y, w_x + w_y), \tag{3.14}$$

and then

$$div\,(\mathbb{H}) = \Delta w + 2w_{xy}. \tag{3.15}$$

For $t > 0$, we have

$$\begin{aligned}E'(t) &= \int_{\Gamma} w_t w_{tt} + (w_{xt} + w_{yt})(w_x + w_y) dS \\ &= \int_{\Gamma} w_t div\,(\mathbb{H}) + \mathbb{H} \cdot \triangledown w_t dS.\end{aligned} \tag{3.16}$$

Since

$$div\,(w_t\mathbb{H}) = w_t div\,(\mathbb{H}) + \mathbb{H} \cdot \triangledown w_t. \tag{3.17}$$

Applying the Green's formula, we have

$$
\begin{aligned}
E'(t) &= \int_{\Gamma} w_t div\,(\mathbb{H}) + \mathbb{H}\cdot\bigtriangledown w_t dS \\
&= \int_{\Gamma} div\,(w_t\mathbb{H})\,dS \\
&= \int_{\partial\Gamma} (w_t\mathbb{H}\cdot\vec{n})\,d\sigma.
\end{aligned}
\tag{3.18}
$$

Notice that $\mathbb{H}\cdot\vec{n}=0$ on the boundaries $\partial\Gamma\setminus(\Gamma_1\cup\Gamma_3)$. By applying the boundary conditions on Γ_1 and Γ_3, respectively, we have

$$
\forall t>0,\quad E'(t)=\sqrt{2}\eta\int_{\Gamma_1}(w_x+w_y)^2 d\sigma+\sqrt{2}\int_{\Gamma_3}(w_x+w_y)^2\left(\alpha-\beta(w_x+w_y)^2\right)d\sigma.
\tag{3.19}
$$

□

Remark 5. *From the above theorem, we can find: if* $\eta>0$*, energy is injected to the system from* Γ_1*. For this reason, we refer to* (3.6) *as an energy injecting boundary condition. Notice that the nonlinearities are distributed on entire* Γ_3*, and the sign of the second term of the RHS of* (3.19) *is dependent of the integral, we may call* (3.7) *a distributed self-excited boundary condition.*

In this section, we will study the chaotic vibration phenomenon of system (3.9).

3.1 Preliminary Analysis

Recall we have the system:

$$
\begin{cases}
w_{tt} = \Delta w + 2w_{xy}, \quad (x,y) \in \mathring{\Gamma}, \ t > 0, \\
w_t = -\eta \left(w_x + w_y \right), \ (x,y) \in \Gamma_1, \ t > 0, \\
w_t = \alpha(w_x + w_y) - \beta(w_x + w_y)^3, \ (x,y) \in \Gamma_3, \ t > 0, \\
w(t,x,y) = 0, \ (x,y) \in \Gamma_2 \cup \Gamma_4, \ t > 0, \\
w(0,x,y) = w_0(x,y) \in C^2(\Gamma), \ w_t(0,x,y) = w_1(x,y) \in C^2(\Gamma).
\end{cases}
\tag{3.20}
$$

where

$$0 < \eta \neq 1, \quad 0 < \alpha < 1, \quad \beta > 0. \tag{3.21}$$

Remark 6. *In the first equation of (3.20), $2w_{xy}$ can be replaced by $-2w_{xy}$.*

Define two linear operators:

$$\mathcal{L}_1 = \frac{\partial}{\partial t} + \frac{\partial}{\partial x} + \frac{\partial}{\partial y}, \quad \mathcal{L}_2 = \frac{\partial}{\partial t} - \frac{\partial}{\partial x} - \frac{\partial}{\partial y}. \tag{3.22}$$

If w is a C^2 function, we have

$$\mathcal{L}_2(w) = w_t - w_x - w_y, \quad \mathcal{L}_1\mathcal{L}_2(w) = w_{tt} - w_{xx} - w_{yy} - 2w_{xy} = 0.$$

Similarly, we have $\mathcal{L}_2\mathcal{L}_1(w) = 0$.

Therefore, we can rewrite the first equation of system (3.20) as

$$\mathcal{L}_1\mathcal{L}_2(w) = \mathcal{L}_2\mathcal{L}_1(w) = 0. \tag{3.23}$$

Let u and v be the Riemann invariants of (3.20) defined by

$$\begin{aligned} u =& \frac{1}{2}\mathcal{L}_1(w) = \frac{w_t + w_x + w_y}{2}, \\ v =& \frac{1}{2}\mathcal{L}_2(w) = \frac{w_t - w_x - w_y}{2}. \end{aligned} \tag{3.24}$$

$\Rightarrow$

$$w_x + w_y = u - v; \quad w_t = u + v.$$

So, the first equation of system (3.20) can be written as

$$\mathcal{L}_2 u = 0,$$

or,

$$\mathcal{L}_1 v = 0.$$

For $t > 0$, the boundary condition on Γ_1 can be represented as a reflection relation between u and v:

$$v(t,x,y) = \frac{\eta+1}{\eta-1}u(t,x,y) := G_\eta\left(u(t,x,y)\right), \quad (x,y) \in \Gamma_1. \tag{3.25}$$

Moreover, the nonlinear condition on Γ_3 is equivalent to the relation of u and v:

$$\beta\left(u(t,x,y) - v(t,x,y)\right)^3 + (1-\alpha)\left(u(t,x,y) - v(t,x,y)\right) + 2v(t,x,y) = 0, \; (x,y) \in \Gamma_3. \tag{3.26}$$

Since $\alpha < 1$ and $\beta > 0$, let $f = u(t,x,y) - v(t,x,y)$, then $f = p(v)$ satisfies the cubic equation

$$\beta f^3 + (1-\alpha)f + 2v = 0. \tag{3.27}$$

Remark 7. *Since we have $\beta > 0$ and $0 < \alpha < 1$, the real solution f is uniquely* *defined by Cardano's formula [33]*

$$f = \big(-\frac{v}{\beta} + \sqrt{D}\big)^{1/3} + \big(-\frac{v}{\beta} - \sqrt{D}\big)^{1/3}, \tag{3.28}$$

where

$$D = \frac{(1-\alpha)^3}{27\beta^3} + \frac{v^2}{\beta^2} > 0.$$

Therefore, the reflection relation between u and v on Γ_3 has the form:

$$u(t,x,y) = v(t,x,y) + p(v(t,x,y)) := F_{\alpha,\beta}(v(t,x,y)), \quad (x,y) \in \Gamma_3. \tag{3.29}$$

On $\Gamma_2 \cup \Gamma_4$, we have

$$w_t = 0, \;\; w_x + w_y = 0.$$

$\Rightarrow$

$$u(t,x,y) = v(t,x,y) = 0, \;\; (x,y) \in \Gamma_2 \cup \Gamma_4, \;\; t > 0.$$

Consequently, for given smooth initial conditions $w_0 \in C^2(\Gamma)$ and $w_1 \in C^2(\Gamma)$, the system (3.20) is equivalent to a system of two coupled first order equations below:

$$\begin{cases} \mathcal{L}_1(v) = \mathcal{L}_2(u) = 0, \quad (x,y) \in \mathring{\Gamma}, \;\; t > 0, \\ v(t,x,y) = G_\eta(u(t,x,y)), \;\; (x,y) \in \Gamma_1, \;\; t > 0, \\ u(t,x,y) = F_{\alpha,\beta}(v(t,x,y)), \;\; (x,y) \in \Gamma_3, \;\; t > 0, \\ u(t,x,y) = v(t,x,y) = 0, \;\; (x,y) \in \Gamma_2 \cup \Gamma_4, \;\; t > 0, \\ u(0,x,y) = u_0(x,y) \in C^1(\Gamma), \;\; v(0,x,y) = v_0(x,y) \in C^1(\Gamma), \end{cases} \tag{3.30}$$

where the initial conditions u_0 and v_0 are now in the form of

$$u_0 = \frac{w_1 + \frac{\partial w_0}{\partial x} + \frac{\partial w_0}{\partial y}}{2}, \quad v_0 = \frac{w_1 - \frac{\partial w_0}{\partial x} - \frac{\partial w_0}{\partial y}}{2}. \tag{3.31}$$

In order to ensure u and v are C^1 functions, we need u_0 and v_0 to be in C^1, and also satisfy some compatible conditions below:

(1)

$$
\begin{aligned}
&\forall(\tilde{x},\tilde{y}) \in \Gamma_1, \quad v_0(\tilde{x},\tilde{y}) = G_\eta(u_0(\tilde{x},\tilde{y})),\\
&\forall(\tilde{x},\tilde{y}) \in \Gamma_3, \quad u_0(\tilde{x},\tilde{y}) = F_{\alpha,\beta}(v_0(\tilde{x},\tilde{y})),\\
&\forall(\tilde{x},\tilde{y}) \in \Gamma_2 \cup \Gamma_4, \ u_0(\tilde{x},\tilde{y}) = v_0(\tilde{x},\tilde{y}) = 0.
\end{aligned}
$$

(2)

$$\forall(\tilde{x},\tilde{y}) \in \Gamma_1, \forall \overrightarrow{v} \in \mathbb{R}^2, \quad \nabla_{\overrightarrow{v}} v_0(x,y)|_{(\tilde{x},\tilde{y})} = \nabla_{\overrightarrow{v}} G_\eta(u_0(x,y))|_{(\tilde{x},\tilde{y})}, \tag{3.32}$$

and

$$\forall(\tilde{x},\tilde{y}) \in \Gamma_1, \forall \overrightarrow{v} \in \mathbb{R}^2, \quad \nabla_{\overrightarrow{v}} u_0(x,y)|_{(\tilde{x},\tilde{y})} = \nabla_{\overrightarrow{v}} F_{\alpha,\beta}(v_0(x,y))|_{(\tilde{x},\tilde{y})}. \tag{3.33}$$

Remark 8. *Note that the two boundary conditions in (3.30) are "reflected" boundary conditions that result in wave reflection on the boundaries.*

Therefore, proving the well-posedness of the main system (3.20) is equivalent to prove the well-posedness of system (3.30). From now on, we will focus on system (3.30).

Lemma 1. *Let u and v be given by* (3.24)*. Then, u keeps constant along the direction $\overrightarrow{l_1}$ and v keeps constant along the direction $\overrightarrow{l_2}$, where*

$$\overrightarrow{l_1} = (1,-1,-1), \quad \overrightarrow{l_2} = (1,1,1). \tag{3.34}$$

Proof. It follows from the fact

$$\nabla_{\overrightarrow{l_1}} u = \left(\frac{\partial}{\partial t} - \frac{\partial}{\partial x} - \frac{\partial}{\partial y}\right) u = \mathcal{L}_2 u = 0. \tag{3.35}$$

Similarly, we have $\nabla_{\overrightarrow{l_1}} v = 0$. $\square$

Next, we show the existence of solutions of system (3.30) on the set $[0,2] \times \Gamma$.

Lemma 2. *Let $t \in [0,2]$ and $(x,y) \in \Gamma$, i.e., $-1 \le x+y \le 1$ and $-1 \le x-y \le 1$. Then, $u(t,x,y)$ and $v(t,x,y)$ can be uniquely solved.*

Proof. First, recall that

$$\Gamma_1 : x+y=-1; \text{and when } (x,y) \in \Gamma_1, v = G_\eta(u(t,x,y)).$$

$$\Gamma_3 : x+y=1; \text{and when } (x,y) \in \Gamma_3, u = F_{\alpha,\beta}(v(t,x,y)).$$

Notice that the points (t,x,y) and $(0, x+t, y+t)$ are in the same characteristics along $\overrightarrow{l_1}$, by applying Lemma 1, we have

$$\begin{aligned} u(t,x,y) &= u(0,x+t,y+t) \\ &= u_0(x+t,y+t), \quad t \le \frac{1-x-y}{2}. \end{aligned} \tag{3.36}$$

When $\frac{1-x-y}{2} < t \le \frac{1-x-y}{2} + 1$, we have

$$\left(x + \frac{1-x-y}{2}, y + \frac{1-x-y}{2}\right) \in \Gamma_3. \tag{3.37}$$

Also, (t,x,y) and $\left(t - \frac{1-x-y}{2}, x + \frac{1-x-y}{2}, y + \frac{1-x-y}{2}\right)$ are in the same characteristics along $\overrightarrow{l_1}$. $(t - \frac{1-x-y}{2}, x + \frac{1-x-y}{2}, y + \frac{1-x-y}{2})$ and $(0, 1-y-t, 1-x-t)$ are in the same characteristics along $\overrightarrow{l_2}$. By applying reflection (3.29) and Lemma 1, we have

$$
\begin{aligned}
u(t,x,y) =& u\left(t-\frac{1-x-y}{2}, x+\frac{1-x-y}{2}, y+\frac{1-x-y}{2}\right)\\
=& F_{\alpha,\beta}\left(v\left(t-\frac{1-x-y}{2}, x+\frac{1-x-y}{2}, y+\frac{1-x-y}{2}\right)\right)\\
=& F_{\alpha,\beta}\left(v\left(0, 1-y-t, 1-x-t\right)\right)\\
=& F_{\alpha,\beta}\left(v_0\left(1-y-t, 1-x-t\right)\right).
\end{aligned}
\tag{3.38}
$$

When $\frac{1-x-y}{2}+1<t\leq 2$, notice that

$$
\begin{aligned}
&\left(x+\frac{1-x-y}{2}-1, y+\frac{1-x-y}{2}-1\right)\in\Gamma_1,\\
&\left(x+\frac{1-x-y}{2}, y+\frac{1-x-y}{2}\right)\in\Gamma_3,
\end{aligned}
\tag{3.39}
$$

from the reflections (3.25), (3.29) and Lemma 1, we have

$$
\begin{aligned}
u(t,x,y) =& u\left(t-\frac{1-x-y}{2}, x+\frac{1-x-y}{2}, y+\frac{1-x-y}{2}\right)\\
=& F_{\alpha,\beta}\left(v\left(t-\frac{1-x-y}{2}, x+\frac{1-x-y}{2}, y+\frac{1-x-y}{2}\right)\right)\\
=& F_{\alpha,\beta}\left(v\left(t-\frac{1-x-y}{2}-1, x+\frac{1-x-y}{2}-1, y+\frac{1-x-y}{2}-1\right)\right)\\
=& F_{\alpha,\beta}\circ G_\eta\left(u\left(t-\frac{1-x-y}{2}-1, x+\frac{1-x-y}{2}-1, y+\frac{1-x-y}{2}-1\right)\right)\\
=& F_{\alpha,\beta}\circ G_\eta\left(u\left(0, x+t-2, y+t-2\right)\right)\\
=& F_{\alpha,\beta}\circ G_\eta\left(u_0\left(x+t-2, y+t-2\right)\right).
\end{aligned}
\tag{3.40}
$$

So u can be solved as:

$$u(t,x,y)=\begin{cases} u_0(x+t,y+t),\ 0\le t\le \frac{1-x-y}{2}, \\ F_{\alpha,\beta}\left(v_0(1-y-t,1-x-t)\right),\ \frac{1-x-y}{2}<t\le\frac{1-x-y}{2}+1, \\ F_{\alpha,\beta}\circ G_\eta\left(u_0(x+t-2,y+t-2)\right)\ \frac{1-x-y}{2}+1<t\le 2. \end{cases}$$

Similarly, v can be solved as:

$$v(t,x,y)=\begin{cases} v_0(x-t,y-t),\ 0\le t\le \frac{x+y+1}{2}, \\ G_\eta\left(u_0(t-y-1,t-x-1)\right),\ \frac{x+y+1}{2}<t\le\frac{x+y+1}{2}+1, \\ G_\eta\circ F_{\alpha,\beta}\left(v_0(x+2-t,y+2-t)\right)\ \frac{x+y+1}{2}+1<t\le 2. \end{cases}$$

For the uniqueness, suppose there is another pair of solution (u',v'), we set $(p,q)=(u'-u,v'-v)$. Then (p,q) will satisfy (3.30) with zero initial conditions. From the explicit solution formulas we obtained above, we have $(p,q)=(0,0)$. So the solution is unique. □

Lemma 3. *For $t\ge 0$ and $(x,y)\in\Gamma$, we have $u(t+2,x,y)=F_{\alpha,\beta}\circ G_\eta\left(u(t,x,y)\right),\ v(t+2,x,y)=G_\eta\circ F_{\alpha,\beta}\left(v(t,x,y)\right)$.*

Proof.

$$\begin{aligned} u(t+2,x,y)=&u\left(t+2-\frac{1-x-y}{2},x+\frac{1-x-y}{2},y+\frac{1-x-y}{2}\right)\\ =&F_{\alpha,\beta}\left(v\left(t+2-\frac{1-x-y}{2},x+\frac{1-x-y}{2},y+\frac{1-x-y}{2}\right)\right)\\ =&F\left(v\left(t+2-\frac{1-x-y}{2}-1,x+\frac{1-x-y}{2}-1,y+\frac{1-x-y}{2}-1\right)\right)\\ =&F\circ G_\eta\left(u\left(t+1-\frac{1-x-y}{2},x+\frac{1-x-y}{2}-1,y+\frac{1-x-y}{2}-1\right)\right)\\ =&F\circ G\left(u\left(t,x,y\right)\right). \end{aligned} \tag{3.41}$$

Similarly, we have $v(t+2,x,y) = G_\eta \circ F_{\alpha,\beta}\left(v(t,x,y)\right)$. $\square$

Theorem 2. *The system* (3.30) *is uniquely solvable on* $[0,+\infty)\times\Gamma$. *Moreover, for any* $t \geq 0$, *we can write* $t = 2n+\tau$ *where* $n \in \mathbb{N}$ *and* $\tau \in [0,2]$. *Then the solution of* (3.30) *is given by*

$$u(t,x,y) = \begin{cases} \left(F_{\alpha,\beta}\circ G_\eta\right)^n\left(u_0(x+\tau,y+\tau)\right), \ 0 \leq \tau \leq \frac{1-x-y}{2}, \\ \left(F_{\alpha,\beta}\circ G_\eta\right)^n\left(F_{\alpha,\beta}\left(v_0(1-y-\tau,1-x-\tau)\right)\right), \ \frac{1-x-y}{2} < \tau \leq \frac{1-x-y}{2}+1, \\ \left(F_{\alpha,\beta}\circ G_\eta\right)^n\left(F_{\alpha,\beta}\circ G_\eta\left(u_0(x+\tau-2,y+\tau-2)\right)\right) \ \frac{1-x-y}{2}+1 < \tau \leq 2. \end{cases} \tag{3.42}$$

and

$$v(t,x,y) = \begin{cases} \left(G_\eta\circ F_{\alpha,\beta}\right)^n\left(v_0(x-\tau,y-\tau)\right), \ 0 \leq \tau \leq \frac{x+y+1}{2}, \\ \left(G_\eta\circ F_{\alpha,\beta}\right)^n\left(G_\eta\left(u_0(\tau-y-1,\tau-x-1)\right)\right), \ \frac{x+y+1}{2} < \tau \leq \frac{x+y+1}{2}+1, \\ \left(G_\eta\circ F_{\alpha,\beta}\right)^n\left(G_\eta\circ F_{\alpha,\beta}\left(v_0(x+2-\tau,y+2-\tau)\right)\right) \ \frac{x+y+1}{2}+1 < \tau \leq 2, \end{cases} \tag{3.43}$$

where $\left(F_{\alpha,\beta}\circ G_\eta\right)^n$ *represents the* n*-times iterative composition of* $F_{\alpha,\beta}\circ G_\eta$ *and* $\left(G_\eta\circ F_{\alpha,\beta}\right)^n$ *represents the* n*-times iterative composition of* $G_\eta\circ F_{\alpha,\beta}$.

Proof. Let $t \geq 0$, there exist unique $\tau \in (0,2)$ and an integer $n \in \mathbb{N}$ such that $t = 2n+\tau$. For $(x,y)\in\Gamma$, by applying Lemmas 1-3 and by induction, we have

$$\begin{aligned} u(t,x,y) =& u(\tau+2n,x,y) \\ &= \left(F_{\alpha,\beta}\circ G_\eta\right)^n\left(u(\tau,x,y)\right), \end{aligned} \tag{3.44}$$

and

$$\begin{aligned} v(t,x,y) =& v(\tau+2n,x,y) \\ &= \left(G_\eta\circ F_{\alpha,\beta}\right)^n\left(v(\tau,x,y)\right). \end{aligned} \tag{3.45}$$

Proof of the uniqueness is similar to the proof in Lemma 2. $\square$

Remark 9. *(i) From (3.42) and (3.43), u and v are chaotic if $F \circ G$ or $G \circ F$ are chaotic.*

(ii) After we obtained the explicit formulas of (u, v), (w_x, w_y, w_t) can be computed by

$$w_x + w_y = u - v; \; w_t = u + v.$$

Together with the initial condition, we can solve for w by the formula

$$w(x, y, t) = \int_0^t (u + v)dt + w_0(x, y).$$

To conclude, we find that the solution (u, v) is fully determined by the maps $G \circ F(\cdot)$ and $F \circ G(\cdot)$. Before introducing the properties of the composite function $H_\eta(\cdot)$, we display the graphics of the composite functions $G_\eta \circ F_{\alpha,\beta}(\cdot)$ and $F_{\alpha,\beta} \circ G_\eta(\cdot)$ for certain values of η, α and β. See Figs. 3.2-3.3. Since $F \circ G = G^{-1} \circ (G \circ F) \circ G$, these two maps are topologically conjugate. So we only need to study one of them. Let's focus on $G \circ F(\cdot)$, from now on, we fix α and β. So $G \circ F(\cdot)$ is a family of maps with a varying parameter η, denoted as

$$H_\eta(\cdot) \triangleq G_\eta \circ F_{\alpha,\beta}(\cdot). \tag{3.46}$$

Moreover, for the case $\eta > 1$, we can apply the transformation $H_{\frac{1}{\eta}}(\cdot) = -H_\eta(\cdot)$. For this reason, from now on we will only study the map $H_\eta(\cdot)$ for the case $\eta \in (0, 1)$.

Remark 10. *From figure 3.2 and figure 3.3, we can also find the that $G_\eta \circ F_{\alpha,\beta}(\cdot)$ and $F_{\alpha,\beta} \circ G_\eta(\cdot)$ are topologically conjugate.*

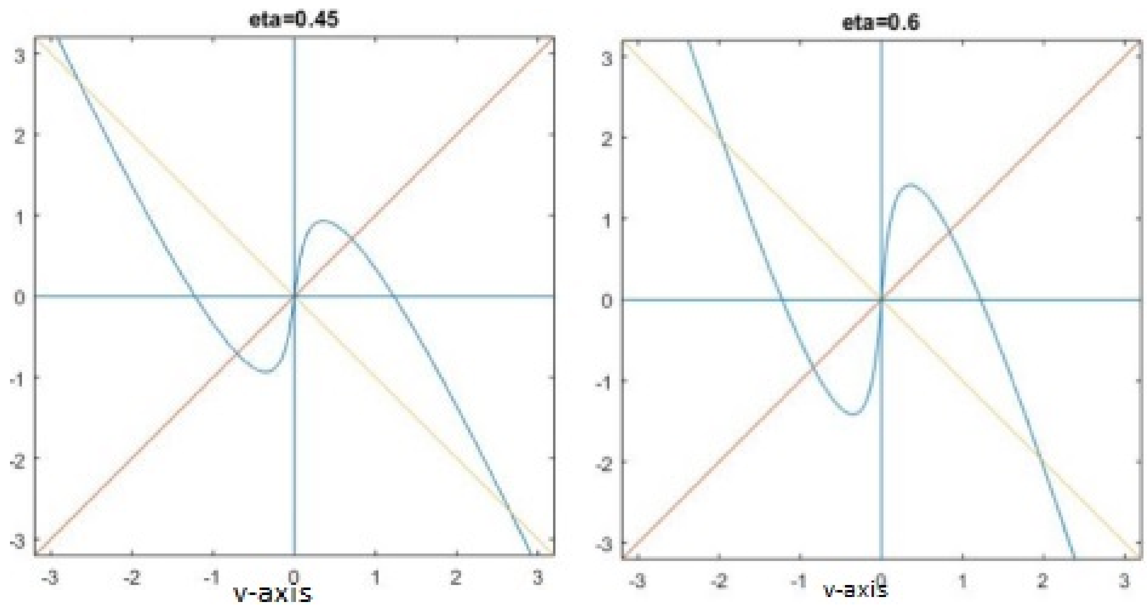

Figure 3.2: The graphs of $G \circ F(v)$, when $\alpha = 0.5$, $\beta = 1$ and (a) $\eta = 0.45$, (b) $\eta = 0.6$.

3.2 Properties of $G_\eta \circ F_{\alpha,\beta}$

Recall from (3.25) and (3.29) that, for any variable s

$$G_\eta(s) = \frac{\eta+1}{\eta-1}s, \qquad \eta \neq 1, \tag{3.47}$$

and

$$F_{\alpha,\beta}(s) = p(s) + s, \tag{3.48}$$

where $f = p(s)$ is the unique real solution of the cubic equation

$$\beta f^3 + (1-\alpha)f + 2s = 0.$$

$$H_\eta(\cdot) \triangleq G_\eta \circ F_{\alpha,\beta}(\cdot).$$

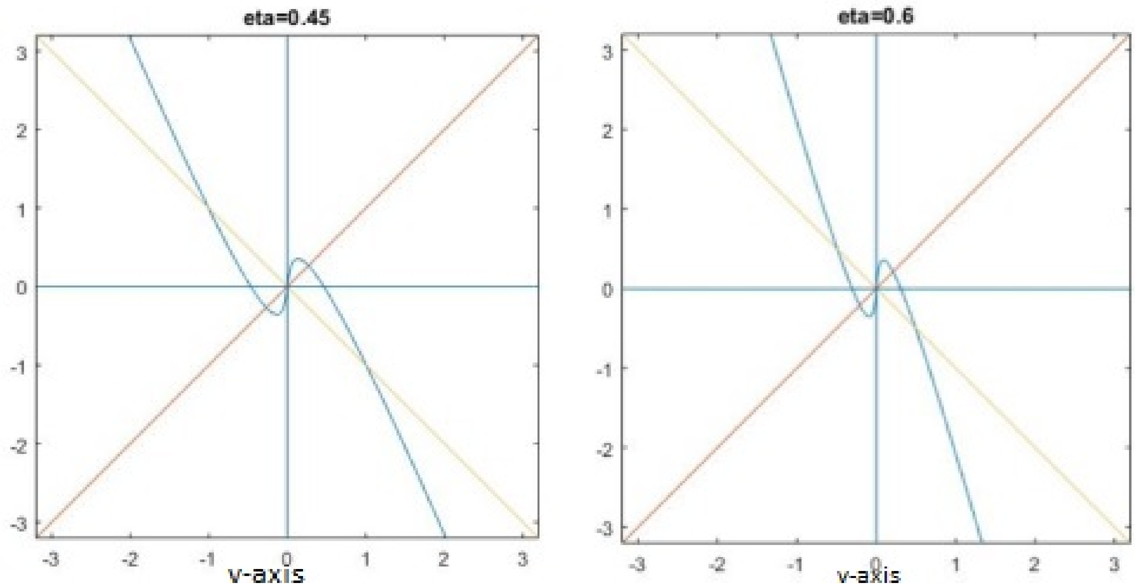

Figure 3.3: The graphs of $F \circ G(v)$, when $\alpha = 0.5$, $\beta = 1$ and (a) $\eta = 0.45$, (b) $\eta = 0.6$.

Lemma 4. *Let $0 < \alpha < 1$, $\beta > 0$. Assume η is varying on the interval $(0, 1)$. Then*

(i) $H_\eta(\cdot)$ is odd;

(ii) $H_\eta(\cdot)$ has three fixed points 0, x_0 and $-x_0$, where

$$x_0 = \frac{\eta + 1}{2}\sqrt{\frac{\eta + \alpha}{\beta}}; \tag{3.49}$$

(iii) $-H_\eta(\cdot)$ has three fixed points 0, x_1 and $-x_1$, where

$$x_1 = \frac{\eta + 1}{2\eta}\sqrt{\frac{1 + \alpha\eta}{\beta\eta}}; \tag{3.50}$$

(iv) The equation $H_\eta(x) = 0$ has three roots 0, x_2 and $-x_2$, where

$$x_2 = \sqrt{\frac{1 + \alpha}{\beta}}; \tag{3.51}$$

(v) The equation $\frac{\partial H_\eta(x)}{\partial x} = 0$ *has two roots* x_3 *and* $-x_3$*, where*

$$x_3 = \frac{2-\alpha}{3}\sqrt{\frac{1+\alpha}{3\beta}}; \tag{3.52}$$

(vi) $H_\eta(\cdot)$ *has two local extremal values* M *and* m *:*

$$\begin{aligned} M = H_\eta(x_3) &= \frac{1+\alpha}{3} \cdot \frac{1+\eta}{1-\eta} \cdot \sqrt{\frac{1+\alpha}{3\beta}}, \\ m = H_\eta(-x_3) &= -H_\eta(x_3) = -M, \end{aligned} \tag{3.53}$$

and $H_\eta(\cdot)$ *is strictly increasing on* $(-x_3, x_3)$*, but strictly decreasing on* $(-\infty, -x_3]$ *and* $[x_3, +\infty)$*.*

Proof. (i) From the formula (3.28), we know that f is odd.
So $H_\eta(-x) = \frac{\eta+1}{\eta-1}(f(-x) - x) = \frac{\eta+1}{\eta-1}(-f(x) - x) = -H_\eta(x)$.
The proofs (ii)-(v) are very similar, so we just write the details for the proof of (ii) here.
(ii) To find the fixed points of $H_\eta(\cdot)$, we set $\frac{\eta+1}{\eta-1}(x + f(x)) = x$.
$\Rightarrow$

$$f(x) + \frac{2}{\eta+1}x = 0.$$

since we have $\beta f^3 + (1-\alpha)f + 2x = 0$, then

$$\beta[(f(x) + \frac{2}{\eta+1}x) - \frac{2}{\eta+1}x]^3 + (1-\alpha)[(f(x) + \frac{2}{\eta+1}x) - \frac{2}{\eta+1}x] + 2x = 0.$$

After simplification, we have

$$-\beta(\frac{2}{\eta+1}x)^3 - (1-\alpha)\frac{2}{\eta+1}x - \frac{2}{\eta+1}x + 2x = 0.$$

Therefore

$$x = 0,\ x = \pm\frac{\eta+1}{2}\sqrt{\frac{\eta+\alpha}{\beta}}.$$

(iii) To find the fixed points of $-H_\eta(\cdot)$, we set $-\frac{\eta+1}{\eta-1}(x+f(x)) = x$ and solve for x.

(iv) To find the zeros of $H_\eta(\cdot)$, we set $\frac{\eta+1}{\eta-1}(x+f(x)) = 0$ and solve for x.

(v) Since $\frac{\partial H_\eta(x)}{\partial x} = \frac{\eta+1}{\eta-1}(1+f')$, we set $\frac{\eta+1}{\eta-1}(1+f') = 0$ and solve for x. Here, after simple calculation, we have $f' = \frac{-2}{1-\alpha+3\beta f^2}$.

(vi) Substituting x_3 and $-x_3$ from (v) to $H_\eta(\cdot)$, we obtain the extremal values. The increasing and decreasing intervals can be obtained by calculating the sign of $\frac{\partial H_\eta(x)}{\partial x}$. It can also be validated from Fig. 3.2. □

Remark 11. *From Fig. 3.2, we find that* $0 < x_3 < x_0 < x_2 < x_1$.

Fix $0 < \alpha < 1$, $\beta > 0$, and consider the equations

$$\begin{aligned} (M =)\frac{1+\alpha}{3}\cdot\frac{1+\eta}{1-\eta}\cdot\sqrt{\frac{1+\alpha}{3\beta}} &= \sqrt{\frac{1+\alpha}{\beta}}(= x_2), \\ (M =)\frac{1+\alpha}{3}\cdot\frac{1+\eta}{1-\eta}\cdot\sqrt{\frac{1+\alpha}{3\beta}} &= \frac{\eta+1}{2\eta}\sqrt{\frac{1+\alpha\eta}{\beta\eta}}(= x_1). \end{aligned} \tag{3.54}$$

(3.54a) and (3.54b) determine two critical values η_1 and η_2, respectively. More specifically, we have

$$\eta_1 = \frac{3\sqrt{3}-(1+\alpha)}{3\sqrt{3}+1+\alpha}, \tag{3.55}$$

and η_2 satisfies the following equation

$$(\frac{1}{\eta_2}-1)\sqrt{\frac{1}{\eta_2}+\alpha} = 2(\frac{1+\alpha}{3})^{\frac{3}{2}}. \tag{3.56}$$

Since

$$(\frac{1}{\eta_1}-1)\sqrt{\frac{1}{\eta_1}+\alpha} = (\frac{1}{\eta_1}+1)\frac{1+\alpha}{3\sqrt{3}}\sqrt{\frac{1}{\eta_1}+\alpha} > 2\frac{1+\alpha}{3\sqrt{3}}\sqrt{1+\alpha} = 2(\frac{1+\alpha}{3})^{\frac{3}{2}},$$

we have

$$0 < \eta_1 < \eta_2 < 1. \tag{3.57}$$

Lemma 5. *Let* $0 < \alpha < 1$, $\beta > 0$ *and* $\eta \in (0,1)$. *Then*

(i) If $0 < \eta \leq \eta_2$, *i.e.,*

$$M \leq x_1,$$

the iterates of every point in the set $V = (-\infty, -x_1)\bigcup(x_1, \infty)$ *escape to* $\pm\infty$, *while those of any point in* $R \backslash \overline{V}$ *are attracted to the bounded invariant interval* $I = [-M, M]$ *of* $H_\eta(\cdot)$.

(ii) If $\eta_2 < \eta < 1$, *there is no bounded invariant interval.*

Proof. The results follow from Lemma 4 and the piecewise monotonic properties of $G_\eta \circ F_{\alpha,\beta}$, as can be confirmed from Fig. 3.2. □

3.3 Period-Doubling Bifurcation Theorem for $G_\eta \circ F_{\alpha,\beta}$

In this section, we will mainly introduce the Period-Doubling Bifurcation theorem for $H = G_\eta \circ F_{\alpha,\beta}$.

Let $\eta \in (0,1)$ and $x_0 \in (0, x_2)$, consider the system

$$\begin{cases} H_\eta(x_0) = x_0, \\ \frac{\partial H_\eta(x)}{\partial x}|_{x=x_0} = -1. \end{cases} \tag{3.58}$$

From (3.58) we obtain an equation for η :

$$3\eta^2 + 2\alpha\eta - 1 = 0.$$

Let η_0 be the unique positive solution of the above equation, i.e.,

$$\eta_0 = \frac{\sqrt{\alpha^2+3}-\alpha}{3}. \tag{3.59}$$

Proposition 1.

$$0 < \eta_0 < \eta_1 < \eta_2 < 1.$$

Proof. From (3.57), we already have $0 < \eta_1 < \eta_2 < 1$. Here, we only need to prove $\eta_0 < \eta_1$.

Since $\alpha < 1$, we have

$$\eta_0 = \frac{\sqrt{\alpha^2+3}-\alpha}{3} < \frac{2-\alpha}{3} < \eta_1.$$

$\square$

Recall the definition of the *period-k orbit of a point p*: a period-k orbit of H is the set of k distinct points $\{H^j(p)|j = 0, ..., k-1\}$ with $H^k(p) = p$. k is the smallest positive integer that satisfy the equality.

Moreover, since H_η is unimodal on $(0, x_2)$ or $(-x_2, 0)$, we consider H_η either on $(0, x_2)$ or $(-x_2, 0)$ in order to be able to apply the Period-Doubling Bifurcation Theorem in ([37, p. 220]).

Now, we are ready to state the first main theorem of this section.

Theorem 3 (Period-Doubling Bifurcation Theorem for H_η)**.** *Let* $0 < \alpha < 1$, $\beta > 0$ *be fixed, and* $\eta \in (0, \eta_2]$ *is a varying parameter. Then* $H_\eta(\cdot)$ *undergoes a period-doubling bifurcation on* $[0, x_2]$ *as the parameter value* η *crosses* η_0*. More specifically,*

(i) H_η *has a unique fixed point in* $[0, x_2]$*. Moreover, if* $\eta \in (0, \eta_0)$*, the fixed point* $x(\eta)$ *is attracting. If* $\eta \in (\eta_0, \eta_2]$*, the fixed point* $x(\eta)$ *is repelling;*

(ii) when $\eta \in (0, \eta_0)$, H_η has no periodic point in $[0, x_2]$ with a period greater than or equal to 2;

(iii) upon η crossing η_0, H_η has an attracting bifurcated period-2 orbit.

Proof. (i) follows from Lemma A.5 in [32]. And

when $\eta \in (0, \eta_0)$, we have

$$|\frac{\partial H_\eta(x)}{\partial x}|_{x=x_0}| < 1.$$

when $\eta \in (\eta_0, \eta_1)$, we have

$$|\frac{\partial H_\eta(x)}{\partial x}|_{x=x_0}| > 1.$$

For (ii), follows from Lemma A.5 in [32].

For (iii), we can check that for $\eta = \eta_0$, we have

$$A \equiv \left[\frac{\partial^2 H}{\partial \eta \partial x} + 0.5(\frac{\partial H}{\partial \eta})\frac{\partial^2 H}{\partial x^2}\right]|_{x=x_0,\eta=\eta_0} \neq 0,$$

and

$$B \equiv \left[\frac{1}{6}\frac{\partial^3 H}{\partial x^3} + 0.25(\frac{\partial^2 H}{\partial x^2})^2\right]|_{x=x_0,\eta=\eta_0} > 0,$$

Then we can apply the Period-Doubling Bifurcation Theorem in ([37, p. 220]) to conclude the proof. $\square$

Theorem 3 can be validated from the bifurcation diagram. In Figure 3.4, we have $\alpha = 0.5,\ \beta = 1$, so $\eta_0 = \frac{\sqrt{0.5^2+3}-0.5}{3} \approx 0.434$. From the graph, the first period-doubling appears near 0.434, matching with Theorem 3.

To prepare for the next main theorem, we recall some properties about periodic points and total variation from literature.

Lemma 6. *[10, Main Theorem 8] Let $f(\cdot) \in C^0(I, I)$, where I is a bounded interval, V is the total variation. Assume that $f(\cdot)$ has two distinct fixed points and a periodic*

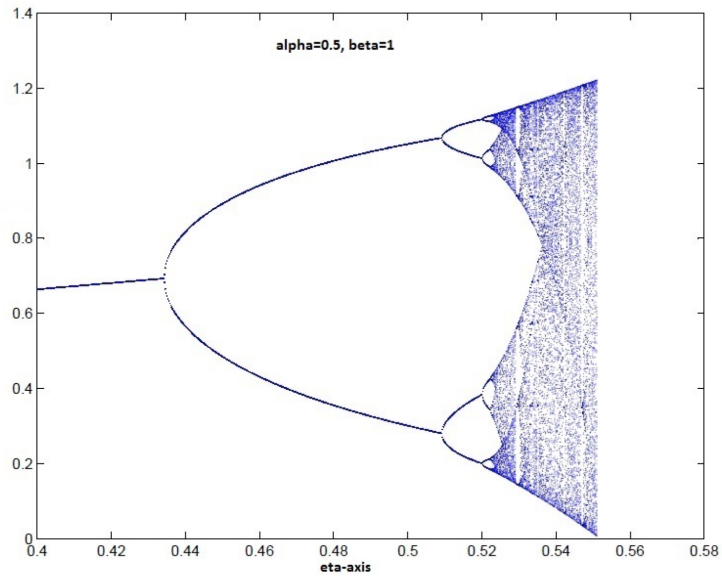

Figure 3.4: Bifurcation diagram of H, when $\alpha = 0.5,\ \beta = 1$.

point with period 2. Then

$$\lim_{n\to\infty} V_{[x_0,p]}(f^n(\cdot)) = \infty, \tag{3.60}$$

where x_0 is the smaller fixed point and p is the periodic point with period 2.

Note that the rate of growth with respect to n in (3.60) is *not exponential*.

Lemma 7. *[6, Section II, Lemma 3] Let $f(\cdot) \in C^0(I, I)$. If $f(\cdot)$ is turbulent, then $f(\cdot)$ has periodic points of all periods.*

Before we state the next Lemma, let's recall the definition of *homoclinic point* and *homoclinic orbit* [21]: if $f(\cdot) \in C^1(I, I)$, let x be a repelling fixed point (i.e., $f(x) = x, |f'(x)| > 1$) and $S^u_{loc}(x)$ be the local unstable set at x, which is the set of points that having a sequence of preimages in I tends toward x. In other words, $S^u_{loc}(x) = \{y \in I | lim_{k\to\infty} d(f^{-k}(y), f^{-k}(x)) = 0\}$.
(i) A point $y \in I$ is said to be *homoclinic* to x if $y \in S^u_{loc}(x)$ and $f^m(y) = x$ for some positive integer m.

(ii) For a *homoclinic point* y, the *homoclinic orbit* of y is the set $\{f^i(y)|i = 1, 2, ..., n\}$. The orbit is *nondegenerate* if $f'(p) \neq 0$ for all points p on the orbit. The orbit is *degenerate* if there exists at least one point q on the orbit such that $f'(q) = 0$.

Lemma 8. *[10, Lemma 7.4] Let $f(\cdot) \in C^0(I, I)$ and f be piecewise monotone. Then the following conditions are equivalent:*

(i) $f(\cdot)$ has a periodic point whose period is not a power of 2 ($1 = 2^0$ is regarded as a power of 2);

(ii) $f(\cdot)$ has a homoclinic point;

(iii) $f(\cdot)$ has positive topological entropy;

(iv) the growth rate of the total variation of $f^n(\cdot)$ is exponential w.r.t. n.

Now let's return to the dynamics of the map $H_\eta(\cdot)$ defined by (3.46). Recall the notation used in Lemma 4 and Lemma 5, such as $x_i, i = 0, 1, 2, 3$, M and m.

Proposition 2. *Let $0 < \alpha < 1$, $\beta > 0$ be fixed, and $\eta \in (0, \eta_2]$ be a varying variable. Given $\eta_i, i = 0, 1$, defined by (3.59) and (3.55) , respectively, then*

(i) if $\eta \in (0, \eta_0)$, $H_\eta(\cdot)$ has no periodic point in $[0, x_2]$ or $[-x_2, 0]$ with period greater than or equal to 2;

(ii) if $\eta \in [\eta_0, \eta_1)$, $H_\eta(\cdot)$ has periodic points in $[0, x_2]$ and $[-x_2, 0]$ each with a period as a power of 2;

(iii) if $\eta \in [\eta_1, \eta_2]$, $H_\eta(\cdot)$ has periodic points in $[-M, M]$ with periods which are not a power of 2.

Proof. Statements (i) and (ii) follow from Theorem 3. For (iii), it follows from [32, Theorem 3.1]. $\square$

From Lemmas 6-8 and Proposition 2, we have the following result.

Proposition 3. *Let $0 < \alpha < 1$, $\beta > 0$ be fixed, and $\eta \in (0, \eta_2]$ is a varying variable. Then the following holds for $n = 0, 1, 2, \ldots$:*

(i) for every $\eta \in (0, \eta_0)$,

$$V_I(H_\eta^n) \leq C, \tag{3.61}$$

where C is a positive constant and $I = [0, x_2]$ or $[-x_2, 0]$;

(ii) for every $\eta \in [\eta_0, \eta_1)$,

$$\lim_{n\to\infty} V_{I_\varepsilon}(H_\eta^n) = \infty, \tag{3.62}$$

where $I_\varepsilon = [0, \varepsilon]$ or $[-\varepsilon, 0]$, for any $\varepsilon > 0$. The increasing rate here is not exponentially with respect to n;

(iii) for every $\eta \in [\eta_1, \eta_2]$,

$$V_{I_\varepsilon}(H_\eta^n) \geq c_1(exp(c_2 n)), \text{ as } n \to \infty. \tag{3.63}$$

where c_1 and c_2 are positive constants.

3.4 Chaotic Vibration Phenomenon of the Main System

Recall the main system we considered in section 1,

$$\begin{cases} w_{tt} = \Delta w + 2w_{xy}, \quad (x,y) \in \mathring{\Gamma}, \ t > 0, \\ w_t = -\eta\,(w_x + w_y)\,, \ (x,y) \in \Gamma_1, \ t > 0, \\ w_t = \alpha(w_x + w_y) - \beta(w_x + w_y)^3, \ (x,y) \in \Gamma_3, \ t > 0, \\ w(t,x,y) = 0, \ (x,y) \in \Gamma_2 \cup \Gamma_4, \ t > 0, \\ w(0,x,y) = w_0(x,y), \ w_t(0,x,y) = w_1(x,y), \ (x,y) \in \Gamma. \end{cases} \tag{3.64}$$

To our knowledge, there is no universally accepted definition of chaos in 2D. Inspired by [10], where they characterized the chaotic behavior by the growth rate of the total variation, we give a suitable definition of chaos for system (3.64) here. First, recall that a *simple curve* $\mathcal{C}$ in a 2D domain Γ is defined through a continuous function g from a real number interval $I = [a, b]$ to Γ. The image $g(I)$ is called a *curve*. *Simple* means g is injective. More specifically, $\mathcal{C}$ is the set of all $g(s)$ when $s \in [a, b]$, where

$$g(s) = (x_{\mathcal{C}}(s), y_{\mathcal{C}}(s)) \in \Gamma.$$

Definition 1. *We say that a PDE system of w in the 2D domain Γ is chaotic or has chaotic vibration phenomenon, if there exists at least one direction $\overrightarrow{l}$ in $\mathbb{R}^3$, such that for any simple curve $\mathcal{C}$ with $g(a), g(b) \in \partial\Gamma$ and $g(j) \in \mathring{\Gamma}$, for any $j \in (a, b)$, the directional derivative $\nabla_{\overrightarrow{l}} w$ satisfies*

(i) $\nabla_{\overrightarrow{l}} w\,(t, x_{\mathcal{C}}(s), y_{\mathcal{C}}(s))$ *is uniformly bounded;*

(ii) $V_{[a,b]}\left(\nabla_{\overrightarrow{l}} w\,(t, x_{\mathcal{C}}(s), y_{\mathcal{C}}(s))\right)$ *is exponentially increasing as time t increases.*

After all these preparations, we are ready to state the last main theorem of this section.

Theorem 4. *Consider the system* (3.20)*. Let $0 < \alpha < 1$, $\beta > 0$ be fixed, for $\eta \in [\eta_1, \eta_2]$, where η_1 and η_2 are given by* (3.55) *and* (3.56)*, respectively. Then, for a certain class of initial conditions the system* (3.64) *is chaotic.*

Proof. Let $\eta \in [\eta_c, \eta_2]$. From Lemma 5, $G_\eta \circ F_{\alpha,\beta}$ has an invariant interval $[-M, M]$, where M is a local maximum of $G_\eta \circ F_{\alpha,\beta}$ as follow

$$M = \frac{1+\alpha}{3} \cdot \frac{1+\eta}{1-\eta} \cdot \sqrt{\frac{1+\alpha}{3\beta}}. \tag{3.65}$$

Choose the initial condition $w_0 = 0$ and $w_1 \in C^2(\Gamma)$ satisfies

$$\begin{aligned} &\forall (x,y) \in \partial\Gamma, \quad w_1(x,y) = 0, \\ &\forall (x,y) \in \mathring{\Gamma}, \quad w_1(x,y) > 0. \end{aligned} \tag{3.66}$$

Furthermore, assume that

$$Range(w_1) \cup Range(\frac{\eta+1}{\eta-1} \cdot w_1) \cup Range(\frac{\eta+1}{\eta-1}(F_{\alpha,\beta}(w_1))) \subset [-M, M]. \tag{3.67}$$

Consider the direction vector $\overrightarrow{l} = (\frac{1}{2}, -\frac{1}{2}, -\frac{1}{2})$, and let

$$v = \nabla_{\overrightarrow{l}} w. \tag{3.68}$$

In fact, v is the same definition as (2.5).

For any simple curve $\mathcal{C}$ in Γ with

$$\begin{aligned} &g(a), g(b) \in \partial\Gamma \\ &g(j) \in \mathring{\Gamma}, \text{ for any } j \in (a,b). \end{aligned} \tag{3.69}$$

Under the assumption (3.67), from Lemmas 2 and 5, we have

$$\forall t \geq 0, \ \forall s \in [a,b], \quad |v\left(t, x_{\mathcal{C}}(s), y_{\mathcal{C}}(s)\right)| \leq M, \tag{3.70}$$

which is to say that $\nabla_{\overrightarrow{l}} w\left(t, x_{\mathcal{C}}(s), y_{\mathcal{C}}(s)\right)$ is uniformly bounded.

Moreover, given any $t \geq 0$, let $t = 2n + \tau$ where $\tau \in (0,2)$ and $n \in \mathbb{N}$. From Theorem 2, we have

$$\forall s \in [a,b], \quad v\left(t, x_{\mathcal{C}}(s), y_{\mathcal{C}}(s)\right) = \left(G_\eta \circ F_{\alpha,\beta}\right)^n \left(v\left(\tau, x_{\mathcal{C}}(s), y_{\mathcal{C}}(s)\right)\right). \tag{3.71}$$

It follows from Proposition 3 (iii) that there exists constants $c_1 > 0$ and $c_2 > 0$ such that for any $\epsilon > 0$

$$V_{[0,\epsilon]} \left(G_\eta \circ F_{\alpha,\beta}\right)^n \geq c_1 e^{c_2 n}, \quad n \in \mathbb{N}. \tag{3.72}$$

Under assumptions (3.66) and (3.69), we have an $\epsilon_0 > 0$ such that

$$[0, \epsilon_0] \subset Range\left(v\left(\tau, x_{\mathcal{C}}(s), y_{\mathcal{C}}(s)\right)\right). \tag{3.73}$$

Take $\epsilon = \epsilon_0$ in (3.72). Consequently, we have

$$\begin{aligned} V_{[a,b]}\left(\nabla_{\vec{l}} w\left(t, x_{\mathcal{C}}(s), y_{\mathcal{C}}(s)\right)\right) &= V_{[a,b]}\left(v\left(t, x_{\mathcal{C}}(s), y_{\mathcal{C}}(s)\right)\right) \\ &= V_{[a,b]}\left(\left(G_\eta \circ F_{\alpha,\beta}\right)^n \left(v\left(\tau, x_{\mathcal{C}}(s), y_{\mathcal{C}}(s)\right)\right)\right), \\ &\geq c_1 e^{c_2 n} \\ &\geq c_1 e^{c_2 \frac{t-\tau}{2}}, \end{aligned} \tag{3.74}$$

Thus, the system (3.64) is chaotic. □

3.5 Numerical Simulations

In this section, we present some numerical simulation results for the system (3.9) to verify the theoretical results in previous sections.

Throughout, we fix $\alpha = 0.5$, $\beta = 1$ and let η be a varying parameter. The initial conditions are chosen as follows:

$$\forall (x,y) \in \Gamma, \quad w_0(x,y) = 0, \quad w_1(x,y) = \frac{1}{10} \cdot \left((x+y)^2 - 1\right)^3 \cdot \left((x-y)^2 - 1\right)^3, \tag{3.75}$$

which satisfies the conditions in the proof of Theorem 4.

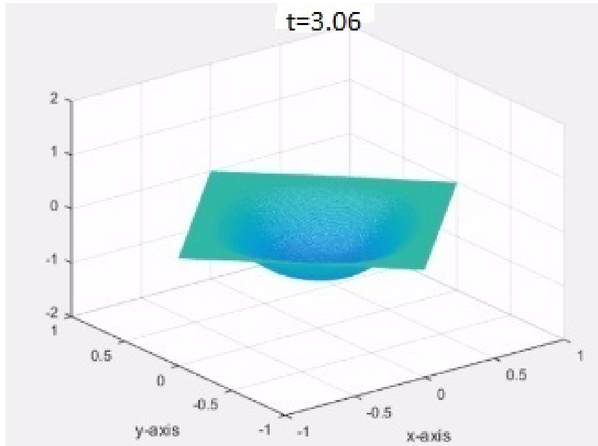

Figure 3.5: The profile of w_t for $\eta = 0.45$ at t=3.06.

We can obtain the three critical parameter values below:

$$\eta_0 \approx 0.434, \qquad \eta_1 \approx 0.552, \qquad \eta_2 \approx 0.667. \tag{3.76}$$

Theorem 4 shows that when $\eta \in [0.552, 0.667]$ the system (3.9) is chaotic. To verify this, in our numerical simulation, we compare two cases: $\eta = 0.45$ and $\eta = 0.6$.

Numerical simulations for w_t are provided in Figures 3.5-3.10.

Video animations can also be found at:

`https://www.dropbox.com/s/1xa8qr29hwfrcbz/nonchaotic.mp4?dl=0`,

with $\eta = 0.45$ and the time range is $[0, 20]$;

`https://www.dropbox.com/s/uljtfbns4hl4dtm/chaotic2.mp4?dl=0`,

with $\eta = 0.6$ and the time range is $[0, 20]$.

All these numerical simulation results match well with the statement in Theorem 4.

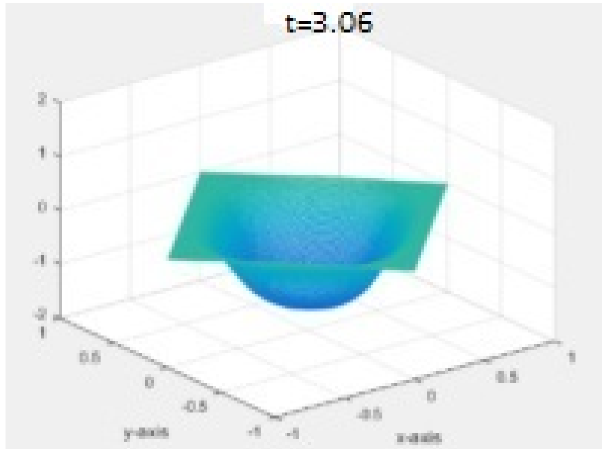

Figure 3.6: The profile of w_t for $\eta = 0.6$ at t=3.06.

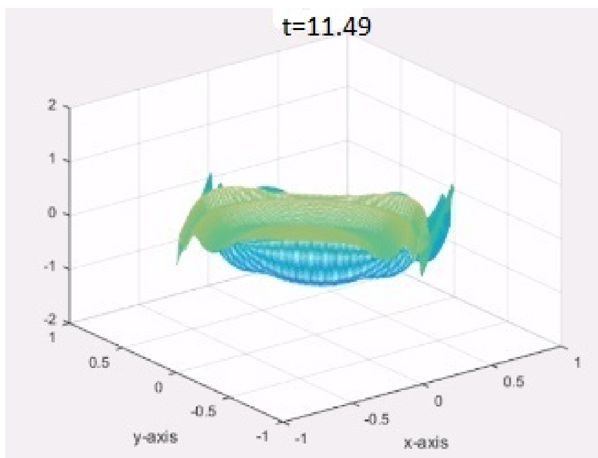

Figure 3.7: The profile of w_t for $\eta = 0.45$ at t=11.49.

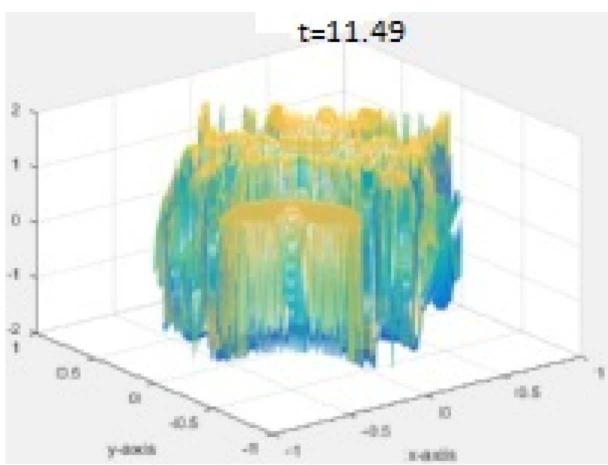

Figure 3.8: The profile of w_t for $\eta = 0.6$ at t=11.49.

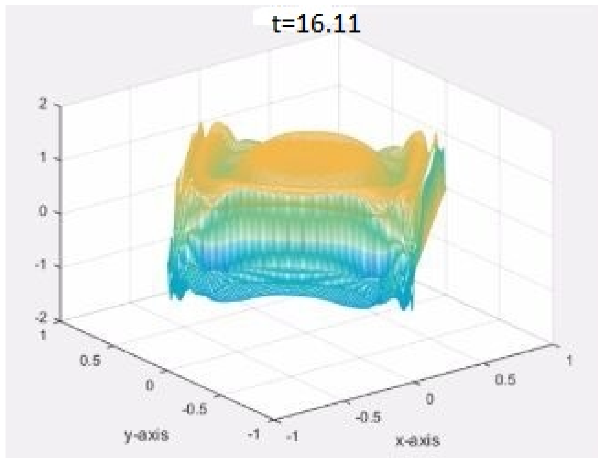

Figure 3.9: The profile of w_t for $\eta = 0.45$ at t=16.11.

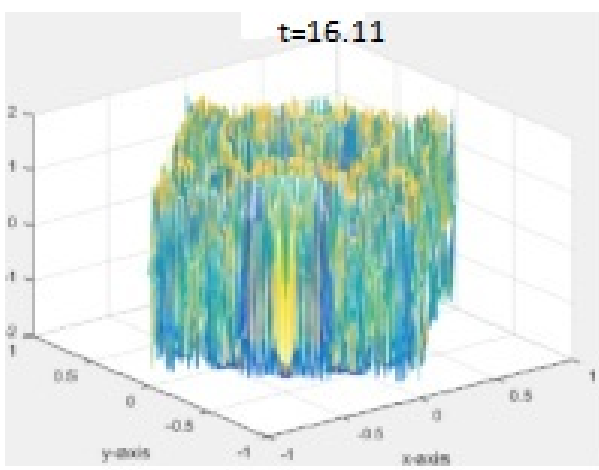

Figure 3.10: The profile of w_t for $\eta = 0.6$ at t=16.11.

4. EMERGENCE OF THE NAVIER-STOKES-ALPHA MODEL FOR CHANNEL FLOWS *

The Navier-Stokes equations (NSE) have been widely used to describe the motion of viscous incompressible fluid flows. In this section, we accept, as done in [16] and [17], that the Navier-Stokes-α model (NS-α) is a good mathematical model for the dynamics of appropriately averaged turbulent fluid flows. We will first give our rationale for this acceptance. The possibility that the NS-α is an averaged version of the NSE, first considered in [12] and [15], was entailed by several auspicious facts. Namely, the NS-α analogue of the Poiseuille, resp, Hagen, solution in a channel, resp, a pipe, displays both the classical Von *Kármán* and the recent Barenblatt-Chorin laws ([28]). Moreover, the NS-α analogue of the Hagen solution, when suitably calibrated, yields good approximations to many experimental data [15]. Furthermore, D. D. Holm found an original, physically sound, statistical averaging of the Euler equations such that the NS-α results from the addition of a linear viscous effect ([28]); see also [13] for a succinct presentation of Holm's averaging. This new averaging is as general as the Reynolds averaging, but unlike the latter, it yields "closed systems of differential equations". We close the above, rather long, argument by quoting the remarkably successful extension of the classic Blasius theory for a turbulent boundary layer ([17]) to a larger range of Reynolds numbers, done by using the NS-α instead of the NSE.

In literature, there are several ways to derive the NS-α model. For example, in 1999, Chen, et al. [13] used the averaged Lagrangian; in 2002, Foias, Holm and Titi [22]

*Part of this section is reprinted from "On the emergence of the Navier-Stokes-alpha model for turbulent channel flows" and "On some properties of incompressible fluid flows in channels" by C. Foias, J. Tian and B. Zhang, a submitted paper [25] and a paper in preparation [24].

rederived the NS-α model by filtering the velocity of the fluid loop in Kelvins circulation theorem for the Navier-Stokes equations. However, almost all these derivation methods are purely mathematical, without taking into account the physical properties. We are interested in finding a connection between NSE and NS-α in terms of the physical properties of the fluid flow. In other words, we need to obtain a simple Reynolds type averaging which will transform the NSE into the NS-α. The organization of this section is as follows: subsection 4.1 introduces the mathematical backgrounds and basic inequalities. In subsection 4.2, we give the definition of the class $\mathcal{P}$. In subsection 4.3, a Reynolds type averaging is introduced. In the last subsection, we present the transition mechanism from NSE to NS-α.

4.1 Specific Preliminaries

First, let's recall the definitions related to the global attractor of the NSE:
The global attractor $\mathcal{A}$ of NSE is defined as $\mathcal{A} = \{u_0 \in H\}$, where H is a phase space and u_0 satisfies the condition that there exists a solution $u(t)$ of the NSE, for all $t \in \mathbb{R}$, such that $u(0) = u_0$ and $\sup_{t\in\mathbb{R}} |u(t)| < \infty$ [42]. In other words, the global attractor is the smallest set in H which uniformly attracts all compact sets [42].
When the topology on H is *weak* topology, the attractor is the weak global attractor ($\mathcal{A}_w$). The definition of $\mathcal{A}_w$ is given in [23]: it is the set of all uniformly bounded global weak solutions in H.
The regular part of the weak global attractor is a weakly open and dense subset of the weak global attractor, and it has the properties that any weak solution passing through the point in the regular part at a given initial time is a strong solution in a neighborhood of the initial time [23].

4.1.1 Mathematical Backgrounds

Throughout, we consider an incompressible viscous fluid in an immobile region $\mathcal{O} \subset \mathbb{R}^3$ subjected to a potential body force $F = -\nabla\Phi$, with a time independent potential $\Phi = \Phi(x) \in C^\infty(\mathcal{O})$. The velocity field of such flows,

$$u = u(x,t) = (u_1(x,t), u_2(x,t), u_3(x,t)),\ \ x = (x_1, x_2, x_3) \in \mathcal{O} \tag{4.1}$$

satisfies the NSE,

$$\frac{\partial}{\partial t}u + (u \cdot \nabla)u = \nu\Delta u - \nabla P, \quad \nabla \cdot u = 0, \tag{4.2}$$

where $P = P(x,t) := p(x,t) + \Phi(x)$, t denotes the time. $\nu > 0$ is the kinematic viscosity, and $p = p(x,t)$ is the pressure.

The NS-α is

$$\frac{\partial}{\partial t}v + (u \cdot \nabla)\, v + \sum_{j=1}^{3} v_j \nabla u_j = \nu\Delta v - \nabla Q, \quad \nabla \cdot u = 0, \tag{4.3}$$

where

$$\begin{aligned} v = (v_1, v_2, v_3) &= (1 - \alpha^2\Delta)u \\ &= \left((1-\alpha^2\Delta)u_1, (1-\alpha^2\Delta)u_2, (1-\alpha^2\Delta)u_3\right), \end{aligned} \tag{4.4}$$

and Q in (4.3) (like P in (4.2)) may depend on the time t.

We consider the following no-slip boundary conditions, for both the NSE (4.2) and the NS-α (4.3),

$$u(x,t) = 0, \quad \text{for } x \in \partial\mathcal{O} := \text{boundary of } \mathcal{O}. \tag{4.5}$$

One can see that if $\alpha = 0$, the NS-α (4.3) become the NSE (4.2), so that (4.3) is also referred as an α-model of (4.2).

In the case of a channel flow, that is, $\mathcal{O} = \mathbb{R} \times \mathbb{R} \times [x_3^{(l)}, x_3^{(u)}]$, where $h := x_3^{(u)} - x_3^{(l)} > 0$ is the "height" of the channel, we recall that a vector of the form

$$(U(x_3), 0, 0) \tag{4.6}$$

is a *stationary* (i.e., time independent) solution of the NSE (4.2) if and only if

$$U(x_3) = b\left(1 - \frac{(x_3 - \frac{x_3^{(u)}+x_3^{(l)}}{2})^2}{(h/2)^2}\right), \quad x_3 \in [x_3^{(l)}, x_3^{(u)}], \tag{4.7}$$

where b is a constant velocity; respectively, $(U(x_3), 0, 0)$ is a stationary solution of the NS-α (4.3) if and only if,

$$U(x_3) = a_1\left(1 - \frac{\cosh\left((x_3 - \frac{x_3^{(u)}+x_3^{(l)}}{2})/\alpha\right)}{\cosh h/(2\alpha)}\right) + a_2\left(1 - \frac{(x_3 - \frac{x_3^{(u)}+x_3^{(l)}}{2})^2}{(h/2)^2}\right), \tag{4.8}$$

for $x_3 \in [x_3^{(l)}, x_3^{(u)}]$, where a_1, a_2 are constant velocities (cf. formula (9.6) in [15]). Above, $\cosh(x) = \frac{e^x+e^{-x}}{2}$ is the hyperbolic cosine function.

To simplify our notation, we will assume up to subsection 4.4 that $x_3^{(l)} = 0$ and $x_3^{(u)} = h$.

4.1.2 Basic Inequalities

(i) Poincaré inequality:

The following classical Poincaré inequality will be used in our discussion.

Lemma 9. *For any C^1 function $\phi(y)$ defined on $[0, h]$, with $\phi(0) = \phi(h) = 0$, we have*

$$\int_0^h (\phi'(y))^2 dy \geq \frac{1}{h^2} \int_0^h (\phi(y))^2 dy. \tag{4.9}$$

Proof. [1] By the fundamental theorem of calculus, we have, for any $x \in \mathbb{R}$, and $x \in [0, h]$,

$$\phi^2(x) = 2 \int_0^x \phi(y)\phi'(y) dy, \tag{4.10}$$

and,

$$\phi^2(x) = -2 \int_x^h \phi(y)\phi'(y) dy. \tag{4.11}$$

Using Cauchy inequality in (4.10), we get,

$$\phi^2(x) \leq 2\left(\int_0^x \phi^2(y) dy \right)^{1/2} \left(\int_0^x (\phi'(y))^2 dy \right)^{1/2},$$

hence

$$\begin{aligned}\int_0^{h/2}\phi^2(x)dx &\le 2\int_0^{h/2}\Big(\int_0^x\phi^2(y)dy\Big)^{1/2}\Big(\int_0^x(\phi'(y))^2dy\Big)^{1/2}dx\\ &\le 2\int_0^{h/2}\Big(\int_0^{h/2}\phi^2(y)dy\Big)^{1/2}\Big(\int_0^{h/2}(\phi'(y))^2dy\Big)^{1/2}dx\\ &\le h\Big(\int_0^{h/2}\phi^2(y)dy\Big)^{1/2}\Big(\int_0^{h/2}(\phi'(y))^2dy\Big)^{1/2},\end{aligned}$$

that is,

$$\int_0^{h/2}\phi^2(x)dx \le h^2\int_0^{h/2}(\phi'(y))^2dy. \tag{4.12}$$

Similarly, using (4.11), and repeating the above steps, we get,

$$\int_{h/2}^{h}\phi^2(x)dx \le h^2\int_{h/2}^{h}(\phi'(y))^2dy. \tag{4.13}$$

Combined (4.12) and (4.13), we obtain (4.9). □

(ii) L^∞ inequality:

For a given function $\phi = \phi(y)$ with periodicity $\Pi > 0$, its average is denoted by $<\phi>$:

$$<\phi>:= \frac{1}{\Pi}\int_0^{\Pi}\phi(y)dy.$$

Lemma 10. *For any continuous function $\phi = \phi(y)$ with periodicity $\Pi > 0$, it holds that*

$$|\phi|_{L^\infty} \le <\phi> + \frac{\Pi}{2\sqrt{3}} <(\phi')^2>^{1/2}. \tag{4.14}$$

Consequently, if

$$< (\phi')^2 > < \infty,$$

then ϕ *is continuous in* $\mathbb{R}$*, and thus* $|\phi(y)| \le |\phi|_{L^\infty}, \forall y \in \mathbb{R}$.

Proof. Without loss of generality, we assume $\phi(0) = |\phi|_{L^\infty}$, then

$$\phi(0) \le \begin{cases} \phi(y) + \int_0^y |\phi'(z)|dz, \ y \ge 0; \\ \phi(y) + \int_y^0 |\phi'(z)|dz, \ y \le 0; \end{cases}$$

thus,

$$\begin{aligned} \frac{\Pi}{2}\phi(0) &\le \begin{cases} \int_0^{\Pi/2} \phi(y)dy + \int_0^{\Pi/2} (\int_z^{\Pi/2} dy)|\phi'(z)|dz \\ \int_{-\Pi/2}^0 \phi(y)dy + \int_{-\Pi/2}^0 (\int_{-\Pi/2}^z dy)|\phi'(z)|dz \end{cases} \\ &= \begin{cases} \int_0^{\Pi/2} \phi(y)dy + \int_0^{\Pi/2} (\Pi/2 - z)|\phi'(z)|dz; \\ \int_{-\Pi/2}^0 \phi(y)dy + \int_{-\Pi/2}^0 (\Pi/2 + z)|\phi'(z)|dz; \end{cases} \end{aligned}$$

hence,

$$\begin{aligned} \Pi|\phi|_{L^\infty} = \Pi\phi(0) &\le \Pi < \phi > + \Big(\int_0^{\Pi/2} (\Pi/2 - z)^2 dz\Big)^{1/2} \Big(\int_0^{\Pi/2} (\phi'(z))^2 dz\Big)^{1/2} \\ &+ \Big(\int_{-\Pi/2}^0 (\Pi/2 + z)^2 dz\Big)^{1/2} \Big(\int_{-\Pi/2}^0 (\phi'(z))^2 dz\Big)^{1/2} \\ &\le \Pi < \phi > + \frac{\Pi^2}{2\sqrt{3}} < (\phi')^2 >^{1/2}, \end{aligned}$$

and (4.14) follows. $\square$

4.2 The Class $\mathcal{P}$

4.2.1 Definition of Class $\mathcal{P}$

We define the class $\mathcal{P}$ by five assumptions: a function $u(x,t)$ belongs to class $\mathcal{P}$ if it satisfies $(\mathbf{A.1}) - (\mathbf{A.5})$,

$(\mathbf{A.1})$ $u(x,t) \in C^\infty(\mathcal{O} \times \mathbb{R})$.

$(\mathbf{A.2})$ $u(x,t)$ is periodic in x_1 and x_2, with periods Π_1 and Π_2, respectively; i.e.,

$$u(x_1+\Pi_1, x_2, x_3, t) = u(x_1, x_2, x_3, t), \quad u(x_1, x_2+\Pi_2, x_3, t) = u(x_1, x_2, x_3, t). \tag{4.15}$$

Remark 12. *From* (4.2) *and* $(\mathbf{A.2})$, *we obtain, for* $1 \leq j \leq 3$,

$$\frac{\partial}{\partial x_j}\left(P(x_1+\Pi_1, x_2, x_3, t) - P(x_1, x_2, x_3, t)\right) = 0,$$

and

$$\frac{\partial}{\partial x_j}\left(P(x_1, x_2+\Pi_2, x_3, t) - P(x_1, x_2, x_3, t)\right) = 0,$$

so $P(x_1+\Pi_1, x_2, x_3, t) - P(x_1, x_2, x_3, t)$ *and* $P(x_1, x_2+\Pi_2, x_3, t) - P(x_1, x_2, x_3, t)$ *are functions only depending on time* t. *For simplicity, we denote*

$$\begin{cases} p_1(t) := P(x_1+\Pi_1, x_2, x_3, t) - P(x_1, x_2, x_3, t), \\ p_2(t) := P(x_1, x_2+\Pi_2, x_3, t) - P(x_1, x_2, x_3, t). \end{cases} \tag{4.16}$$

Remark 13. *We also assume that the time independent potential function* $\Phi(x)$ *is periodic in* x_1 *and* x_2 *with periods* Π_1 *and* Π_2, *respectively. Then, physically,* $p_1(t)$ *and* $p_2(t)$ *represent the pressure drops of the flows in* x_1 *and* x_2 *directions, respectively.*

($\mathbf{A}.\mathbf{3}$) $u(x,t)$ exists for all $t \in \mathbb{R}$ and has bounded energy per mass, i.e.,

$$\int_0^{\Pi_1}\int_0^{\Pi_2}\int_0^{h} u(x,t)\cdot u(x,t)dx < \infty, \forall t \in \mathbb{R}. \tag{4.17}$$

($\mathbf{A}.\mathbf{4}$) there exists a constant $0 < \bar{p} < \infty$ for which,

$$0 < -p_1(t) \leq \bar{p}$$
$$|p_2(t)| \leq \bar{p}$$

for all $t \in \mathbb{R}$, where $p_1(t)$ and $p_2(t)$ are defined in (4.16).

($\mathbf{A}.\mathbf{5}$) $P = P(x,t)$ is bounded in the x_2 direction, i.e.,

$$\sup_{x_2 \in \mathbb{R}} P(x_1, x_2, x_3, t) < \infty,\ \forall x_1, x_3, t \in \mathbb{R}.$$

Remark 14. *In fact,* ($\mathbf{A}.\mathbf{5}$) *can be replaced with the following weaker assumption* ($\mathbf{A}.\mathbf{5}'$)*. We will provide the proof for this claim later.*

($\mathbf{A}.\mathbf{5}'$)

$$\limsup_{x_2 \to \pm\infty} P(x_1, x_2, x_3, t) < \infty, \tag{4.18}$$

for any given x_1, x_3 and $t \in \mathbb{R}$.

Remark 15. *(i):* ($\mathbf{A}.\mathbf{4}$) *and* ($\mathbf{A}.\mathbf{5}$) *imply*

$$p_2(t) \equiv 0, \tag{4.19}$$

i.e., P is periodic in x_2 direction. Indeed, for all $m \in \mathbf{Z}$,

$$P(x_1, x_2 + m\Pi_2, x_3, t) = P(x_1, x_2, x_3, t) + mp_2(t),$$

one then concludes that $p_2(t)$ must equal zero by using $(\mathbf{A}.\mathbf{5})$ and letting $m \to \infty$.

(ii). The reasons and appropriateness for making these assumptions are as follows: regularity property $(\mathbf{A}.\mathbf{1})$ guarantees the pointwise convergence for various Fourier series discussed in this section. In particular, it plays an important role in the proof in Lemma 11. However, this condition could be weakened using the concept of Leray-Hopf weak solutions as defined in [23].

Since the periods Π_1 and Π_2 could be taken to be arbitrarily large, assuming the periodicity in x_1 and x_2 is a reasonable approximation for experimental channel flow simulations. A technical convenience of assuming $(\mathbf{A}.\mathbf{2})$ is the availability of the Fourier series expansion.

The boundedness assumption $(\mathbf{A}.\mathbf{3})$ comes from the definition of weak global attractor of the NSE as given in [23], however, we remark that even though there are several equivalent ways to define the global attractors for many dissipative systems (see [41], [20]), in some particular systems without having full dissipations, the appropriate notion for attractors should be defined using the boundedness (see [4]).

Assumptions $(\mathbf{A}.\mathbf{4})$ and $(\mathbf{A}.\mathbf{5})$ are physically reasonable, since the pressure drops, i.e., $p_1(t)$, $p_2(t)$, can be easily controlled by experiments.

In our following discussion, we will consider solutions of NSE (4.2) and of NS-α (4.3) in the class $\mathcal{P}$.

4.2.2 Energy Estimate

We can use the inequality (4.14) in Lemma 10 to get an inequality estimating the energy of the velocity field $u(x,t) \in \mathcal{P}$.

Proposition 4. *For $u(x,t) \in \mathcal{P}$, we have*

$$\begin{aligned} \frac{d}{dt}\int_\Omega |u|^2 d^3x + 2\nu \int_\Omega \sum_{k,l=1}^{3} (\frac{\partial u_k}{\partial x_l})^2 d^3x - \nu \int_\Omega ((\frac{\partial u_1}{\partial x_1})^2 + (\frac{\partial u_2}{\partial x_2})^2) d^3x \\ \leq \frac{\bar{p}^2 \Pi_1 \Pi_2 h}{6\nu} + \bar{p}^{3/2}(\Pi_1 + \Pi_2)h + \bar{p}^{1/2} \sum_{j=1}^{2} \int_0^{\Pi_{j'}} \int_0^h < u_j >_j^2 dx_3 dx_{j'}. \end{aligned} \tag{4.20}$$

Proof. Taking the dot product of the NSE (4.2) with u and integrating over $\Omega := [0,\Pi_1] \times [0,\Pi_2] \times [0,h]$, we get

$$\frac{1}{2}\frac{d}{dt}\int_\Omega |u|^2 d^3x + \nu \int_\Omega |\nabla u|^2 d^3x = -\sum_{j=1}^{3} \int_\Omega \frac{\partial P}{\partial x_j} u_j d^3x, \tag{4.21}$$

since the nonlinear term $\int_\Omega (u \cdot \nabla) u \cdot u d^3x$ vanishes.

Indeed, using integration by parts and the periodicity conditions (**A.2**), one gets, for $j = 1, 2$,

$$\int_0^{\Pi_j} u_k \frac{\partial}{\partial x_j}(u_j u_k) dx_j = -\int_0^{\Pi_j} u_j u_k \frac{\partial}{\partial x_j} u_k dx_j, \forall k = 1, 2, 3;$$

similarly, using the boundary condition (4.5) and integration by parts, we obtain

$$\int_0^h u_k \frac{\partial}{\partial x_3}(u_3 u_k) dx_3 = -\int_0^h u_3 u_k \frac{\partial}{\partial x_3} u_k dx_3, \forall k = 1, 2, 3;$$

so,

$$
\begin{aligned}
\int_\Omega (u\cdot\nabla)u\cdot u d^3x &= \int_\Omega \sum_{k=1}^3\sum_{j=1}^3 u_j(\frac{\partial}{\partial x_j}u_k)u_k d^3x \\
&= \int_\Omega \sum_{k=1}^3\sum_{j=1}^3 u_k\frac{\partial}{\partial x_j}(u_j u_k) d^3x \\
&= -\sum_{k=1}^3\int_\Omega (u_1u_k\frac{\partial}{\partial x_1}u_k + u_2u_k\frac{\partial}{\partial x_2}u_k + u_3u_k\frac{\partial}{\partial x_3}u_k)d^3x \\
&= -\sum_{k=1}^3\int_\Omega u_k\sum_{j=1}^3 u_j\frac{\partial}{\partial x_j}u_k d^3x \\
&= -\int_\Omega (u\cdot\nabla)u\cdot u d^3x,
\end{aligned}
$$

hence,

$$\int_\Omega (u\cdot\nabla)u\cdot u d^3x = 0.$$

Remark 16. *Observe that the above proof can be applied to show*

$$\int_\Omega (u\cdot\nabla)v\cdot v d^3x = 0, \tag{4.22}$$

for $u, v \in \mathcal{P}$.

For the term on the right hand side of (4.21), we have, by (4.16),

$$
\begin{aligned}
\int_\Omega \frac{\partial P}{\partial x_1}u_1 d^3x &= \int_0^{\Pi_2}\int_0^h \left((Pu_1)|_{x_1=\Pi_1} - (Pu_1)|_{x_1=0} - \int_0^{\Pi_1} P\frac{\partial u_1}{\partial x_1}dx_1\right)dx_3dx_2 \\
&= p_1(t)\int_0^{\Pi_2}\int_0^h u_1|_{x_1=0}dx_3dx_2 - \int_\Omega P\frac{\partial u_1}{\partial x_1}d^3x;
\end{aligned}
$$

similarly,

$$\int_\Omega \frac{\partial P}{\partial x_2} u_2 d^3x = p_2(t) \int_0^{\Pi_1} \int_0^h u_2|_{x_2=0} dx_3 dx_1 - \int_\Omega P \frac{\partial u_2}{\partial x_2} d^3x;$$

and, from no-slip boundary condition (4.5),

$$\int_\Omega \frac{\partial P}{\partial x_3} u_3 d^3x = -\int_\Omega P \frac{\partial u_3}{\partial x_3} d^3x;$$

so,

$$\begin{aligned}\int_\Omega \nabla P \cdot u d^3x = &-\int_\Omega P \nabla \cdot u d^3x + p_1(t) \int_0^{\Pi_2} \int_0^h u_1|_{x_1=0} dx_3 dx_2 \\ &+ p_2(t) \int_0^{\Pi_1} \int_0^h u_2|_{x_2=0} dx_3 dx_1 \\ &= p_1(t) \int_0^{\Pi_2} \int_0^h u_1|_{x_1=0} dx_3 dx_2 + p_2(t) \int_0^{\Pi_1} \int_0^h u_2|_{x_2=0} dx_3 dx_1,\end{aligned}$$

where in the last line, the incompressibility condition (i.e., the second equation in (4.2)) is used.

Therefore, using (4.14) in Lemma 10, relations (4.16), and denoting $j' = 3 - j$ for $j = 1, 2$, (4.21) becomes

$$\begin{aligned}&\frac{1}{2}\frac{d}{dt}\int_\Omega |u|^2 d^3x + \nu \int_\Omega |\nabla u|^2 d^3x \\ &= -p_1(t) \int_0^{\Pi_2} \int_0^h u_1|_{x_1=0} dx_3 dx_2 - p_2(t) \int_0^{\Pi_1} \int_0^h u_2|_{x_2=0} dx_3 dx_1 \\ &\leq \sum_{j=1}^{2} |p_j(t)| \int_0^{\Pi_{j'}} \int_0^h \left(< u_j >_j + \frac{\Pi_j}{2\sqrt{3}} < (\frac{\partial u_j}{\partial x_j})^2 >_j^{1/2} \right) dx_3 dx_{j'} \\ &= \sum_{j=1}^{2} |p_j(t)| \int_0^{\Pi_{j'}} \int_0^h \left(< u_j >_j + \frac{{\Pi_j}^{1/2}}{2\sqrt{3}} \Big(\int_0^{\Pi_j} (\frac{\partial u_j}{\partial x_j})^2 dx_j \Big)^{1/2} \right) dx_3 dx_{j'},\end{aligned} \tag{4.23}$$

where $<\cdot>_j$ denotes the average in the x_j direction, i.e., $<\cdot>_j := \frac{1}{\Pi_j}\int_0^{\Pi_j} \cdot dx_j$. Applying Young's inequality and (**A**.**4**), we get

$$|p_j(t)| \int_0^{\Pi_{j'}} \int_0^h \frac{\Pi_j{}^{1/2}}{2\sqrt{3}} \Big(\int_0^{\Pi_j} (\frac{\partial u_j}{\partial x_j})^2 dx_j \Big)^{1/2} dx_3 dx_{j'} \leq \frac{\bar{p}^2 \Pi_1 \Pi_2 h}{24\nu} + \frac{\nu}{2} \int_\Omega (\frac{\partial u_j}{\partial x_j})^2 d^3x,$$

for $j = 1, 2$.

Hence,

$$\begin{aligned}
&\frac{d}{dt}\int_\Omega |u|^2 d^3x + 2\nu \int_\Omega \sum_{k,l=1}^{3} (\frac{\partial u_k}{\partial x_l})^2 d^3x - \nu \int_\Omega \Big((\frac{\partial u_1}{\partial x_1})^2 + (\frac{\partial u_2}{\partial x_2})^2 \Big) d^3x \\
&\leq \frac{\bar{p}^2 \Pi_1 \Pi_2 h}{6\nu} + 2\bar{p} \sum_{j=1}^{2} \int_0^{\Pi_{j'}} \int_0^h < u_j >_j dx_3 dx_{j'} \\
&\leq \frac{\bar{p}^2 \Pi_1 \Pi_2 h}{6\nu} + 2\bar{p} \sum_{j=1}^{2} (\Pi_{j'} h)^{1/2} \Big(\int_0^{\Pi_{j'}} \int_0^h < u_j >_j^2 dx_3 dx_{j'} \Big)^{1/2} \\
&\leq \frac{\bar{p}^2 \Pi_1 \Pi_2 h}{6\nu} + \bar{p}^{3/2} (\Pi_1 + \Pi_2) h + \bar{p}^{1/2} \sum_{j=1}^{2} \int_0^{\Pi_{j'}} \int_0^h < u_j >_j^2 dx_3 dx_{j'}.
\end{aligned}$$

□

4.2.3 Properties Related to $\mathcal{P}$

We note the following properties for the velocity fields that belong to $\mathcal{P}$:

Lemma 11. *If $u(x,t) = (u_1(x,t), u_2(x,t), u_3(x,t)) \in \mathcal{P}$ is a solution of the NSE* (4.2) *(or the NS-α* (4.3)*), we have*

$$u_3(x,t) \equiv 0, \forall x \in \Omega, t \in \mathbb{R}.$$

Proof. By the periodicity (**A**.**2**) and no-slip boundary condition (4.5), we can express

u as follows,

$$u(x,t) = \sum_{k\in\mathbb{Z}^2\times\mathbb{N}} \hat{u}(t;k)E(x;k),$$

where $k = (k_1, k_2, k_3)$, $\mathbb{N}$ denotes the set of positive integers, and

$$E(x;k) := e^{2\pi i(\frac{k_1 x_1}{\Pi_1} + \frac{k_2 x_2}{\Pi_2})} \sin(\frac{\pi k_3 x_3}{h}).$$

The incompressibility condition in (4.2) can be written as

$$0 = \nabla \cdot u = \sum_{k\in\mathbb{Z}^2\times\mathbb{N}} \hat{u}_1(t;k)\frac{\partial}{\partial x_1}E(x;k) + \sum_{k\in\mathbb{Z}^2\times\mathbb{N}} \hat{u}_2(t;k)\frac{\partial}{\partial x_2}E(x;k) + \frac{\partial u_3}{\partial x_3},$$

hence,

$$\frac{\partial u_3}{\partial x_3} = -i2\pi \sum_{k\in\mathbb{Z}^2\times\mathbb{N}} \left(\hat{u}_1(k)\frac{k_1}{\Pi_1} + \hat{u}_2(k)\frac{k_2}{\Pi_2}\right) \sin(\frac{\pi k_3 x_3}{h}) e^{2\pi i(\frac{k_1 x_1}{\Pi_1} + \frac{k_2 x_2}{\Pi_2})}; \tag{4.24}$$

on the other hand,

$$\frac{\partial u_3}{\partial x_3} = \sum_{k\in\mathbb{Z}^2\times\mathbb{N}} \hat{u}_3(k)\frac{k_3\pi}{h}\cos(\frac{\pi k_3 x_3}{h}) e^{2\pi i(\frac{k_1 x_1}{\Pi_1} + \frac{k_2 x_2}{\Pi_2})}. \tag{4.25}$$

From (4.24) and (4.25), we deduce that

$$\sum_{k_3\in\mathbb{N}} \left(\hat{u}_3(k)\frac{k_3\pi}{h}\cos(\frac{\pi k_3 x_3}{h}) + 2\pi i[\hat{u}_1(k)\frac{k_1}{\Pi_1} + \hat{u}_2(k)\frac{k_2}{\Pi_2}]\sin(\frac{\pi k_3 x_3}{h})\right) = 0, \tag{4.26}$$

for all $(k_1, k_2) \in \mathbb{Z}^2$ and for all $x_3 \in [0, h]$.

Now, we can rewrite (4.26) as

$$\sum_{k_3\in\mathbb{N}}\left(\frac{k_3\pi}{2h}\hat{u}_3(k)+\pi[\hat{u}_1(k)\frac{k_1}{\Pi_1}+\hat{u}_2(k)\frac{k_2}{\Pi_2}]\right)e^{i\frac{\pi k_3 x_3}{h}}$$
$$+\sum_{k_3\in\mathbb{N}}\left(\frac{k_3\pi}{2h}\hat{u}_3(k)-\pi[\hat{u}_1(k)\frac{k_1}{\Pi_1}+\hat{u}_2(k)\frac{k_2}{\Pi_2}]\right)e^{-i\frac{\pi k_3 x_3}{h}}=0,$$

from which we obtain, for all $k_3 \in \mathbb{N}$, the followings

$$\frac{k_3\pi}{2h}\hat{u}_3(k)+\pi[\hat{u}_1(k)\frac{k_1}{\Pi_1}+\hat{u}_2(k)\frac{k_2}{\Pi_2}]=0,$$

and

$$\frac{k_3\pi}{2h}\hat{u}_3(k)-\pi[\hat{u}_1(k)\frac{k_1}{\Pi_1}+\hat{u}_2(k)\frac{k_2}{\Pi_2}]=0,$$

so,

$$\hat{u}_3(k)k_3 \equiv 0, \tag{4.27}$$

and

$$\hat{u}_1(k)\frac{k_1}{\Pi_1}+\hat{u}_2(k)\frac{k_2}{\Pi_2}\equiv 0,$$

from (4.27), we have,

$$\hat{u}_3(k)\equiv 0, \forall k\in\mathbb{Z}^2\times\mathbb{N},$$

that is, $u_3(x,t)=0$. □

The following Lemma is a generalized form of Lemma 11 without the regularity assumption (**A.1**).

Lemma 12. *For any solution* $u(x,t) = (u_1(x,t), u_2(x,t), u_3(x,t))$ *of* (4.2) *which satisfies* (**A.2**) *and* (4.5), *we have*

$$u_3(x,t) \equiv 0. \tag{4.28}$$

Proof. Different from the proof in the previous lemma, here, we provide a more general proof using the theory of distribution.

First, the solution $u(x,t)$ can be expanded (see [40]) as follows,

$$u(x,t) = \sum_{k_1,k_2\in\mathbb{Z},k_3\in\mathbb{N}} \hat{u}(t;k)E(x;k),$$

where

$$E(x;k) := e^{2\pi i(\frac{k_1x_1}{\Pi_1}+\frac{k_2x_2}{\Pi_2})}\sin(\frac{\pi k_3x_3}{h}).$$

The incompressibility condition in (4.2) can be written as

$$0 = \nabla\cdot u = \sum_{k\in\mathbb{Z}^2\times\mathbb{N}} \hat{u}_1(t;k)\frac{\partial}{\partial x_1}E(x;k) + \sum_{k\in\mathbb{Z}^2\times\mathbb{N}} \hat{u}_2(t;k)\frac{\partial}{\partial x_2}E(x;k) + \frac{\partial u_3}{\partial x_3},$$

hence,

$$\frac{\partial u_3}{\partial x_3} = -i2\pi \sum_{k\in\mathbb{Z}^2\times\mathbb{N}} \left(\hat{u}_1(k)\frac{k_1}{\Pi_1} + \hat{u}_2(k)\frac{k_2}{\Pi_2}\right)\sin(\frac{\pi k_3x_3}{h})e^{2\pi i(\frac{k_1x_1}{\Pi_1}+\frac{k_2x_2}{\Pi_2})};$$

on the other hand,

$$\frac{\partial u_3}{\partial x_3} = \sum_{k\in\mathbb{Z}^2\times\mathbb{N}} \hat{u}_3(k)\frac{k_3\pi}{h}\cos(\frac{\pi k_3 x_3}{h})e^{2\pi i(\frac{k_1x_1}{\Pi_1}+\frac{k_2x_2}{\Pi_2})}.$$

Denoting

$$k_{12}^2 = \frac{4k_1^2}{\Pi_1^2} + \frac{4k_2^2}{\Pi_2^2},$$

then

$$(-\Delta)u(x,t) = \sum_{k_1,k_2\in\mathbb{Z},k_3\in\mathbb{N}} \pi^2(k_{12}^2 + k_3^2/h^2)\hat{u}(t;k)E(x;k).$$

Recall that

$$\mathcal{T}_{t_0} = \{t \in [t_0,\infty) : |(-\Delta)u(t)|^2 < \infty\}$$

is a set of full measure in $[t_0,\infty)$, where

$$|(-\Delta)u(t)|^2 = \sum_{k_1,k_2\in\mathbb{Z},k_3\in\mathbb{N}} c_1\pi^2(k_{12}^2 + k_3^2/h^2)|\hat{u}(t;k)|^2,$$

for some dimensional constant $c_1 > 0$.

Now,

$$\frac{\partial u_3}{\partial x_3} = \sum_{k_1,k_2\in\mathbb{Z},k_3\in\mathbb{N}} -i\pi(\hat{u}_1(t;k)\frac{2k_1}{\Pi_1} + \hat{u}_2(t;k)\frac{2k_2}{\Pi_2})E(x;k),$$

hence,

$$|\frac{\partial u_3}{\partial x_3}|^2 \leq \sum_{k_1,k_2\in\mathbb{Z},k_3\in\mathbb{N}} \pi^2 k_{12}^2 |\hat{u}(t;k)|^2 \leq c_1^{-1}|(-\Delta)u(t)|^2,$$

it follows then from Fubini's theorem that, for each $t \in \mathcal{T}_{t_0}$, there exists $\mathcal{R}_t \subset [0,\Pi_1]\times[0,\Pi_2]$ that is of full measure, such that if $(x_1,x_2)\in\mathcal{R}_t$, then

$$\int_0^h |\frac{\partial u_3}{\partial x_3}|^2 dx_3 < \infty, \text{ and, } \int_0^h |u_3|^2 dx_3 < \infty.$$

To continue, we consider $t \in \mathcal{T}_{t_0}$ and $(x_1,x_2)\in\mathcal{R}_t$ being fixed, and thus $\phi(x_3) := u_3(x_1,x_2,x_3,t)$ will "be" a function of x_3 only.

We have,

$$\phi(x_3) = \sum_{k_3\in\mathbb{N}} \hat{\phi}(k_3)\sin(\frac{\pi k_3 x_3}{h}), \text{ for } x_3 \in (0,h),$$

where, $\hat{\phi}(k_3) = \sum_{k_1,k_2\in\mathbb{Z}} \hat{u}_3(k_1,k_2,k_3)e^{2i\pi(\frac{k_1x_1}{\Pi_1}+\frac{k_2x_2}{\Pi_2})}$.

Clearly, $\hat{\phi}(k_3)$ satisfies

$$\int_0^{\Pi_1}\int_0^{\Pi_2} |\hat{\phi}(k_3)|^2 dx_1 dx_2 = \Pi_1\Pi_2 \sum_{k_1,k_2\in\mathbb{Z}} |\hat{u}_3(k_1,k_2,k_3)|^2,$$

thus,

$$\begin{aligned}\int_0^{\Pi_1}\int_0^{\Pi_2} \sum_{k_3\in\mathbb{N}} |\hat{\phi}(k_3)|^2 dx_1 dx_2 &\leq \Pi_1\Pi_2 \sum_{k_1,k_2\in\mathbb{Z},k_3\in\mathbb{N}} |\hat{u}_3(k_1,k_2,k_3)|^2 \\ &\leq \frac{c_2}{h}|u_3|^2_{L^2(\Omega)} < \infty.\end{aligned}$$

Moreover,

$$
\begin{aligned}
\int\int_{\mathcal{R}_t}(\sum_{k_3\in\mathbb{N}}|\hat{\phi}(k_3)|k_3)dx_1dx_2 &\leq \int\int_{\mathcal{R}_t}(\sum_{k_3\in\mathbb{N}}|\hat{\phi}(k_3)|k_3^2\times\frac{1}{k_3})dx_1dx_2\\
&\leq \int\int_{\mathcal{R}_t}(\sum_{k_3\in\mathbb{N}}|\hat{\phi}(k_3)|^2k_3^4)^{1/2}\times(\sum_{k_3\in\mathbb{N}}\frac{1}{k_3^2})^{1/2}dx_1dx_2\\
&\leq \frac{\pi}{\sqrt{6}}\int\int_{\mathcal{R}_t}(\sum_{k_3\in\mathbb{N}}|\hat{\phi}(k_3)|^2k_3^4)^{1/2}dx_1dx_2\\
&= \frac{\pi}{\sqrt{6}}\int\int_{\mathcal{R}_t}(\sum_{k\in\mathbb{Z}^2\times\mathbb{N}}|\hat{u}_3(k)|^2k_3^4)^{1/2}dx_1dx_2\\
&\leq \frac{\pi}{\sqrt{6}}\left(\int\int_{\mathcal{R}_t}(\sum_{k\in\mathbb{Z}^2\times\mathbb{N}}|\hat{u}_3(k)|^2k_3^4)dx_1dx_2\right)^{1/2}(\Pi_1\Pi_2)^{1/2}\\
&\leq \frac{\pi\Pi_1\Pi_2h}{\sqrt{6}}\left(\sum_{k\in\mathbb{Z}^2\times\mathbb{N}}|\hat{u}_3(k)|^2(k_3^2/h^2+k_{12}^2)^2\right)^{1/2}\\
&< \infty,
\end{aligned}
$$

therefore,

$$\sum_{k_3\in\mathbb{N}}|\hat{\phi}(k_3)|k_3 < \infty,$$

for a.e. $(x_1, x_2) \in [0, \Pi_1] \times [0, \Pi_2]$.

It follows immediately that the series

$$\sum_{k_3\in\mathbb{N}}\hat{u}_3(k)\sin(\frac{\pi k_3 x_3}{h})e^{2\pi i(\frac{k_1x_1}{\Pi_1}+\frac{k_2x_2}{\Pi_2})}$$

and

$$\sum_{k_3\in\mathbb{N}}\hat{u}_3(k)\cos(\frac{\pi k_3 x_3}{h})e^{2\pi i(\frac{k_1x_1}{\Pi_1}+\frac{k_2x_2}{\Pi_2})}$$

are both absolutely convergent. This ensures that the two different Fourier series (4.24) and (4.25) must be "equal", and their sums be continuous.

Therefore,

$$\sum_{k_3\in\mathbb{N}}\left(\hat{u}_3(k)\frac{k_3\pi}{h}\cos(\frac{\pi k_3x_3}{h})+2\pi i[\hat{u}_1(k)\frac{k_1}{\Pi_1}+\hat{u}_2(k)\frac{k_2}{\Pi_2}]\sin(\frac{\pi k_3x_3}{h})\right)=0,$$

for all $(k_1,k_2)\in\mathbb{Z}^2$ and for all $x_3\in[0,h]$,

or, equivalently,

$$\begin{aligned}&\sum_{k_3\in\mathbb{N}}\left(\frac{k_3\pi}{2h}\hat{u}_3(k)+\pi[\hat{u}_1(k)\frac{k_1}{\Pi_1}+\hat{u}_2(k)\frac{k_2}{\Pi_2}]\right)\exp{(i\frac{\pi k_3x_3}{h})}\\&+\sum_{k_3\in\mathbb{N}}\left(\frac{k_3\pi}{2h}\hat{u}_3(k)-\pi[\hat{u}_1(k)\frac{k_1}{\Pi_1}+\hat{u}_2(k)\frac{k_2}{\Pi_2}]\right)\exp{(-i\frac{\pi k_3x_3}{h})}=0,\end{aligned}$$

from which we obtain, for all $k_3\in\mathbb{N}$, the followings

$$\frac{k_3\pi}{2h}\hat{u}_3(k)+\pi[\hat{u}_1(k)\frac{k_1}{\Pi_1}+\hat{u}_2(k)\frac{k_2}{\Pi_2}]=0,$$

and

$$\frac{k_3\pi}{2h}\hat{u}_3(k)-\pi[\hat{u}_1(k)\frac{k_1}{\Pi_1}+\hat{u}_2(k)\frac{k_2}{\Pi_2}]=0.$$

Therefore,

$$\hat{u}_3(k)k_3\equiv0,$$

and

$$\hat{u}_1(k)\frac{k_1}{\Pi_1} + \hat{u}_2(k)\frac{k_2}{\Pi_2} \equiv 0.$$

Hence,

$$\hat{u}_3(k) \equiv 0, \forall k \in \mathbb{Z}^2 \times \mathbb{N},$$

that is, $u_3(x,t) = 0$. $\square$

Besides $u_3 = 0$, further relations between the three components of the u can be exploited: roughly speaking, u_1 and u_2 are not totally independent, one of them is, at least locally, a function of the other component.

Theorem 5.

$$\frac{\partial(u_1,u_2)}{\partial(x_1,x_2)} = \begin{vmatrix} \frac{\partial u_1}{\partial x_1} & \frac{\partial u_1}{\partial x_2} \\ \frac{\partial u_2}{\partial x_1} & \frac{\partial u_2}{\partial x_2} \end{vmatrix} = 0. \tag{4.29}$$

Proof. (4.29) is obtained by using the fourth relation in (4.30), and the fact that the left hand side in (4.31) equals zero. $\square$

From Lemma 11, the NSE (4.2) becomes

$$\begin{cases} \frac{\partial}{\partial t}u_1 + u_1\frac{\partial}{\partial x_1}u_1 + u_2\frac{\partial}{\partial x_2}u_1 - \nu(\frac{\partial^2}{\partial x_1^2} + \frac{\partial^2}{\partial x_2^2} + \frac{\partial^2}{\partial x_3^2})u_1 = -\frac{\partial}{\partial x_1}P, \\ \frac{\partial}{\partial t}u_2 + u_1\frac{\partial}{\partial x_1}u_2 + u_2\frac{\partial}{\partial x_2}u_2 - \nu(\frac{\partial^2}{\partial x_1^2} + \frac{\partial^2}{\partial x_2^2} + \frac{\partial^2}{\partial x_3^2})u_2 = -\frac{\partial}{\partial x_2}P, \\ 0 = -\frac{\partial}{\partial x_3}P, \\ \frac{\partial}{\partial x_1}u_1 + \frac{\partial}{\partial x_2}u_2 = 0. \end{cases} \tag{4.30}$$

Proposition 5. *Let $u(x,t) \in \mathcal{P}$, then $P = P(x_1, x_2, t)$ is harmonic in the space variables x_1 and x_2.*

Proof. From (4.30), by taking $\partial/\partial x_1$ in the first equation and $\partial/\partial x_2$ in the second equation and then summing the two resulting equations, we can obtain the following,

$$(\frac{\partial u_1}{\partial x_1})^2 + 2\frac{\partial u_1}{\partial x_2}\frac{\partial u_2}{\partial x_1} + (\frac{\partial u_2}{\partial x_2})^2 = -(\frac{\partial^2}{\partial x_1^2} + \frac{\partial^2}{\partial x_2^2})P, \tag{4.31}$$

where $P = P(x_1, x_2, t)$ is independent of x_3 (see the third equation in (4.30)).

In (4.31), the left hand side (LHS) takes values zero at $x_3 = 0$ and $x_3 = h$, while the right hand side (RHS) is independent of x_3, hence

$$-(\frac{\partial^2}{\partial x_1^2} + \frac{\partial^2}{\partial x_2^2})P = 0, \tag{4.32}$$

for all $x_1, x_2 \in \mathbb{R}$. $\square$

From (4.16), we see $P(x_1 + n\Pi_1, x_2, t) - P(x_1, x_2, t) = np_1(t), \forall n \in \mathbb{N}^+$. Now, for any $y \in \mathbb{R}^+$, choose $n \in \mathbb{N}$, such that $n\Pi_1 \leq y < (n+1)\Pi_1$, then

$$\begin{aligned} P(y, x_2, t) &= P(y - n\Pi_1, x_2, t) + np_1(t) \\ &\leq \sup\{|P(x_1, x_2, t)| : 0 \leq x_1 < \Pi_1\} + np_1(t) \\ &\leq \sup\{|P(x_1, x_2, t)| : 0 \leq x_1 < \Pi_1\} + \frac{y}{\Pi_1}\bar{p}; \end{aligned}$$

similar arguments apply to the case when $y \leq 0$, and we get the next result.

Lemma 13. *Let $u(x,t) \in \mathcal{P}$ be a solution of* (4.2)*. The estimate*

$$P(y, x_2, t) \leq \sup\{|P(x_1, x_2, t)| : 0 \leq x_1 < \Pi_1\} + \frac{|y|}{\Pi_1}\bar{p} \tag{4.33}$$

holds for all $y, x_2, t \in \mathbb{R}$, where $\bar{p}$ is as given in (**A**.**4**).

Moreover, we have

Lemma 14. *For the pressure related term $P = P(x_1, x_2, t)$, we have,*

$$\sup_{x_1,x_2} |\frac{\partial}{\partial x_1} P(x_1, x_2, t)| < \infty, \tag{4.34}$$

for all $t \in \mathbb{R}$.

Proof. According to Poisson's formula (see [30]; see also [27]), we have, for any $a > 0,\ a \in \mathbb{R}$,

$$P(z,t) = \int_{|y|=a} H(y,z)P(y,t)dy, \quad \text{for } |z| < a,$$

where $z = (x_1, x_2)$, and

$$H(y,z) = \frac{1}{2\pi a} \frac{a^2 - |z|^2}{|z-y|^2}.$$

So,

$$\begin{aligned} P(z,t) = P(x_1,x_2,t) &= \frac{1}{2\pi} \int_{|y|=1} \frac{1 - |\frac{z}{a}|^2}{|\frac{z}{a} - y|^2} P(ay_1, ay_2, t)dy \qquad (4.35) \\ &= \frac{1}{2\pi} \int_0^{2\pi} \frac{1 - \frac{x_1^2+x_2^2}{a^2}}{1 - 2(\frac{x_1^2+x_2^2}{a^2})^{1/2} \cos(\theta - \omega) + \frac{x_1^2+x_2^2}{a^2}} P(a\cos\theta, a\sin\theta, t)d\theta, \end{aligned}$$

where $x_1 + ix_2 = |z|e^{i\omega}$ and $y_1 + iy_2 = |y|e^{i\theta}$.

However, we will work with the following equivalent form of (4.35), namely,

$$P(x_1,x_2,t) = \frac{1}{2\pi} \int_0^{2\pi} H(z/a,\theta)P(a\cos\theta, a\sin\theta, t)d\theta, \tag{4.36}$$

where, for $|z| < 1$,

$$
\begin{aligned}
H(z,\theta) &= \frac{1 - x_1^2 - x_2^2}{(x_1 - \cos\theta)^2 + (x_2 - \sin\theta)^2} \\
&= \frac{1 - x_1^2 - x_2^2}{1 + x_1^2 + x_2^2 - 2(x_1\cos\theta + x_2\sin\theta)}.
\end{aligned}
$$

A direct calculation gives that

$$
\frac{\partial}{\partial x_1} H(x_1, x_2, \theta) = \frac{-4x_1 + 2\cos\theta + 2x_1^2\cos\theta - 2x_2^2\cos\theta + 4x_1x_2\sin\theta}{[1 + x_1^2 + x_2^2 - 2(x_1\cos\theta + x_2\sin\theta)]^2},
$$

this implies, for $a > 4|z| + 1$, the following

$$
\begin{aligned}
\frac{\partial}{\partial x_1} H(z/a, \theta) &= \frac{1}{a}\frac{\partial H}{\partial x_1}(z,\theta)|_{z=z/a} \\
&\leq \frac{4(\frac{|x_1|}{a} + 2\frac{|z|^2}{a^2} + 1)}{a(1 + \frac{|z|^2}{a^2} - 2\frac{|z|}{a})^2} \\
&\leq 32.
\end{aligned}
$$

Therefore, from (4.36), recalling the bound (4.33) given in Lemma 13, we have,

$$
|\frac{\partial}{\partial x_1} P(x_1, x_2, t)| \leq \frac{32\bar{p}}{\Pi_1} + 32a\sup\{|P(x_1, x_2, t)| : 0 \leq x_1 < \Pi_1\},
$$

where $\sup\{|P(x_1, x_2, t)| : 0 \leq x_1 < \Pi_1\}$ is a periodic function in x_2 with period Π_2, and hence

$$
\max_{x_2 \in \mathbb{R}} \sup\{|P(x_1, x_2, t)| : 0 \leq x_1 < \Pi_1\} < \infty,
$$

consequently,

$$\sup_{x_1,x_2} |\frac{\partial}{\partial x_1} P(x_1,x_2,t)| < \infty,$$

for all $t \in \mathbb{R}$. □

Moreover, we have the following explicit formula for the pressure related term $P(x,t)$.

Proposition 6. *The term $P = P(x_1,x_2,t)$ in the Navier-Stokes equations* (4.30) *is of the following form,*

$$\begin{aligned} P(x_1,x_2,t) &= \tilde{p}_0(t) + x_1\tilde{p}_1(t) \\ &= \tilde{p}_0(t) + x_1 p_1(t)/\Pi_1. \end{aligned} \tag{4.37}$$

Proof. Using (4.34) in Lemma 14, and Liouville's theorem for harmonic function $\frac{\partial}{\partial x_1}P(x_1,x_2,t)$, we conclude that

$$\frac{\partial}{\partial x_1} P(x_1,x_2,t) = \tilde{p}_1(t),$$

for some function $\tilde{p}_1(t)$ of time t, so that

$$P = P(x_1,x_2,t) = \tilde{p}_0(x_2,t) + x_1\tilde{p}_1(t), \tag{4.38}$$

and, due to the harmonicity of $P(x_1,x_2,t)$ in x_1 and x_2,

$$\frac{\partial^2}{\partial x_2^2}\tilde{p}_0(x_2,t) = 0,$$

so, $\tilde{p}_0(x_2,t)$ is a linear function in x_2, but then periodicity of $P(x_1,x_2,t)$ in x_2 would imply that $\tilde{p}_0(x_2, t)$ is only a function of time t, say

$$\tilde{p}_0(x_2, t) = \tilde{p}_0(t).$$

Finally, the second equality in (4.37), namely,

$$\Pi_1 \tilde{p}_1(t) = p_1(t), \tag{4.39}$$

follows from (4.38) and relation (4.16). □

Remark 17. *It follows from the harmonicity of the pressure related term P and Proposition* 6 *that* (**A.5**) *can be replaced by a weaker condition, namely,*

$$\limsup_{x_2 \to \pm\infty} P(x_1, x_2, x_3, t) < \infty, \tag{4.40}$$

for any given x_1, x_3 and $t \in \mathbb{R}$.

4.3 A Simple Reynolds Averaging

The Reynolds type averaging with which we will work throughout is given in the following definition:

Definition 2. *For any given scalar/vector function $\phi = \phi(x)$,*

$$< \phi > (x_3) := \frac{1}{\Pi_1 \Pi_2} \int_0^{\Pi_1} \int_0^{\Pi_2} \phi \, dx_2 dx_1. \tag{4.41}$$

Applying the operation $< \cdot >$ to the first and second equations in (4.30) , one gets the following Reynolds type equations

$$\frac{\partial}{\partial t}\begin{pmatrix} < u_1(t) > \\ < u_2(t) > \end{pmatrix} - \nu \frac{\partial^2}{\partial x_3^2}\begin{pmatrix} < u_1(t) > \\ < u_2(t) > \end{pmatrix} = -\begin{pmatrix} \frac{p_1(t)}{\Pi_1} \\ \frac{p_2(t)}{\Pi_2} \end{pmatrix}. \tag{4.42}$$

Using (4.19), we can easily obtain,

Proposition 7. *For all $u(x,t) \in \mathcal{P}$, we have*

$$< u_2(t) > (x_3) \equiv 0, \ \forall x_3 \in [0,h], \ t \in \mathbb{R}. \tag{4.43}$$

Therefore, the averaged velocity field takes the form

$$< u(t) > (x_3) = \begin{pmatrix} < u_1(t) > (x_3) \\ < u_2(t) > (x_3) \\ < u_3(t) > (x_3) \end{pmatrix} = \begin{pmatrix} < u_1(t) > (x_3) \\ 0 \\ 0 \end{pmatrix} \tag{4.44}$$

Theorem 6. *For given $p_1(t)$ and $p_2(t)$, the set*

$$\{< u >: u \in \mathcal{P}\}$$

is a nonzero singleton.

Proof. Let u and v be any two elements in $\mathcal{P}$ which are the solutions of the NSE (4.2). Denoting

$$w(x_3,t) = (w_1(x_3,t), w_2(x_3,t), w_3(x_3,t)) := < u(t) > (x_3) - < v(t) > (x_3),$$

then

$$w_2(x_3,t) = w_3(x_3,t) = 0,$$

for all $x_3 \in [0,h]$, $t \in \mathbb{R}$.

Moreover, from (4.42),

$$\frac{\partial}{\partial t} w_1(x_3,t) - \nu \frac{\partial^2}{\partial x_3^2} w_1(x_3,t) = 0,$$

hence,

$$\frac{1}{2}\frac{d}{dt}\int_0^h w_1^2(x_3,t)dx_3 + \nu \int_0^h |\frac{\partial w_1}{\partial x_3}(x_3,t)|^2 dx_3 = 0.$$

Notice that

$$w_1(x_3,t)|_{x_3=0,h} = 0,$$

then Poincaré inequality (4.9) is applicable, so we obtain,

$$\frac{1}{2}\frac{d}{dt}\int_0^h w_1^2(x_3,t)dx_3 + \frac{\nu}{h^2}\int_0^h w_1^2(x_3,t)dx_3 \leq 0,$$

therefore, for any $t_0 < t$,

$$0 \leq \int_0^h w_1^2(x_3,t)dx_3 \leq e^{-\frac{2}{h^2}(t-t_0)} \int_0^h w_1^2(x_3,t_0)dx_3,$$

the uniqueness follows from using assumption (**A**.**3**) and letting $t_0 \to -\infty$ in the last inequality.

Finally, if this singleton is zero, then from (4.42), $p_1(t)$ must be zero, which contradicts with the assumption ($\mathbf{A}.\mathbf{4}$) that $p_1(t)$ is never zero. $\square$

By (4.42), $< u_1(t) > (x_3)$ satisfies

$$\frac{\partial}{\partial t} < u_1(t) > (x_3) - \nu \frac{\partial^2}{\partial x_3^2} < u_1(t) > (x_3) = -p_1(t)/\Pi_1, \tag{4.45}$$

with boundary conditions

$$< u_1(t) > (x_3)|_{x_3=0,h} = 0. \tag{4.46}$$

In order to get an explicit form of $< u_1(t) > (x_3)$, we apply the Duhamel principal in a form adapted for (4.45) and (4.46). We can obtain the following integral representation for $< u_1(t) > (x_3)$.

Proposition 8. *The following relation holds for* $u(x,t) \in \mathcal{P}$

$$< u_1(t) > (x_3) = \int_{-\infty}^{t} K(x_3, t-\tau) p_1(\tau) d\tau, \tag{4.47}$$

where, the kernel function $K(x,t)$ *is defined by the series,*

$$K(x,t) = \sum_{k=1}^{\infty} \frac{2\left((-1)^k - 1\right)}{\Pi_1 k \pi} e^{-\nu(\frac{\pi k}{h})^2 t} \sin \frac{\pi k x}{h}. \tag{4.48}$$

Proof. It is well known that (see [40]) an orthonormal basis for

$$\mathcal{D}(A) := \{\phi(x) \in C^2([0,h]) : \phi(x)|_{x=0,h} = 0\}, \tag{4.49}$$

where $A := -\frac{\partial^2}{\partial x^2}$, is

$$\left\{\sqrt{2/h}\sin(\pi kx/h)\right\}_{k=1}^{\infty}.$$

Therefore, $< u_1(t) > (x_3)$ can be expanded as,

$$< u_1(t) > (x_3) = \sum_{k=1}^{\infty} < u_1(t) >\hat{}\,(k)\sqrt{\frac{2}{h}}\sin\frac{\pi k x_3}{h}.$$

To obtain an explicit form for $< u_1(t) >\hat{}\,(k)$, the coefficients in the Fourier sine series expansion, we introduce the Fourier expansion in equation (4.45) to get

$$\begin{aligned}\frac{\partial}{\partial t} < u_1(t) >\hat{}\,(k) + \nu(\frac{\pi k}{h})^2 < u_1(t) >\hat{}\,(k) &= \int_0^h -\frac{p_1(t)}{\Pi_1}\sqrt{\frac{2}{h}}\sin\frac{\pi k x_3}{h}dx_3 \\ &= -\sqrt{\frac{2}{h}}\frac{p_1(t)}{\Pi_1}\frac{h}{\pi k}\left(1-(-1)^k\right),\end{aligned}$$

whence, for $t_0 < t$,

$$\begin{aligned}< u_1(t) >\hat{}\,(k) =& e^{-\nu(\frac{\pi k}{h})^2(t-t_0)} < u_1(t_0) >\hat{}\,(k) \\ &+ \sqrt{\frac{2}{h}}\frac{h}{\Pi_1 \pi k}\left((-1)^k - 1\right)\int_{t_0}^t e^{-\nu(\frac{\pi k}{h})^2(t-\tau)}p_1(\tau)d\tau.\end{aligned}$$

Letting $t_0 \to -\infty$ and using $(\mathbf{A}.\mathbf{3})$, we have

$$< u_1(t) >\hat{}\,(k) = \sqrt{\frac{2}{h}}\frac{h}{\Pi_1 \pi k}\left((-1)^k - 1\right)\int_{-\infty}^t e^{-\nu(\frac{\pi k}{h})^2(t-\tau)}p_1(\tau)d\tau,$$

and the result follows. $\square$

Lemma 15. *The kernel function $K(x,t)$ defined by* (4.48) *satisfies the following properties:*

1.

$$\int_{-\infty}^{t} K(x,t-\tau)d\tau = \frac{-1}{2\Pi_1\nu}x(h-x), \tag{4.50}$$

2.

$$\frac{\partial}{\partial t}K(x,t) - \nu\frac{\partial^2}{\partial x^2}K(x,t) = 0. \tag{4.51}$$

Proof.

$$\begin{aligned}
\int_{-\infty}^{t} K(x,t-\tau)d\tau &= \int_{-\infty}^{t}\sum_{k=1}^{\infty}\frac{2((-1)^k-1)}{\Pi_1 k\pi}e^{-\nu(\frac{\pi k}{h})^2(t-\tau)}\sin(\frac{\pi kx}{h})d\tau \\
&= \sum_{k=1}^{\infty}\int_{-\infty}^{t}\frac{2((-1)^k-1)}{\Pi_1 k\pi}e^{-\nu(\frac{\pi k}{h})^2(t-\tau)}\sin(\frac{\pi kx}{h})d\tau \\
&= \sum_{k=1}^{\infty}\frac{2((-1)^k-1)}{\Pi_1 k\pi}\sin(\frac{\pi kx}{h})\int_{-\infty}^{t}e^{-\nu(\frac{\pi k}{h})^2(t-\tau)}d\tau \\
&= \sum_{k=1}^{\infty}\frac{2((-1)^k-1)}{\Pi_1 k\pi}\sin(\frac{\pi kx}{h})\frac{h^2}{\nu(\pi k)^2},
\end{aligned}$$

thus, (4.50) is obtained by comparing the above with the following expansion

$$x(h-x) = \sum_{k=1}^{\infty}\frac{4h^2(1-(-1)^k)}{(\pi k)^3}\sin(\frac{\pi kx}{h}). \tag{4.52}$$

Furthermore, (4.51) follows from a direct computation using the series representation (4.48) of $K(x,t)$. □

Using Proposition 8 and (4.50) in Lemma 15, we recover the classic Poiseuille flow in the particular case when $p_1(t)$ is a constant.

Theorem 7. *If, moreover, $p_1(t) = p_{10} < 0$ for some constant $p_{10} \in \mathbb{R}$, then*

$$< u_1(t) > (x_3) = \mu x_3(h - x_3), \tag{4.53}$$

where the coefficient μ is given by

$$\mu = \frac{-p_{10}}{2\Pi_1 \nu}. \tag{4.54}$$

Remark 18. *From Theorem 6 and Theorem 7, we see that*

$$\{< u >: u \in \mathcal{P}, p_1(t) = p_{10}\} = \{(\frac{-p_{10}}{2\Pi_1 \nu} x_3(h - x_3), 0, 0)\}. \tag{4.55}$$

From (4.42), one can easily deduce the following simple mathematical connection between the NSE (4.2) and the NS-α (4.3).

Theorem 8. *Let $u(x,t) \in \mathcal{P}$. Define, for any $\alpha \in \mathbb{R}$, $\alpha > 0$,*

$$V(x,t) = (1 - \alpha^2 \frac{\partial^2}{\partial x_3^2}) < u_1(t) > (x_3), \tag{4.56}$$

and,

$$Q(x,t) = -\frac{1}{2}\left(< u_1(t) >^2 (x_3) - \alpha^2 \big(\frac{\partial}{\partial x_3} < u_1(t) > (x_3)\big)^2\right) + \frac{x_1 p_1(t)}{\Pi_1}, \tag{4.57}$$

then,

$$\begin{cases} \frac{\partial}{\partial t} V(x,t) - \nu \frac{\partial^2}{\partial x_3^2} V(x,t) = -\frac{\partial}{\partial x_1} Q, \\ 0 = -\frac{\partial}{\partial x_2} Q, \\ V \frac{\partial}{\partial x_3} < u_1(t) > (x_3) = -\frac{\partial}{\partial x_3} Q \end{cases} \tag{4.58}$$

Equivalently, $(< u_1(t) > (x_3), 0, 0)$ is a solution of the NS-α (4.3) with corresponding

$Q(x,t)$ *defined by* (4.57).

4.4 Transition Mechanism from NSE to NS-α

4.4.1 Motivations

The flows we considered here are driven by the pressure drop, as we only consider a potential body force, thus, the pressure term will play essential roles in the study of these equations. Moreover, from (4.47), we see that, for any $T > 0$,

$$
\begin{aligned}
U_1(x_3) :&= \frac{1}{T}\int_0^T < u_1(t) > (x_3)dt \\
&= \frac{1}{T}\int_0^T \int_{-\infty}^t K(x_3, t-\sigma)p_1(\sigma)d\sigma dt \\
&\overset{\xi=t-\sigma}{=} \int_0^\infty K(x_3,\xi)P_1(\xi)d\xi \\
&= \sum_{k=1}^\infty \frac{2((-1)^k-1)}{\Pi_1 k\pi}\left(\int_0^\infty e^{-\nu(\frac{k\pi}{h})^2\xi}P_1(\xi)d\xi\right)\sin\frac{k\pi x_3}{h},
\end{aligned}
$$

where $P_1(\xi) = \frac{1}{T}\int_0^T p_1(t-\xi)dt$. It follows from the Plancherel's theorem that

$$
\begin{aligned}
||U_1||^2_{L^2([0,h])} &= \sum_{k=1}^\infty \frac{4((-1)^k-1)^2}{(\Pi_1 k\pi)^2}\left(\int_0^\infty e^{-\nu(\frac{k\pi}{h})^2\xi}P_1(\xi)d\xi\right)^2 ||\sin\frac{k\pi x_3}{h}||^2_{L^2([0,h])} \\
&= \sum_{k=1}^\infty \frac{2h((-1)^k-1)^2}{(\Pi_1 k\pi)^2}\left(\int_0^\infty e^{-\nu(\frac{k\pi}{h})^2\xi}P_1(\xi)d\xi\right)^2 \\
&\leq (\text{use the bound for } p_1(t) \text{ in } (\mathbf{A.4})) \\
&\leq \bar{p}^2\sum_{k=1}^\infty \frac{2h^5((-1)^k-1)^2}{\Pi_1^2\nu^2 k\pi^6} \\
&\leq \bar{p}^2\frac{2h^5}{\Pi_1^2\nu^2(\pi)^6}\sum_{k=1}^\infty \frac{4}{(2k-1)^2}.
\end{aligned}
$$

Using the identity

$$\sum_{k=1}^{\infty} \frac{1}{(2k-1)^2} = \frac{\pi^2}{8}, \tag{4.59}$$

we obtain the following theorem

Theorem 9. *If the NSE describe the fluid, then necessarily we have*

$$Re \leq \frac{\bar{p}h^3}{\Pi_1 \nu^2 \pi^2}, \tag{4.60}$$

where,

$$Re := \frac{h^{1/2}||U_1||_{L^2([0,h])}}{\nu} \tag{4.61}$$

is the Reynolds number related to the flow.

From (4.60) in Proposition 9 we see that the magnitude of the pressure drop forms an upper estimate of that of the velocity in the channel, thus if the magnitude of flows velocity become significant, or equivalently, the Reynolds number Re of the flow is large, then the solution of the velocity from the NSE will no longer satisfy this upper estimate. At this moment, the fluid will "select" the NS-α model instead of the NSE. This motivates our considerations in this section.

The Prandtl's wall roughness idea suggests our conjecture for the transition from the NSE to the NS-α. That is, the roughness of the wall in the x_3 direction may "introduce" the operator $(1 - \alpha^2\Delta)$.

To model the effect of the wall roughness onto the fluid flow, it is necessary to consider the general channel geometry $\mathcal{O} = \mathbb{R} \times \mathbb{R} \times [x_3^{(l)}, x_3^{(u)}]$, since we have to consider the effects of both the upper and lower walls. However, we stress that, in order to keep the symmetry property of the fluid flow, it is reasonable to assume that the wall roughness also satisfies the appropriate symmetry property such that the center of the channel does not move after taking into account the change of vertical distance of the channel due to the wall rugosities, and consequently, only the change of the height matters. Therefore, without loss of generality, it suffices to consider the particular case where $x_3^{(l)} = 0$ and $x_3^{(u)} = h$.

4.4.2 Roughness Model

We consider the solution $< u_1(t) > (x_3)$, represented in (4.47) to be also a function of the wall height h, that is,

$$< u_1(t) > (x_3; h) = \int_{-\infty}^{t} K(x_3, t-\tau; h) p_1(\tau) d\tau, \tag{4.62}$$

where

$$K(x,t;h) = \sum_{k=1}^{\infty} \frac{2\left((-1)^k - 1\right)}{\Pi_1 k\pi} e^{-\nu(\frac{\pi k}{h})^2 t} \sin\frac{\pi k x}{h}. \tag{4.63}$$

Lemma 16. *The kernel $K(x,t;h)$ also satisfies,*

$$\frac{\partial K}{\partial h} = -\frac{x}{h}\frac{\partial K}{\partial x} - \frac{2t}{h}\frac{\partial K}{\partial t}. \tag{4.64}$$

We introduce the effect of the wall roughness to update the pressure drop $p_1(t)$ by considering it to be a function of the roughness $\mathfrak{R} = \mathfrak{R}(x_1, x_2)$, which is only a function of the variables x_1 and x_2.

Motivated by (4.45), we replace $p_1(t)$ by the following expression,

$$p_1(t;h+\mathfrak{R}) := \Pi_1 \left(-\frac{\partial}{\partial t} < u_1(t) > (x_3; h+\mathfrak{R}) + \nu \frac{\partial^2}{\partial x_3^2} < u_1(t) > (x_3; h+\mathfrak{R}) \right), \tag{4.65}$$

where, recall the Reynolds type average $< \cdot >= \frac{1}{\Pi_1 \Pi_2} \int_0^{\Pi_1} \int_0^{\Pi_2} \cdot dx_2 dx_1$, defined in (4.41).

Now, we use the first order linear approximation, that is, we approximate $p_1(t; h+\mathfrak{R})$ by

$$\Pi_1 \left((-\frac{\partial}{\partial t} + \nu \frac{\partial^2}{\partial x_3^2}) < u_1(t) > (x_3; h) + \mathfrak{R}(x_1, x_2)(-\frac{\partial}{\partial t} + \nu \frac{\partial^2}{\partial x_3^2}) \frac{\partial}{\partial h} < u_1(t) > (x_3; h) \right). \tag{4.66}$$

By the identity (4.64) in Lemma 16, (4.66) equals

$$p_1(t) + \Pi_1 \mathfrak{R}(x_1, x_2)(-\frac{\partial}{\partial t} + \nu \frac{\partial^2}{\partial x_3^2}) H, \tag{4.67}$$

where $H = \int_{-\infty}^{t} \left((-\frac{x_3}{h}) \frac{\partial K}{\partial x_3}(x_3, t-\tau; h) - \frac{2(t-\tau)}{h} \frac{\partial K}{\partial t}(x_3, t-\tau; h) \right) p_1(\tau) d\tau$.
For (4.67), after using (4.51) in Lemma 15, can be simplified to be

$$p_1(t) \left(1 + \mathfrak{R}(x_1, x_2) \Pi_1 \frac{x_3}{h} \frac{\partial K}{\partial x_3}(x_3, 0; h) \right). \tag{4.68}$$

However, the expression in (4.68) depends on x_3, thus, we take average in x_3 in

(4.68) to get the form of updated $p_1(t)$, namely,

$$
\begin{aligned}
p_1^{new}(t) &:= \frac{1}{h}\int_0^h p_1(t)\left(1+\Pi_1\mathfrak{R}(x_1,x_2)\frac{x_3}{h}\frac{\partial K}{\partial x_3}(x_3,0;h)\right)dx_3 \qquad (4.69)\\
&= p_1(t)\left(1+\frac{\mathfrak{R}}{h}\sum_{k=1}^{\infty}\frac{2\left((-1)^k-1\right)^2}{(k\pi)^2}\right)\\
&= (\text{use } (4.59))\\
&= p_1(t)\left(1+\frac{\mathfrak{R}}{h}\right).
\end{aligned}
$$

Replacing $p(t)$ in the expression (4.62) by the updated form (4.69), we get the following,

$$
\begin{aligned}
&\int_{-\infty}^{t} K(x_3,t-\tau;h)p_1^{new}(\tau)d\tau \qquad (4.70)\\
&= \int_{-\infty}^{t} K(x_3,t-\tau;h)p_1(\tau)d\tau + \int_{-\infty}^{t} K(x_3,t-\tau;h)\frac{\mathfrak{R}}{h}p_1(\tau)d\tau\\
&=< u_1(t) > (x_3;h) + \frac{1}{h}\int_{-\infty}^{t}\sum_{k=1}^{\infty}\frac{2((-1)^k-1)}{\Pi_1 k\pi}e^{-\nu(\frac{k\pi}{h})^2(t-\tau)}\mathfrak{R})\left(\sin\frac{k\pi x_3}{h}\right)p_1 d\tau.
\end{aligned}
$$

In order to update $< u_1(t) > (x_3;h)$, we need a mathematical description for the roughness. Our mathematical definition of the wall roughness is an application of Mandelbrot's paradigm(see [34]) that the roughness of a wall is produced by a sum of small decreasing rugosities of the walls which are assumed to be connected by adequate self-similarities.

For this purpose, we first introduce the following definitions: for $j = 1,2$, let $r_j : \mathbb{R} \to \mathbb{R}$ denote a function satisfying

$$r_j(x) = r_j(x+\pi_j), \forall x \in \mathbb{R},$$

where

$$\pi_j = \frac{\Pi_j}{N_j}, \qquad r_j(x) = \begin{cases} r_j(0) & |x| < \delta_j \\ 0 \quad \delta_j \leq |x| < \frac{\pi_j}{2} \end{cases}$$

for some $N_j \in \mathbb{N}, N_j > 0$ $(j = 1, 2)$, and $2\delta_1, 2\delta_2$ are the lengths of the edges in the x_1 and x_2 directions, respectively, of the rectangular parallelepiped we will define later.

In fact, we note that the periods π_j $(j = 1, 2)$ are properties of the walls and it is plausible to consider that our previously defined periods Π_j are connected to the $\pi_j' s, j = 1, 2$.

The progenitor of the roughness system is

$$rug_1 = \{x = [x_1, x_2, x_3] : 0 \leq x_3 \leq \frac{r_1(x_1)r_2(x_2)}{h}\}.$$

Note that rug_1 is a system of rectangular parallelepipeds with volume

$$vol_1 = \frac{4\delta_1\delta_2 r_1(0)r_2(0)}{h}.$$

The descendant generations of the rugosities rug_n $(n = 2, 3, ...)$ are

$$rug_n = \{x = [x_1, x_2, x_3] : 0 \leq x_3 \leq \frac{r_1(nx_1)r_2(nx_2)}{n^2 h}\}$$

with volume

$$vol_n = \frac{1}{n^4} vol_1.$$

Since the roughness is the superposition of different rugosities that bear similarities, mathematically we have

$$\mathfrak{R}(x_1, x_2) = \sum_{n=1}^{\infty} \mathfrak{R}_{(n,k)}(x_1, x_2), \tag{4.71}$$

where

$$\mathfrak{R}_{(n,k)}(x_1, x_2) = e(n)s(n, k)\frac{r_1(nx_1)r_2(nx_2)}{n^2 h}, \tag{4.72}$$

where $e(n)$ represents the effect of the rugosity rug_n onto the fluid and $s(n, k)$ represents how the rugosities "pick" the wavenumber. When the fluid flows through the wall, the smallest rectangular parallelepiped will have the strongest effect to the fluid. So the smaller the volume is, the stronger it effects. It is reasonable to assume $e(n) = \frac{c_1}{vol_n} = \frac{c_1 n^4}{vol_1}$, where c_1 is a dimensional constant.

As mentioned in the introduction, assuming that the rugosity rug_n will only affect the wave numbers having size comparable with its own size, the rugosity will "see" the size of the wavenumber of the fluid field, and "pick" its favorable wavenumber to interact. Also from (4.62) and (4.63) we notice that k needs to be odd. Similarly, we need n to be odd. So we can assume $s(n, k) = \chi_{(\frac{h-\epsilon_n h}{n}, \frac{h-\epsilon_{n-1} h}{n-1}]}(\frac{h}{k}) \times \chi_{2\mathbb{Z}+1}(n)$, where $\epsilon_n = h^{-1} h_1 \sum_{l=1}^{n} \frac{1}{l^2}$, h_1 is a fixed small constant, and h is sufficiently small.

Proposition 9. *For each fixed odd number k, $\sum_{n=1}^{\infty} \mathfrak{R}_{(n,k)}(x_1, x_2) = \mathfrak{R}_{(k,k)}(x_1, x_2)$.*

Proof. For any odd number k, we have

$$\sum_{n=1}^{\infty} \mathfrak{R}_{(n,k)}(x_1, x_2) = \sum_{n=1}^{\infty} e(n)s(n, k)\frac{r_1(nx_1)r_2(nx_2)}{n^2 h},$$

where $s(n, k) \neq 0$ only if n is odd and $\frac{h}{k} \in (\frac{h-\epsilon_n h}{n}, \frac{h-\epsilon_{n-1} h}{n-1}]$.

Now,

$$\frac{h}{k} \in (\frac{h-\epsilon_n h}{n}, \frac{h-\epsilon_{n-1}h}{n-1}] \Rightarrow n \in (k(1-\epsilon_n), k(1-\epsilon_{n-1})+1].$$

Since $h_1 << h$, ϵ_1 is very small, we have

$$1 < [k(1-\epsilon_{n-1})+1] - [k(1-\epsilon_n)] = 1 + \frac{k\epsilon_1}{n^2} < 2,$$

this implies that there are at most two consecutive integers locate in between the interval $(k(1-\epsilon_n), k(1-\epsilon_{n-1})+1]$. The only two possibilities are k and $k-1$, but n need to be odd, so we have $n = k$. $\square$

Then the second term of the RHS of (4.70) becomes

$$\begin{aligned}
&\frac{1}{h}\int_{-\infty}^{t}\sum_{k=1}^{\infty}\frac{2((-1)^k-1)}{\Pi_1 k\pi}e^{-\nu(\frac{k\pi}{h})^2(t-\tau)}\mathfrak{R}(x_1,x_2)(\sin\frac{k\pi x_3}{h})p_1(\tau)d\tau \\
&= \frac{1}{h}\int_{-\infty}^{t}\sum_{k=1}^{\infty}\left(\frac{2((-1)^k-1)}{\Pi_1 k\pi}e^{-\nu(\frac{k\pi}{h})^2(t-\tau)}\sum_{n=1}^{\infty}\mathfrak{R}_{(n,k)}(x_1,x_2)\sin\frac{k\pi x_3}{h}\right)p_1(\tau)d\tau \\
&= \frac{1}{h}\int_{-\infty}^{t}\sum_{k=1}^{\infty}\left(\frac{2((-1)^k-1)}{\Pi_1 k\pi}e^{-\nu(\frac{k\pi}{h})^2(t-\tau)}\mathfrak{R}_{(k,k)}(x_1,x_2)\sin\frac{k\pi x_3}{h}\right)p_1(\tau)d\tau \\
&= \frac{1}{h}\int_{-\infty}^{t}\sum_{k=1}^{\infty}\frac{2((-1)^k-1)}{\Pi_1 k\pi}e^{-\nu(\frac{k\pi}{h})^2(t-\tau)}\frac{c_1k^4}{vol_1}\frac{r_1(kx_1)r_2(kx_2)}{k^2h}\sin\frac{k\pi x_3}{h}p_1(\tau)d\tau \\
&= \frac{1}{h}\int_{-\infty}^{t}\sum_{k=1}^{\infty}\frac{2((-1)^k-1)}{\Pi_1 k\pi}e^{-\nu(\frac{k\pi}{h})^2(t-\tau)}\frac{c_1k^2}{vol_1h}r_1(kx_1)r_2(kx_2)\sin\frac{k\pi x_3}{h}p_1(\tau)d\tau,
\end{aligned}$$

averaging with respect to x_1 and x_2, we have

$$\frac{1}{h}\int_{-\infty}^{t}\sum_{k=1}^{\infty}\frac{2((-1)^k-1)}{\Pi_1 k\pi}e^{-\nu(\frac{k\pi}{h})^2(t-\tau)}\frac{c_1k^2}{vol_1h}r_1(0)r_2(0)\sin\frac{k\pi x_3}{h}p_1(\tau)d\tau.$$

Thus, the updated averaged velocity after taking into account the wall roughness is,

$$< u_1(t) >^{new} (x_3; h) =< u_1(t) > (x_3; h) - \frac{c_1 r_1(0) r_2(0)}{\pi^2 vol_1} \Delta < u_1(t) > (x_3; h), \quad (4.73)$$

whence the Laplacian operator arises naturally. We obtain the NS-α with $\alpha = \sqrt{\frac{c_1 r_1(0) r_2(0)}{\pi^2 vol_1}} = \sqrt{\frac{c_1 h}{4\pi^2 \delta_1 \delta_2}}$:

$$< u_1(t) >^{new} (x_3; h) = (1 - \alpha^2 \Delta) < u_1(t) > (x_3; h). \quad (4.74)$$

5. CONCLUDING REMARKS

In this dissertation, the outcomes of the study of two problems in nonlinear dynamics have been presented. The two problems are the chaotic vibration phenomenon in high-dimensional partial differential equations and the emergence of the Navier-Stokes alpha model for channel flows.

First, we presented the study of the chaotic vibration phenomenon in high-dimensional partial differential equations. It included two parts:
(i) by building our own solver in OpenFOAM, we studied the chaotic vibration phenomenon in the 2D wave equation numerically;
(ii) by applying the method of characteristics, we provided a rigorous proof of the chaotic vibration phenomenon of the 2D non-strictly hyperbolic equation.

Moreover, we also studied the problem related to the Navier-Stokes-alpha model, which is a mathematical model for the dynamics of appropriately averaged turbulent fluid flows. By introducing a Reynolds type average, we developed the transition from Navier-Stokes equations to the Navier-Stokes-alpha model.

The effect of these studies is to create a better understanding of both attractors and chaos. Moreover, the combination of the numerical simulations and theoretical analysis makes possible a deep understanding of the nonlinear dynamic phenomena.

REFERENCES

[1] *Lecture four: The poincare inequalities*, http://ocw.mit.edu/courses/mathematics/18, Accessed: 2016-04-21.

[2] *Openfoam user guide*, http://cfd.direct/openfoam/user-guide/cavity/, Accessed: 2016-04-21.

[3] *What is thrust*, http://www.grc.nasa.gov/WWW/k-12/airplane/thrust1.html, Accessed: 2016-04-21.

[4] Animikh Biswas, Ciprian Foias, and Larios Adam, *A generalized notion of attractor for the semi-dissipative boussinesq equations*, In preparation.

[5] Paul Blanchard, Robert L. Devaney, and Glen R. Hall, *Differential equations*, Thompson, 2006.

[6] Louis Stuart Block and William Andrew Coppel, *Dynamics in one dimension*, Springer, 1992.

[7] Ronald N Bracewell, *The fourier transform*, Scientific American **260** (1989), no. 6, 86–95.

[8] Goong Chen, Sze-Bi Hsu, and Jianxin Zhou, *Chaotic vibrations of the one-dimensional wave equation due to a self-excitation boundary condition. iii. natural hysteresis memory effects*, International Journal of Bifurcation and Chaos **8** (1998), no. 03, 447–470.

[9] Goong Chen, Sze-Bi Hsu, Jianxin Zhou, Guanrong Chen, and Giovanni Crosta, *Chaotic vibrations of the one-dimensional wave equation due to a self-excitation boundary condition. part i: Controlled hysteresis*, Transactions of the American Mathematical Society **350** (1998), no. 11, 4265–4311.

[10] Goong Chen, Tingwen Huang, and Yu Huang, *Chaotic behavior of interval maps and total variations of iterates*, International Journal of Bifurcation and Chaos **14** (2004), no. 07, 2161–2186.

[11] Goong Chen, Liangliang Li, and Jing Tian, *Chaotic vibration of a 2d non-strictly hyperbolic equation*, In preparation.

[12] Shiyi Chen, Ciprian Foias, Darryl D. Holm, Eric Olson, Edriss S. Titi, and Shannon Wynne, *Camassa-holm equations as a closure model for turbulent channel and pipe flow*, Phys. Rev. Lett. **81** (1998), 5338–5341.

[13] Shiyi Chen, Ciprian Foias, Darryl D Holm, Eric Olson, Edriss S Titi, and Shannon Wynne, *The camassa–holm equations and turbulence*, Physica D: Nonlinear Phenomena **133** (1999), no. 1, 49–65.

[14] Chen, Goong and Hsu, Sze-Bi and Zhou, Jianxin, *Chaotic vibration the one-dimensional wave equation due to a self-excitation boundary condition partii: Energy pumping, period doubling and homoclinic orbits*, International Journal of Bifurcation and Chaos **8** (1998), no. 3, 423–445.

[15] Chen, Shiyi and Foias, Ciprian and Holm, Darryl D and Olson, Eric and Titi, Edriss S and Wynne, Shannon, *A connection between the camassa–holm equations and turbulent flows in channels and pipes*, Physics of Fluids (1994-present) **11** (1999), no. 8, 2343–2353.

[16] Alexey Cheskidov, *Turbulent boundary layer equations*, Comptes Rendus Mathematique **334** (2002), no. 5, 423–427.

[17] Cheskidov, Alexey, *Boundary layer for the navier-stokes-alpha model of fluid turbulence*, Archive for rational mechanics and analysis **172** (2004), no. 3, 333–362.

[18] Ferruccio Colombini, Enrico Jannelli, and Sergio Spagnolo, *Well-posedness in the gevrey classes of the cauchy problem for a non-strictly hyperbolic equation with coefficients depending on time*, Annali della Scuola Normale Superiore di Pisa-Classe di Scienze **10** (1983), no. 2, 291–312.

[19] Ferruccio Colombini and Sergio Spagnolo, *An example of a weakly hyperbolic cauchy problem not well posed inc*, Acta Mathematica **148** (1982), no. 1, 243–253.

[20] Peter Constantin and Ciprian Foias, *Navier-stokes equations*, University of Chicago Press, 1988.

[21] Robert L Devaney and Luke Devaney, *An introduction to chaotic dynamical systems*, vol. 13046, Addison-Wesley Reading, 1989.

[22] Ciprian Foias, Darryl D Holm, and Edriss S Titi, *The three dimensional viscous camassa–holm equations, and their relation to the navier–stokes equations and turbulence theory*, Journal of Dynamics and Differential Equations **14** (2002), no. 1, 1–35.

[23] Ciprian Foias, Ricardo Rosa, and Roger Temam, *Topological properties of the weak global attractor of the three-dimensional navier-stokes equations*, Discrete Contin. Dyn. Syst **27** (2010), no. 4, 1611–1631.

[24] Ciprian Foias, Jing Tian, and Bingsheng Zhang, *On some properties of incompressible fluid flows in channels*, In preparation.

[25] Foias, Ciprian and Tian, Jing and Zhang, Bingsheng, *On the emergence of the navier-stokes-alpha model for turbulent channel flows*, Submitted.

[26] Russell Herman, *A second course in ordinary differential equations: Dynamical systems and boundary value problems*, 2008.

[27] Kenneth Hoffman, *Banach spaces of analytic functions*, Dover Publications, Inc., New York, 1988, Reprint of the 1962 original. MR 1102893

[28] Darryl D Holm, *Fluctuation effects on 3d lagrangian mean and eulerian mean fluid motion*, Physica D: Nonlinear Phenomena **133** (1999), no. 1, 215–269.

[29] John W Jewett and Raymond A Serway, *Physics for scientists and engineers with modern physics*, Cengage Learning EMEA, 2008.

[30] Fritz John, *Partial differential equations*, Springer-Verlag, New York-Berlin, 1971, Applied Mathematical Sciences, Vol. 1. MR 0304828

[31] Randall J LeVeque, *Finite volume methods for hyperbolic problems*, vol. 31, Cambridge University Press, 2002.

[32] Liangliang Li, Yuanlong Chen, and Yu Huang, *Nonisotropic spatiotemporal chaotic vibrations of the one-dimensional wave equation with a mixing transport term and general nonlinear boundary condition*, Journal of Mathematical Physics **51** (2010), no. 10, 102703.

[33] Jun Liu, Yu Huang, Haiwei Sun, and Mingqing Xiao, *Numerical methods for weak solution of wave equation with van der pol type nonlinear boundary conditions*, Numerical Methods for Partial Differential Equations **32** (2016), no. 2, 373–398.

[34] Benoit B Mandelbrot, *Multifractals and 1/ noise: Wild self-affinity in physics (1963–1976)*, Springer, 2013.

[35] Mandelbrot, Benoit B, *The fractal geometry of nature*, vol. 173, Macmillan, 1983.

[36] Takuya Oshima and Masashi Imano, *A full finite-volume time-domain approach towards general-purpose code development for sound propagation prediction with unstructured mesh*, Proceedings of Inter-Noise, 2008.

[37] Clark Robinson, *Dynamical systems, stability, symbolic dynamics and chaos*, CRC Press, 1998.

[38] Noriyuki Sasaki, Mitsunori Murakami, Kazuo Nozawa, Shunji Soejima, Akira Shiraki, Takeshi Aono, Tomeo Fujimoto, Isao Funeno, Norio Ishii, and Hiroshi Onogi, *Design system for optimum contra-rotating propellers*, Journal of marine science and technology **3** (1998), no. 1, 3–21.

[39] James Johnston Stoker, *Nonlinear vibrations in mechanical and electrical systems*, 1950.

[40] Béla Sz.-Nagy, *Introduction to real functions and orthogonal expansions*, Oxford University Press, New York, 1965. MR 0181711

[41] Roger Temam, *Infinite-dimensional dynamical systems in mechanics and physics*, vol. 68, Springer Science & Business Media, 2012.

[42] Jing Tian and Bingsheng Zhang, *On solutions of the 2d navier-stokes equations with constant energy and enstrophy*, Indiana University Mathematics Journal **64** (2015).